KAUNAS UNIVERSITY OF TECHNOLOGY

MUHAMMAD USMAN MUNIR

# DEVELOPMENT OF ELECTROSPUN FIBERS FOR APPLICATION IN MEDICAL DEVICES

Doctoral dissertation
Technological Sciences, Materials Engineering (T 008)

2024, Kaunas

This doctoral dissertation was prepared at Kaunas University of Technology, Faculty of Mechanical Engineering and Design, Department of Production Engineering during the period of 2019–2023.

**Scientific Supervisor:**
Prof. Dr. Daiva MIKUČIONIENĖ (Kaunas University of Technology, Technological Sciences, Materials Engineering, T 008).

Edited by: English language editor Dr. Armandas Rumšas (Publishing House *Technologija*), Lithuanian language editor Aurelija Gražina Rukšaitė (Publishing House *Technologija*).



The public defense of the dissertation will be held at 10 a. m. on 12 March 2024 at the public meeting of the Dissertation Defence Board of Materials Engineering Science Field in Rectorate Hall at Kaunas University of Technology.

Address: K. Donelaičio 73-402, LT-44249, Kaunas, Lithuania.
Phone: (+370) 608 28 527; e-mail doktorantura@ktu.lt

The doctoral dissertation was sent out on 12 February, 2024.
The doctoral dissertation is available on the internet at http://ktu.edu and at the library of Kaunas University of Technology (Gedimino 50, LT-44239, Kaunas, Lithuania).

KAUNO TECHNOLOGIJOS UNIVERSITETAS

MUHAMMAD USMAN MUNIR

# MEDICININĖS PASKIRTIES PRIEMONĖMS SKIRTŲ PLUOŠTŲ KŪRIMAS ELEKTRINIO VERPIMO BŪDU

Daktaro disertacija
Technologijos mokslai, medžiagų inžinerija (T 008)

2024, Kaunas

Disertacija rengta 2019–2023 metais Kauno technologijos universiteto Mechanikos inžinerijos ir dizaino fakulteto Gamybos inžinerijos katedroje.

**Mokslinė vadovė:**
prof. dr. Daiva MIKUČIONIENĖ (Kauno technologijos universitetas, technologijos mokslai, medžiagų inžinerija, T 008).

Disertaciją redagavo: anglų kalbos redaktorius dr. Armandas Rumšas (leidykla „Technologija“), lietuvių kalbos redaktorė Aurelija Gražina Rukšaitė (leidykla „Technologija“).

**Medžiagų inžinerijos mokslo krypties disertacijos gynimo taryba:**
prof. dr. Rimvydas MILAŠIUS (Kauno technologijos universitetas, technologijos mokslai, medžiagų inžinerija, T 008) – **pirmininkas**;
doc. habil. dr. Marcin BARBURSKI (Lodzės technikos universitetas, Lenkija, technologijos mokslai, medžiagų inžinerija, T 008);
doc. dr. Jurgita DOMSKIENĖ (Kauno technologijos universitetas, technologijos mokslai, medžiagų inžinerija, T 008);
prof. dr. Saulius GRIGALEVIČIUS (Kauno technologijos universitetas, technologijos mokslai, medžiagų inžinerija, T 008);
prof. habil. dr. Malgorzata MATUSIAK (Lodzės technikos universitetas, Lenkija, technologijos mokslai, medžiagų inžinerija, T 008).

Disertacija bus ginama viešame medžiagų inžinerijos mokslo krypties disertacijos gynimo tarybos posėdyje 2024 m. kovo 12 d. 10 val. Kauno technologijos universiteto Rektorato salėje.

Adresas: K. Donelaičio g. 73-402, LT-44249 Kaunas, Lietuva.
Tel: (+370) 608 28 527; el. paštas doktorantura@ktu.lt

Disertacija išsiųsta 2024 m. vasario 12 d.
Su disertacija galima susipažinti interneto svetainėje http://ktu.edu ir Kauno technologijos universiteto bibliotekoje (Gedimino g. 50, LT-44239 Kaunas, Lithuania).

**TABLE OF CONTENTS**

**LIST OF TABLES**

**LIST OF FIGURES**

## LIST OF ABBREVIATIONS AND DEFINITIONS

### Abbreviations

| | | |
|---|---|---|
| PVA | – | Poly vinyl alcohol |
| PLA | – | Poly lactic acid |
| DMF | – | Dimethyl formamide |
| CNDs | – | Carbon nanodots |
| ZnO | – | Zinc oxide |
| AV | – | Aloe vera |
| NPs | – | Nanoparticles |
| TGA | – | Thermogravimetric analysis |
| FTIR | – | Fourier transform infrared |
| CFU | – | Colony forming unit |
| DOE | – | Design of experiment |
| $TiO_2$ | – | Titanium dioxide |
| EDANA | – | European Disposable and Nonwoven Association |
| SARS | – | Severe acute respiratory syndrome |
| CA | – | Cellulose acetate |
| PEG | – | Polyethylene glycol |
| PCL | – | Polycaprolactone |
| PEO | – | Polyethylene oxide |
| PBS | – | Polybutylene succinate |
| PVP | – | Polyvinylpyrrolidone |
| ISO | – | International Organization for Standardization |
| SI | – | Système international |
| PAN | – | Polyacrylonitrile |
| PMMA | – | Poly (methyl methacrylate) |
| ROS | – | Reactive oxygen species |
| IONP | – | Iron oxide nanoparticles |
| HEPA | – | High efficiency particulate air (filter) |
| PPE | – | Personal protective equipment |
| SEM | – | Scanning electron microscope |

## INTRODUCTION

In December 2019, the very first case of SARS-CoV-2 was reported. [1]. Then, in as little as 3 months, this virus was found to be so contagious that, on 11 March 2020, WHO declared it as a global pandemic [2]. As this virus attacks the respiratory system, initially, people were advised to adopt safety precautions, such as maintaining safe distance and using personal protective equipment. [3]. This unfortunate development has caused an unusual usage and demand for PPEs. In 2020, due to SARS-CoV-2, the market size of personal protective equipment increased by 17% as compared to 2019. The global market size of PPEs was 80 billion in 2022, and was projected to increase to 111 billion USD by 2029 [4, 5].

Just like influenza and severe acute respiratory syndrome (SARS), SARS-CoV-2 is transmitted mainly by droplets of cough or sneeze of the patient. The average size of droplets exhaled by cough, sneeze, speak or sig is 5 microns, and the range to which a patient can spread virus was found to equal 1–2 meters. That is why people were asked to maintain a safe distance of 6 feet from each other, just to contain the virus from further spreading [6]. Poor ventilation in crowded indoor activities is also a main reason that SARS-CoV-2 spreads at a faster pace in winters as compared to summers. As a matter of fact, in summers, normally, windows and doors are open for proper ventilation [6]. In 2020, before the availability of a vaccine against this deadly virus, the only way one could adopt to reduce the spread was by keeping the safe distance, and by using proper PPEs, especially facemasks. Medical facemasks were highly helpful in that time as they cover the nose and mouth of the user and act as a barrier to any outgoing droplets of virus by cough, sneeze, or by speaking [7].

Conventionally, a three-layered structure of spunbond and meltblown nonwoven sheets is used for medical facemasks and respirators [8]. Technical textiles, especially nanofibres, have been reported to manifest superior properties as compared to macro fibres. This is due to the fact that nanofibres have their diameter in the the much smaller nanometre range, and they form a functional nonwoven web which can efficiently filter out particles in nano and micro sizes as well [9].

There are different methods to obtain these nanofibres. One of the widely used techniques to obtain nanofibres is electrospinning. In 1900, John Francis Cooley filed the first patent in electrospinning. Then, a mathematical model of cone formation from the surface of a droplet in an electric filed was proposed in 1964 by Sir Geoffrey Ingram Taylor. Formerly, it was known as the Taylor cone, named after Geoffrey Ingram Taylor. Since 1995, the formation of nanofibres by electrospinning has become a field of prominent interest among the researchers [10].

Nanofibre sheets prepared by electrospinning show superior performance and thus can be used as a filtration layer in the medical face mask as well as in respirator filters. Sustainability and the environmental impact of the disposable face mask is still an issue. Hence, polymeric nanomembranes were being prepared by using different sustainable polymers. These polymers were functionalised with antimicrobial materials to cope with contagious diseases.

**Aim of Doctoral Thesis**

The aim of the research is to develop sustainable electrospun fibre layers and functionalise them with antibacterial materials for application in medical face masks and to determine the barrier performance of functionalised nonwoven layers.

To achieve this aim, the following objectives were set:

- To optimise the solution parameters for electrospinning of sustainable PVA and PLA polymers.
- To analyse the surface morphology and chemical composition of the resulting fibres and identify the optimal weight percentage of polymers for electrospinning.
- To evaluate the antibacterial properties of nanofibres functionalised with *Aloe vera*, zinc oxide, and carbon nanodots.
- To assess the barrier performance of prototype facemasks for medical applications.

**Scientific Novelty of the Research**

The doctoral research presents approaches in the development of sustainable and highly functionalised nanofibres using a cutting-edge electrospinning technique. Extensive investigations have been conducted to explore the remarkable antibacterial capabilities of natural and photoactive materials, such as *Aloe vera*, ZnO, and carbon nanodots, which resulted in a comprehensive and compelling comparison of their performance.

Particularly noteworthy are the carbon nanodots-loaded PLA nanofibres which not only exhibit sustainability and biodegradability, but also demonstrate exceptional functional properties under visible light, courtesy of the inherent photoactive behaviour of CNDs. These nanofibres present a breakthrough solution which combines environmental consciousness with enhanced functionality, thereby setting a new standard for sustainable materials in various applications.

Furthermore, when applied in the field of medical devices, both PVA and PLA nanofibres showcased superior barrier performance compared to the conventional nanofibres. This finding holds immense potential for revolutionizing the medical industry by offering enhanced protection and ensuring the highest standards of safety.

**Practical Value of the Work**

This research has demonstrated that functionalised nanofibres can be used as a potential filtration layer in medical devices. The proposed sandwich-layered model, in which the middle layer is composed of nanofibres, and the outer layers are composed of spunbond can also be used in respirators as well as in nonwoven surgical gowns. The model presented in this research satisfies the international requirements of Type I/Level 1 medical facemasks. The upscaling and industrial use of such electrospun fibres is very easy and feasible too, and it would also reduce cost compared to the conventional meltblown nonwoven sheets used in medical face masks.

**Author's Contribution**

This doctoral thesis presents results which have been originally collected and analysed by the author. The author has published the output of this doctoral thesis.

Some of the doctoral research was done in collaboration with the Nanotechnology Research Lab of the National Textile University, Faisalabad, Pakistan. The author worked on the development of eco-friendly electrospun fibres of *Aloe vera*/PVA/ZnO and advised their potential applications in textiles. The author planned and conducted all the experiments for the fabrication of AV/PVA/ZnO nanofibres by the solution electrospinning technique.

Other major part of the doctoral research was conducted in collaboration with Dr. Thomas Mayer-Gall's laboratory in German Textile Research Center North-West (DTNW), Germany. The author planned and conducted all the fabrication of PLA/CNDs nanofibres by solution electrospinning.

# 1. LITERATURE REVIEW

## 1.1. Medical Devices

According to Clause 3 of ISO 13485:2016(E) Medical devices – Quality management systems – Requirements for regulatory purposes, "a medical device is an instrument, apparatus, implement, machine, appliance, implant, reagent for in vitro use, software, material or other similar or related article, intended by the manufacturer to be used, alone or in combination, for human beings, for one or more of the specific medical purpose(s) of:

- diagnosis, prevention, monitoring, treatment, or alleviation of disease.
- diagnosis, monitoring, treatment, alleviation of or compensation for an injury.
- investigation, replacement, modification, or support of the anatomy or of a physiological process.
- supporting or sustaining life.
- control of conception.
- disinfection of medical devices.
- providing information by means of in vitro examination of specimens derived from the human body."

According to this description, face masks, barrier face coverings, surgical masks, and respirators for COVID-19 fall under the category of medical devices. This has also been approved by FDA, confer: "The FDA regulates face masks, including cloth face coverings, barrier face coverings, and surgical masks as medical devices when they are intended for a medical purpose. Medical purposes include uses related to helping prevent the spread of COVID-19" [11]. WHO has also approved this definition, and, under the Global Model Regulatory Framework for Medical Devices including in vitro diagnostic medical devices, it supports Member States while encouraging them to develop and implement regulatory controls and regional guidelines for good manufacturing to ensure the quality, safety and efficacy of medical devices available in their countries [12].

## 1.2. Generic Structure of Medical Face Masks and Respirators

A face mask is a type of a medical device which covers the nose and mouth of the wearer. The face mask is 'kind of' a physical barrier which filters the airflow in and out of the wearer's mouth and nose. Therefore, if the user sneezes, coughs, or speaks, the droplets coming out are filtered at the face mask, and they do not reach out the surrounding environment; similarly, during inhalation, the droplets outside of face masks are also filtered, and the user is protected from the outside impact, too. This way, face masks save the wearer and the people in the surroundings as well [8].

Generally, medical face masks are made of nonwoven fabrics which filter out some of the incoming and outgoing viruses, bacteria, particles, and droplets by trapping them in their filtration later, but they are denoted by loose fitting to the face, and some of the air is not filtered during breathing. The common structure of a medical

face mask contains three layers: two supporting outer layers and one inner filtration layer [13], as presented in Fig. 1. Typically, the outer layers are made of spunbond nonwoven fabric, and the inner layer(s) are made of a meltblown nonwoven layer [14].

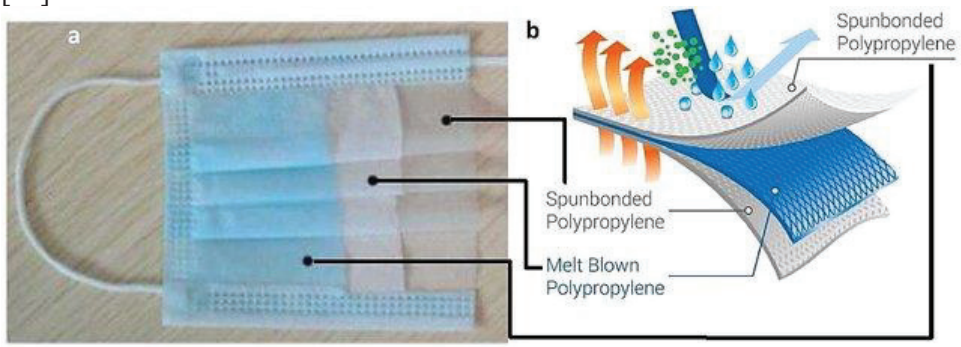


**Fig. 1**. Generic structure of medical face mask [13]

Face masks may or may not meet the fluid barrier performance and have just some loose strips, thus being not tight to the face. These face masks must not be confused with respirators N95/KN95, as these respirators are a type of the medical device designed to give a very close fit to the face and nose of the user while also covering them [15]. The minimum requirements of PFE and BFE are almost the same, as used in a medical face mask and a respirator. Respirators may or may not have a breathing value reducing the breathing resistance during inhalation/exhalation, as shown in Fig. 2 [16].

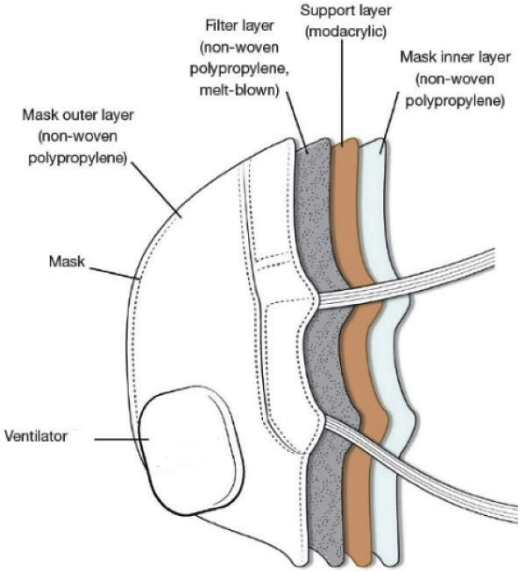


**Fig. 2**. Typical structure of N95 respirator [17]

## 1.3. Nonwoven Fabrics

Nonwovens, weaving, and knitting are three types of fabric formation techniques. In nonwovens, the fibres/filaments are placed randomly, which forms a web with specific properties. The term 'nonwoven' has already been used for a number of decades. Nonwoven fabrics are known to be cheaper than the conventional woven fabrics. ISO 9092:2019 defines nonwovens as "engineered fibrous assembly, primarily planar, which has been given a designed level of structural integrity by physical and/or chemical means, excluding weaving, knitting and papermaking" [18]. The *European Disposable and Nonwoven Association* (EDANA) defines nonwovens as "a manufactured sheet, web or batt of directionally or randomly orientated fibres, bonded by friction, and/or cohesion and/or adhesion and it excludes a number of materials such as paper, woven and knitted fabrics, tufted or stitch-bonded, and felted by wet-milling" [19]. INDA (the *Association of the Nonwoven Fabrics Industry*) explains nonwoven fabrics as "sheet or web structures bonded together by entangling fibres or filaments, by various mechanical, thermal and/or chemical processes" [20, 21].

One of the most significant features of nonwoven fabrics is that they usually are made directly from raw material, thus skipping a lot of other processes, such as carding, roving, opening, spinning, and weaving/knitting. The comparably simple process allows nonwovens to compete with complex fabric formation techniques like weaving and knitting. In this context, nonwovens are comparatively cheap and cost-effective, and they also have a much wider application area as compared to woven/knitted fabrics [22, 23] .

Due to their low weight, strength, permeability and filtration properties, nonwovens are being used in a wide range of applications. One of the best uses of nonwovens is in the medical field. Nonwovens made of synthetic fibres have a low lint, good mechanical properties, and their disposability makes them a perfect material to be used in growing healthcare and hygiene applications [24].

Nonwoven fabric formation starts from the polymer melt, followed by passing the melt through the spinneret, thus forming either fibres or filaments. There are three main stages in the formation of nonwoven fabric: 1) web formation, 2) web bonding, 3) finishing treatment [25]. Nonwoven fabrics used in medical devices, especially medical face masks, are commonly made of spunbond and meltblown fabrics, and these form different nonwoven fabrics due to different web formation techniques being used [26].

### 1.3.1. Spunbond

Generally, spun melt describes the formation of nonwovens from thermoplastic polymers. It encompasses spunbond and meltblown web formation techniques.

The spunbond process is a web formation technique. Firstly, a polymer melt is passed through the spinneret containing many holes. As soon as the fibres/filaments exit the spinneret, the filaments are cooled down by a supply of conditioned air. The filaments are laid randomly on a moving conveyor belt. This random lying of filaments is caused by the turbulence in the air stream. Then conveyor belt then carries

the spunbonded web for further processing of bonding and the finishing treatment depending upon the end application [27]. Fig. 3 presents the spunbond nonwoven fabric formation process.

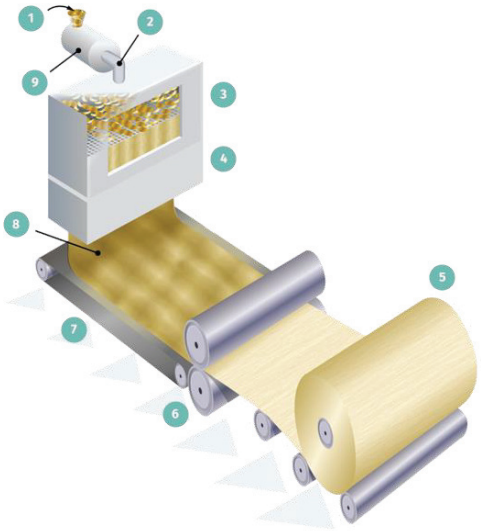


**Fig. 3**. Spunbond nonwoven fabric formation process: 1) polymer chips feed, 2) liquid polymer, 3) extrusion die, 4) filament attenuator (cooling and stretching), 5) wind up, 6) calendar bonding, 7) laydown, 8) fibre dispersion, 9) extruder [28]

### 1.3.2. Meltblown

Meltblown is a different type of nonwoven web formation technique, only involving a minor difference compared to the spun laid technique. Instead of the filaments being stretched as they exit the spinneret, rather, they are blown by hot air, which keeps them in the partially molten state. This way, thinner fibres or filaments are formed, but the resultant nonwoven sheet offers comparably low tensile strength as compared to the spunbond samples [29–31]. Fig. 4 presents the meltblown, nonwoven fabric formation process.

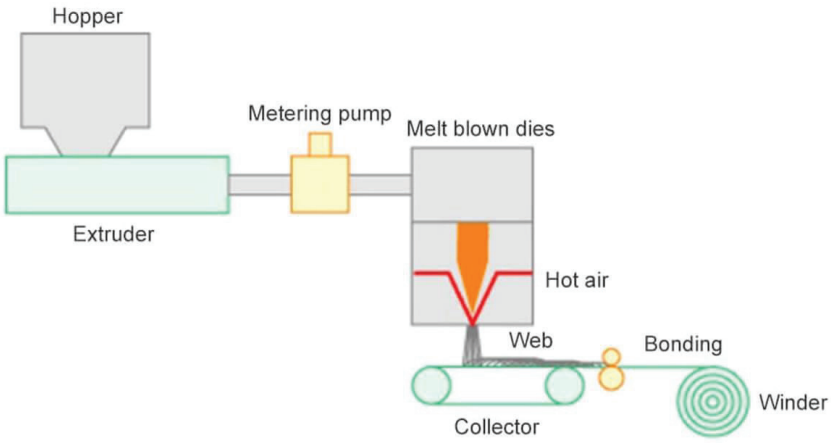


**Fig. 4**. Meltblown process [32]

### 1.4. Nanofibres

As the term 'nano' depicts, the diameter of the fibres must be in the nano scale, from tens to some hundreds of nanometres. As defined in the SI units, the prefix *nano* means one billionth, or $10^{-9}$, hence one nanometre is one billionth part of a metre [33]. There is no formal or universally accepted definition of *nanofibre* as such, but, generally, fibres with a diameter in the range of 1–500 nanometres fall under the criteria of nanofibres, and the ratio between the length and the width should be greater than 50 [34]. Fig. 5 presents a comparison of the nanometre size to some common things.

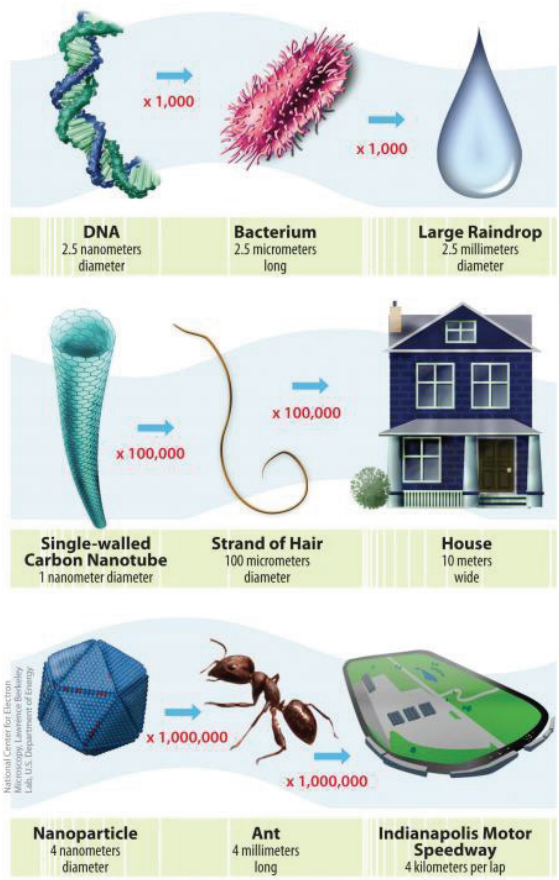


**Fig. 5**. Nanometre: size comparison of different objects in nanometres [35]

Due to their nano size, the fibres with a diameter in the nano range exhibit exceptional properties as compared to micro fibres. This is due to the fact that the surface area of nanofibres to volume is much higher, and also the porosity in the nano size makes them unique [36]. The above mentioned properties make them suitable for use in medical devices for filtration, drug delivery, etc. [37]. Following are the techniques used to form fibres with a diameter in the nanoscale:

- Drawing [38].
- Phase separation, template synthesis [39].
- Self-assembly.
- Centrifugal spinning [40].
- Electrospinning [41].

### 1.5. Electrospinning

Electrospinning is a nanofibre formation technique in which a high voltage is required. The electric field between the polymer source and the collector stretches the polymer chains from the source to the collector, and thus nanofibres are formed [42, 43]. This

phenomenon was first reported in 1887 and described by Charles Vernon Boys. In an electric field, he observed the formation of fibres from a solution when it approaches the edge of a dish [10]. The process of electrospinning is relatively simple; it only requires a source – a stock solution (whether in a syringe or a needle), and a collector (a metallic plate or drum) and some potential difference between the source and the collector. Generally, the positive terminal from the voltage device is connected to the syringe or directly to the stock solution (in case of needleless electrospinning), whereas the other terminal from the voltage device is grounded [44]. Due to the potential difference between the source (a needle or solution) and the collector, the polymer is stretched due to the electrostatic force of repulsion, and charged species get accumulated at the tip of the needle. The potential difference applied is in some 1000s of Volts. When the forces surpass the surface tension, the charged polymer solution stretches out of the polymer solution in the conical shape which is called the Taylor cone, as shown in Fig. 6 .

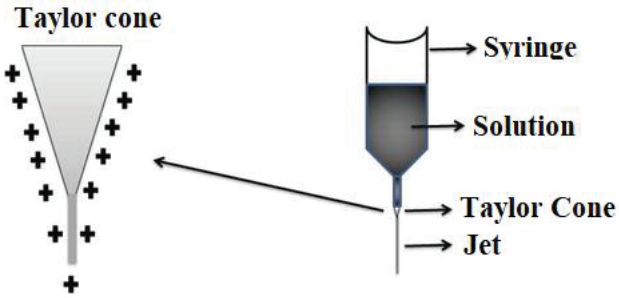


**Fig. 6**. Taylor cone formation in the process of electrospinning [46]

As mentioned above, due to a much high potential difference, the Taylor cone gets stretched and is attracted to the surface of the collector. The nanofibres also solidify as they arrive at the collector [47]. This electrospinning technique is very versatile, and it produces fibres in the micro and nanometric scales, depending on the properties of the stock solution and the process parameters [48]. Due to easy processing, electrospinning is being used to form fibres for a number of applications involving tissue engineering, drug delivery, biomedical, textiles, filtration, sensors, catalysis, electronic devices, energy storage, and environmental applications [49–55].

A lot of materials can be fabricated by this technique. These include polymers, ceramics, and composites [56]. Hollow nanofibres and core-shell structure nanofibres can also be formed [57]. On the basis of the phase of the polymer state, the electrospinning process has two categories: one is solution electrospinning, and the other is melt electrospinning [58]. An illustration of the process of electrospinning is shown in Fig. 7.

Melt electrospinning is also known as solvent-free electrospinning [59]. As compared to solution electrospinning, melt electrospinning utilises no solvent for the polymer; rather, the polymers in the filament form are directly electrospun in from the molten state. This solvent-free aspect makes it a greener, safer, and more sustainable technique for the formation of nanofibres. The only drawback of melt spinning is the

resultant larger diameter of nanofibres, which is a deficiency of suitable polymers for the melt electrospinning process [60–62].

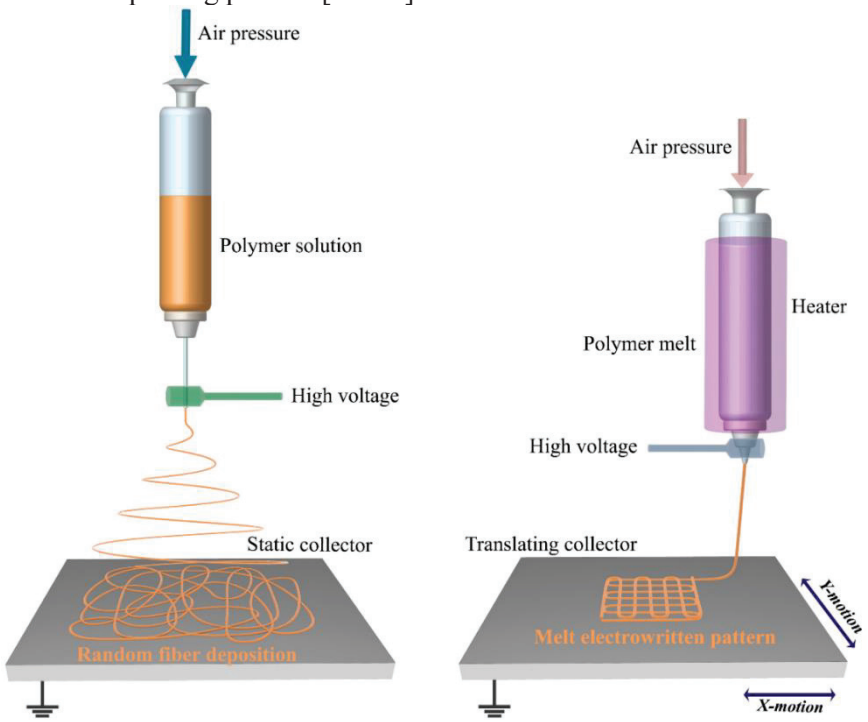


**Fig. 7**. Solution and melt electrospinning [63]

Based on the direction between the collector and the syringe, the electrospinning technique features 2 different types. One is horizontal, in which the syringe is placed horizontally to the collector. The other is vertical, in which the syringe/needle is placed vertically to that of the plane of the collector [64]. A schematic representation of the vertical and horizontal directions is shown in Fig. 8.

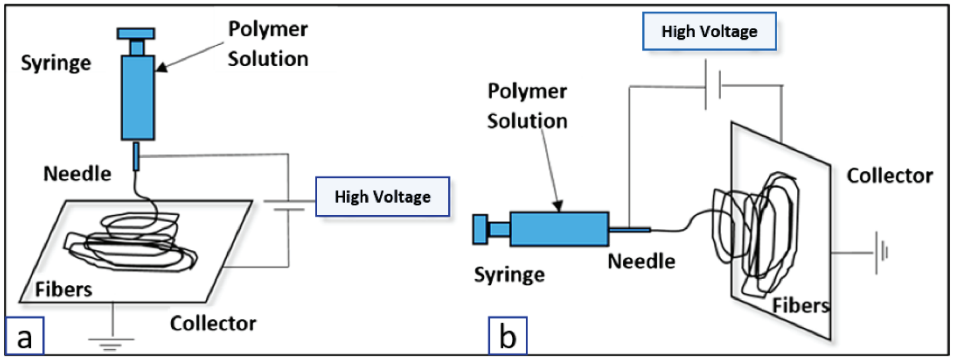


**Fig. 8**. (a) Vertical and (b) horizontal electrospinning [65]

Based on the fibre generation from the stock solution, electrospinning is categorised into two categories: 1) needle electrospinning; 2) needleless electrospinning. Needle electrospinning further contains multi needle, core-shell, and coaxial electrospinning techniques [66–68]. The multi-needle technique is used to increase the production rate of the nanofibre formation. Core-shell is used for incorporating different materials in the core and shell of the nanofibres. Whereas, the coaxial is technique is used when we want to use 2 or more incompatible materials (with each other), every material generates nanofibres from different needles or nozzles, and they are collected as a composite nanofibre sheet on the collector [69–71]. In needleless electrospinning, as shown by its name, no needle is used for the generation of nanofibres. Rather, the whole stock solution is made to have a potential, and nanofibres are stretched from the surface of the stock solution to the collector [72, 73]. Fig. 9 shows a description of needleless electrospinning.

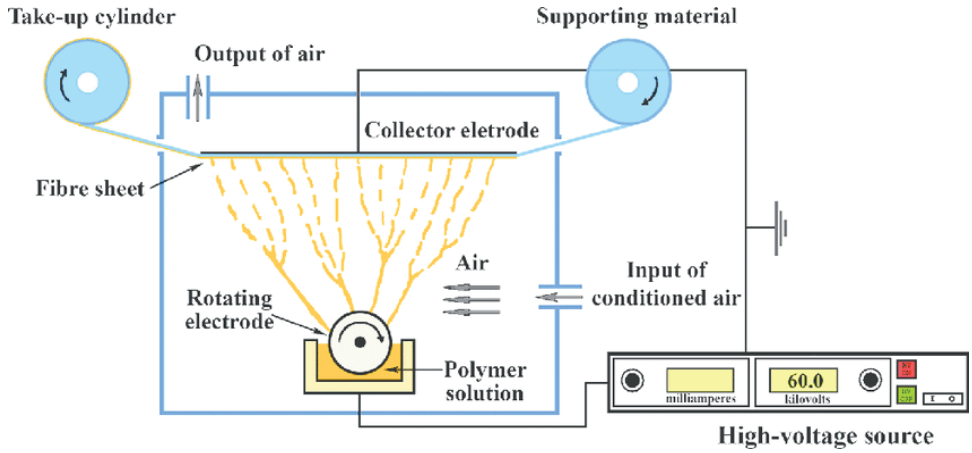


**Fig. 9**. Needleless electrospinning [74]

## 1.6. Nanofibres in Medical Textiles

The simple electrospinning process and the nanofibre generation process make it suitable to fabricate a wide range of polymers including natural and synthetic polymers, and also biodegradable and nonbiodegradable polymers. Due to various concerns, mainly health-related and environmental, a lot of focus has been made on sustainable and biodegradable polymers [75, 76]. These include collagen, alginate, chitosan, cellulose acetate (CA), gelatine, poly(ethylene glycol) (PEG), poly(lactic acid) (PLA), poly(glycolic acid) (PGA), poly(D, L-lactide- co-glycolide) (PLGA), polycaprolactone (PCL), polybutylene succinate (PBS), polyvinyl alcohol (PVA), and polyethylene oxide (PEO) [77–82]. Some natural polymers do exhibit antimicrobial properties, and some are made antimicrobial by incorporating antimicrobial materials in them. These fibres shall be discussed in the sections below.

### 1.6.1. Nanofibres with inherited antimicrobial properties

Nanofibres with inherited antimicrobial properties are extensively used in different applications due to their biocompatibility, non-toxicity, and biodegradability. Chitosan is a natural and linear polysaccharide. In the chemical structure of chitosan, it contains randomly oriented D-glucosamine and N-acetyl-D-glucosamine linked by a β- (1–4). Fig. 10 shows the chemical structure of chitosan. One of the unique things about chitosan is that it is the only positively charged naturally alkaline polysaccharide material described so far [83]. One more thing about chitosan is that it possesses inherited antimicrobial properties, which is associated with the cationic nature of this natural polymer. There are several mechanisms proposed on how the cationic charge develops antimicrobial properties [84] which are described below:

1. The positive charge on the chitosan surface interacts with the cell wall of the bacteria and either damages it or creates disturbance in the permeability of the negatively charged cell wall of bacteria.
2. As the cationic nature creates diffused hydrolysis products with the DNA, it inhibits mRNA and eventually protein synthesis.
3. Chelation of nutrients and essential metals is achieved.

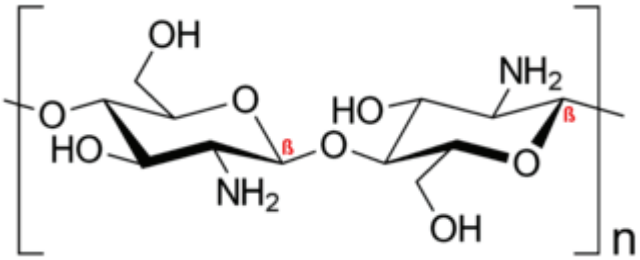


**Fig. 10**. Chemical structure of chitosan [85]

### 1.6.2. Nanofibres doped with natural antimicrobial properties.

Naturally derived bioactive agents are widely studied as they pose no threat and have no toxicity when used in medical textiles. Some bioactive plant crude extracts are easily obtained by organic solvent extraction, and these have already been doped in nanofibre to gain antimicrobial properties. Mikučionienė *et al.* [86] developed Baltic amber-based polyamide electrospun fibres and also investigated their antibacterial properties. They found a significant antibacterial behaviour of samples containing Baltic amber in them as compared to the control samples. Yao *et al*. [87] studied the wound healing effects of a herbal medicine, *Centella asiatica* (CA). They found that when gelatine nanofibres are incorporated with *Centella asiatica* extract, the wound healing process is facilitated by collagen synthesis, and also by fibroblast proliferation. They also found that *Centella asiatica* exhibits antibacterial activity. Fig. 11 shows the actual image of the *Centella asiatica* plant.

**Fig. 11**. *Centella asiatica* plant – visual representation [88]

Chan *et al*. [89] developed natural silk fibroin protein (SFP) nanofibres by incorporating it with Chinese herbal extract (baicalein, BAI). They found that the SFP/PVP/BAI nanofibre sheet has antimicrobial properties against *S. aureus*. Sadri *et al*. [90] studied and developed chitosan-based polyethylene oxide nanofibres and also blended this solution with green tea extract, a natural and eco-friendly antibiotic and antimicrobial material. They found that the resultant nanofibres have good antimicrobial properties and good healing properties when chitosan/PEO/GT was used as wound dressing.

Suwantong *et al*. [91] developed dichloromethane extracted (dGM) and acetone extracted (aGM) (*Garcinia mangostana Linn*) loaded PLA nanofibres. They found that dichloromethane extracted *Garcinia mangostana Linn* offers good antimicrobial properties against *S. aureus* DMST 20654, whereas acetone extracted *Garcinia mangostana Linn* has good antimicrobial properties against *S. epidermidis* and against *S. aureus* ATCC 25923. Fig. 12 shows an actual image of *Garcinia mangostana Linn*.

**Fig. 12**. *Garcinia mangostana Linn* – a fruit-based natural antimicrobial agent [92]

Suganya *et al*. [93] developed a *Tecomella undulata* extract loaded PCL/PVP nanofibres, which is a widely known traditional medicine in the field of wound healing. They found that these *Tecomella undulata* loaded PCL/PVP nanofibres exhibit good antimicrobial properties against *S. aureus* with a 24 mm zone of inhibition and against *E. Coli* with a 28 mm zone of inhibition, respectively. Fig. 13 shows the actual image of the *Tecomella undulata* plant.

**Fig. 13**. *Tecomella undulata* – leaves and flowers [94]

***Aloe vera***

The abundantly used antimicrobial material with good softness properties is the *Aloe vera* leaf gel. Due to its soft feel and antimicrobial properties, *A*loe vera gel is being used in many types of cosmetics [95]. *Aloe vera* gel is extracted from the leaves of the *A*loe vera plant, and it constitutes many elements, of which, glucomannan and acemanan are considered to be the active antimicrobial agents [96]. Fig. 14 shows an actual image of the *Aloe vera* leaf and its gel. It has also been used in tissue engineering [97].

Several researchers checked the antimicrobial activity of *Aloe vera* leaf gel, and found that *A*loe vera gel has more antimicrobial activity against gram-positive bacteria rather than against gram-negative bacteria [98].

The antimicrobial activity of *Aloe vera* gel is primarily attributed to the presence of various bioactive compounds found in the plant. Here are some key factors that contribute to its antimicrobial properties:

1. Polysaccharides: *Aloe vera* gel contains several polysaccharides, such as acemannan, which have shown antimicrobial activity against a wide range of bacteria, fungi, and viruses. These polysaccharides disrupt the cell walls of microorganisms, thereby leading to their death or inhibition of growth.

2. Phenolic compounds: *Aloe vera* gel contains various phenolic compounds, including catechins, coumarins, and flavonoids. These compounds possess antimicrobial properties by interfering with microbial enzymes, disrupting their cellular processes, and inhibiting their growth.

3. Saponins: *Aloe vera* gel contains saponins, which are natural compounds with detergent-like properties. Saponins can disrupt the cell membranes of

microorganisms, thus leading to leakage of their cellular contents and ultimately causing their death.

4. Salicylic acid: *Aloe vera* gel contains salicylic acid which exhibits antimicrobial activity. Salicylic acid has been shown to inhibit the growth of bacteria and fungi by interfering with their metabolic processes.

5. Polypeptides: *Aloe vera* gel contains several polypeptides, such as aloverin, which have demonstrated antimicrobial effects. These polypeptides can disrupt microbial membranes and inhibit their growth.

It is of importance to note that the antimicrobial properties of Aloe vera gel can vary depending on such factors as the plant species, processing methods, and storage conditions. Additionally, the antimicrobial activity may differ against different types of microorganisms.

Suganya *et al*. [99] found that when *Aloe vera* is added with PCL and nanofibres are formed, *Aloe vera*/PCL nanofibres tend to be thinner, more hydrophilic, and this also adds antimicrobial activity to the formed nanofibres. Fatemah *et al*. [100] developed *Aloe vera*-loaded polyvinyl alcohol nanofibres and found that 60% *Aloe vera* is released in 60 minutes, and almost 100% gets released in 120–240 minutes in a phosphate buffer solution. Ibrahim *et al*. [101] developed *Aloe vera*-based chitosan nanofibres, and also optimised the conditions for the formation of nanofibres. They found that acetic acid (90% pure), a federate of 0.3 mL/hour and a distance of 10 cm from the nozzle to the collector are the optimum conditions for the formation of *Aloe vera*/chitosan nanofibres.

**Fig. 14**. *Aloe vera* leaf – cross sectional view of gel inside the *Aloe vera* leaf [102]

### 1.6.3. Nanofibres doped with synthetic antimicrobial agents

Other than natural available antimicrobial agents, researchers have also developed synthetic antimicrobial agents for specific applications. Nowadays, the synthetic based antimicrobials are made in the size of nanometres, because nano-sized materials offer far superior properties as compared to their macro size. Also, another reason to discuss nano-sized antimicrobial agents is that these are to be electrospun

with suitable polymers in nano-sized fibres – this makes them suitable for nanofabrication. These nanoparticles embedded in the structure of nanofibres have different antimicrobial mechanisms, and some of them inhibit the growth by their charged nature, and some make reactive oxygen species as the active antimicrobial agent [103].

**Silver based nanofibres**

For decades, silver nanoparticles (Ag NPs) have been used as antimicrobial agents, and also Ag NPs loaded nanofibres have captured the attention of researchers as they can be used in medical applications, too [104]. A high antibacterial activity, biocompatibility, and minimal toxicity in eukaryotic cells are among the characteristics of AgNPs [105]. Erika *et al.* [106] developed *Propolis Ethanolic Extract* (PEE) and silver nanoparticles (AgNPs) based PLA electrospun fibres. The formed fibres were in the range of micrometres. They found that samples without AgNPs did not show significant antibacterial and/or antifungal properties, and this could be attributed to low quantities of PEE in the electrospun solution. The highest antimicrobial activity was observed for nonwoven materials from PLA microfibres containing AgNPs against gram-negative bacteria, *Pseudomonas aeruginosa*, and gram-positive bacteria, *Staphylococcus aureus*. Fig. 15 shows different antimicrobial mechanisms proposed for silver nanoparticles.

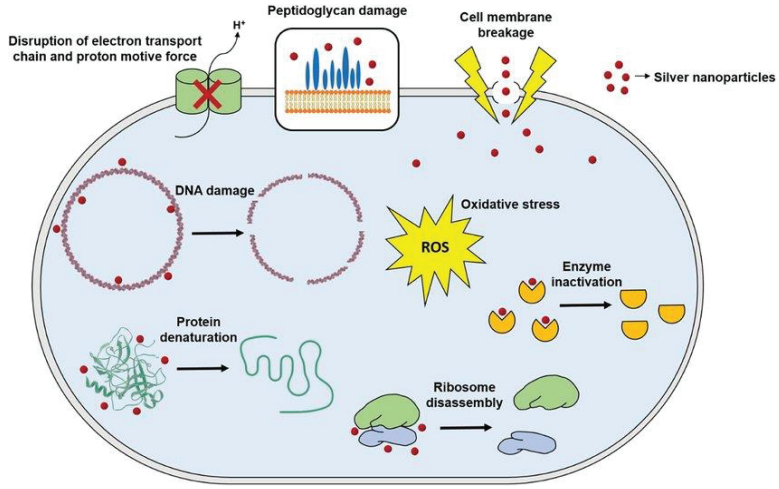


**Fig. 15**. Different antimicrobial mechanisms of silver nanoparticles [107]

Ag NPs of various sizes and concentrations were examined in one of the *in vitro* studies, and their antiviral properties against SARS-CoV-2 were studied At concentrations between 1 and 10 ppm, particles having a diameter of around 10 nm efficiently suppressed extracellular SARS-CoV-2; however, the cytotoxic impact was shown at doses of 20 ppm and higher [108]. In addition, hospital health workers were administered mouthwash and nasal rinse containing AgNPs in order to prevent SARS-CoV-2 infection. The group using AgNPs experienced a significantly lower rate of

SARS-CoV-2 infection (1.8%) compared to the group using the regular mouth and nose rinse (28.2%) [109].

Blosi *et al*. [110] observed that 97.7% filtration efficiency was achieved for nano-sized aerosol particles using electrospun nanowebs made from PVA/AgNPs. Additionally, electrospun nanofibres exhibited remarkable antimicrobial activity attributed to the presence of AgNPs. Selvam *et al*. [111] created PA/AgNPs-based electrospun nanofibres and discovered a 99% BFE, as well as effectiveness against both gram-positive and gram-negative bacteria. *HeiQ® Viroblock* [112] is a commercial silver-based antibacterial finish which claims to be 99.9% effective against SARS-CoV-2 virus in 30 minutes. Fig. 16 presents a face mask made with the *Viroblock* finish. A team of researchers created composite nanowebs using *Viroblock*/ZnO/PAN materials. They found that these nanowebs exhibited strong antibacterial properties, with 92.59% effectiveness against *S. aureus* bacteria and 88.64% effectiveness against *Pseudomonas aeruginosa* bacteria, when loaded with 5% *Viroblock*. Additionally, they observed a significant reduction in viral titter by 37% when using nanofibre sheets made from 5% *Viroblock*/PAN/ZnO [113].


**Fig. 16**. Viroblock – silver emits silver ions for bacterial killing [114]

**Copper based nanofibres**

Because of their strong antiviral and antibacterial capabilities, copper, its alloys, and some specific insoluble copper compounds are attractive materials for use in the battle against bacteria and viruses [115]. Copper(I) iodide is white in colour and has strong antiviral effects; hence it was used in masks, filters, and other surfaces [116]. A molecular docking research was also conducted to further understand the interaction of Cu(I) with the major protease of SARS-CoV-2 [117].

Moreover, the effectiveness of copper nanoparticles, Cu(I) and Cu(II) oxides as powerful antiviral agents has been demonstrated through their deposition on non-woven polypropylene textiles which are used as the outer and inner fabric layers in commercial respirators [118]. Researchers have developed a reusable and self-sterilizing surgical face mask by applying a combination of shellac (a natural hydrophobic polymer) and copper nanoparticles onto a non-woven fabric. In addition to the already available antimicrobial properties, this technique enhanced the hydrophobic nature of the mask, effectively blocking the transmission of droplets

carrying pathogens [119]. Furthermore, the KN94 mask with antiviral properties was developed through the application of the vacuum deposition technique to construct a 20 nm copper layer. Researchers observed that KN94 face masks with copper-deposited polypropylene exhibited a particle filtration efficiency of 95.1% for NaCl and 91.6% for paraffin oil. Upon contact with a copper-coated face mask, the virus was found to be eradicated by 75% [120]. Copper@ZIF-8 core-shell nanowires on a non-woven polypropylene surface were used to create a medical face mask. After 48 hours, 1 g of Cu@ZIF-8 NW per well inhibited viral proliferation by 55% [121]. Although copper is an essential trace mineral for our body's normal metabolism [122], it is important to consider the potential risks and adverse effects of copper nanoparticles, as well as the possibility of other serious issues, despite the assertion that wearing textiles coated with small amounts of copper-derived particles is assumed not to result in health problems [123].

**Zinc oxide based nanofibres**

Zinc oxide nanoparticles (ZnO NPs) had their effectiveness established in combating various pathogens, such as *Escherichia coli*, *Klebsiella pneumonia*, *Pseudomonas aeruginosa*, *Pseudomonas vulgaris*, and *Campylobacter jejuni*, due to their strong antibacterial properties. Moreover, these nanoparticles are considered safe for human contact [103]. Unfortunately, few investigations on the antiviral activities of ZnO NPs have been conducted. A recent study looked at the efficiency of ZnO nanoparticles against SARS-CoV-2. ZnO NPs were extensively characterised after being synthesised by utilising an environmentally friendly and scalable electrochemical process. Their antiviral effectiveness against SARS-CoV-2 was examined *in vitro*, with a reduction in the viral load ranging from 70% to 90% depending on the material's composition. ZnO NPs would be ideal coatings for routinely touched surfaces [124]. Fig. 17 shows the molecular structure of ZnO NP.

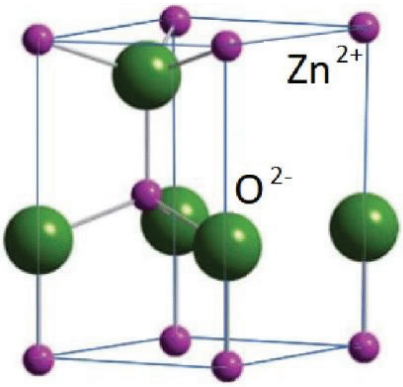


**Fig. 17.** Molecular structure of ZnO NP [125]

Nanofibres made of poly(methyl methacrylate) (PMMA) through electrospinning have been developed to tackle multiple functions. These nanowebs

have demonstrated their effectiveness in fighting against both gram-positive and gram-negative bacteria; they also exhibited antiviral properties against SARS-CoV-2. Additionally, they possess self-cleaning features to remove contaminants [126]. Fig. 18 presents the antimicrobial mechanism of ZnO nanoparticles.

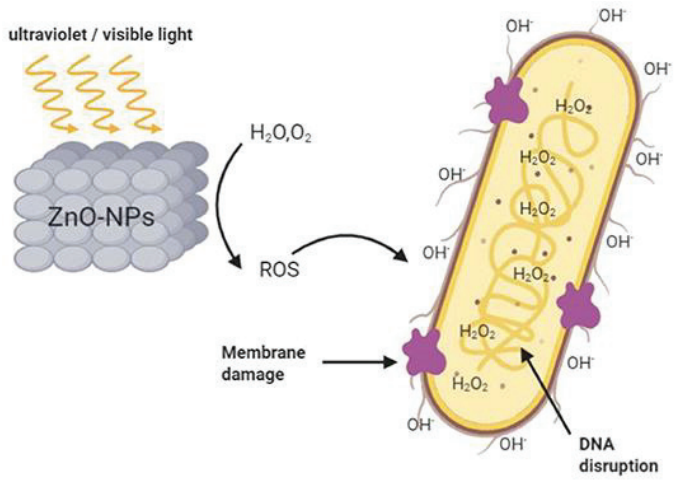


**Fig. 18**. Antimicrobial mechanism of ZnO NPs [127]

ZnO-loaded PVDF nanofibres demonstrate effective antiviral properties, and the arrangement of 5% ZnO/PVDF nanofibres in a nanoweb configuration prevents virus growth and entry. These nanowebs could potentially be used in half-face respirators with integrated filters. Due to the difficulty of separating the extremely thin layer of nanofibres from the electrospinning machine, the researchers employed a non-woven film on the collector plate to allow the nanofibres to directly accumulate on its surface. They created polyacrylonitrile (PAN)/ZnO nanofibres, which were then scaled up to non-woven spunbonded polypropylene (SPP) with weight bases of 0.4 g/m$^2$ and 0.8 g/m$^2$. The researchers suggested that a symmetric setup consisting of SPP/PAN/PAN/SPP was the optimal choice as it reduced SPP usage while maintaining the FFP2-type filtering efficiency and decreasing the breathing resistance, particularly under high airflow conditions, such as FFP2 exhalation. Additionally, the incorporation of ZnO nanoparticles in their sheets resulted in remarkable antibacterial properties [128].

**Titanium oxide-based nanofibres**

Titanium dioxide possesses the necessary qualities, particularly minimal human toxicity and good UV-activated inhibition of viruses and bacteria [129]. The photocatalytic generation of reactive oxygen species (ROS), which are very unstable and swiftly engage with biomolecules in electron-exchange processes, is involved in the antibacterial and antiviral mechanism. This process alters the structure of

biopolymers and lipids, rendering ROS harmful to a wide range of species [130]. Fig. 19 shows the antimicrobial mechanism of $TiO_2$ nanoparticles.

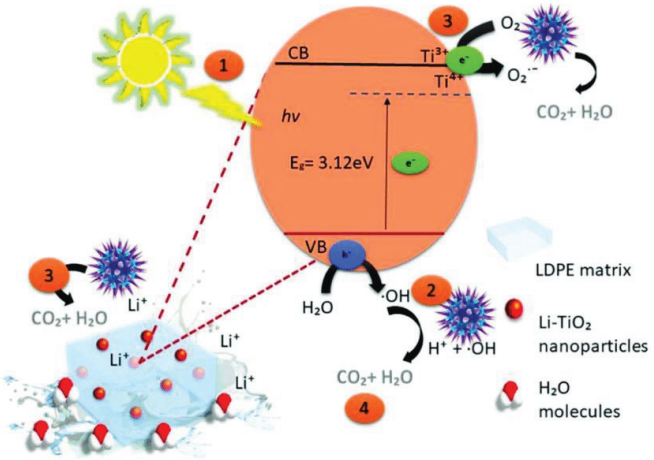


**Fig. 19**. Antimicrobial mechanism of heterostructure nanocomposites of Li-$TiO_2$/LDPE against *S. aureus* [131]

$TiO_2$/PVP nanofibres have also been demonstrated to have a high filtering efficiency. The antibacterial properties of $TiO_2$ made it a good material for the filtering medium, especially in face masks and respirators. PAN/$TiO_2$/Ag nanofibres with a particulate matter filtering efficiency of 96.9% have also been created. Because of their outstanding antibacterial and UV-resistant qualities, these nanofibres are appropriate for the filtering media in facemasks and respirators [132].

**Iron oxide-based nanofibres**

Iron oxide nanoparticles (IONPs) have demonstrated a significant potential in the field of medicine due to their exceptional biocompatibility and magnetic properties. These nanoparticles have been approved by the FDA and various European Union agencies for their application as nanoparticle-based pharmaceuticals. They have garnered considerable interest in medical practices, such as cancer treatment, magnetic drug targeting, and serving as contrast agents for MRI scans [133]. IONPs exhibit antiviral and antimicrobial properties against diverse viruses and bacteria, employing various mechanisms to combat viral infections. These mechanisms include the generation of reactive oxygen species (ROS), lipid peroxidation, and binding to viral surface proteins, effectively hindering viral attachment to the host cells. To enhance their antiviral activity, stability, and safety, it is possible to coat IONPs with the appropriate polymers, such as polyvinylpyrrolidone or polyethylene glycol [134].

### Carbon based nanofibres

Carbon-based nanomaterials, such as graphene, have demonstrated their value in a variety of applications. The infective ability of SARS-CoV-2 can be inhibited by graphene and graphene oxide. When they are mixed into polyurethane or cotton, the resultant fabric retains these qualities, thus effectively limiting the viral and bacterial infectivity [135, 136].

Additionally, carbon nanotubes and carbon dots have demonstrated notable efficacy. By incorporating carbon nanotubes into a polyester substrate, a filter with a comparable efficiency to HEPA filters was created, which was capable of being sanitised through resistive heating. Meanwhile, carbon dots which are present in poly(vinylidene fluoride) membranes offer self-sterilisation through solar-induced absorption of sunlight, subsequent dissipation of heat, and various other technological benefits [137].

One of the emerging materials to have antimicrobial properties is carbon nanodots or carbon quantum dots [138]. These carbon nanodots (CNDs) demonstrate photocatalytic properties comparable to those of semiconductor nanoparticles. The primary advantage of using CNDs instead of semiconductor nanomaterials lies in their ability to exhibit photocatalytic activities under visible light. CNDs possess broad and strong absorption capabilities in both the visible and near-infrared ranges. Recent research suggests that the antibacterial effects of CNDs are attributed to the generation of reactive oxygen species (ROS). When CNDs are exposed to light, they activate the oxygen which is present in the surrounding air or water, thus leading to the formation of hydroxyl-free radicals (OH) or individual oxygen atoms. These ROS can eradicate the biomolecules/cells of bacteria which encounter the CNDs. Meziani *et al.* [138] first reported that CNDs under visible/natural light could effectively inhibit *E. coli* cells both in suspensions and on the agar surface.

## 1.7. Environmental Aspects of PPEs Disposal

Because of the abrupt surge in the use of disposable PPEs, particularly medical face masks, these PPEs created an estimated 7200 tons of garbage every day globally, with medical face masks accounting for a larger amount of this waste [139]. Nonwoven polypropylene sheets or synthetic fibres/polymers are commonly used to manufacture medical face masks and gowns. These polymers are typically not biodegradable, and therefore they present a considerable threat to the wellbeing of land and marine organisms. As stated by the UN Environment Program, approximately 75% of discarded face masks end up either in landfills or floating in the ocean [140]. Microplastics were examined in artificial weathering studies by Saliu *et al.* [141] who found that subjecting a lone surgical mask to 180 hours of UV-light exposure and intense stirring in synthetic seawater can lead to the release of as many as 173,000 microplastic fibres per day. This leakage of microplastics poses a threat to marine plant life, animals, and human health. In response to this environmental concern,

numerous scholars have shifted their attention to creating biodegradable and eco-friendly medical face masks.

The face mask made from wheat gluten biopolymer was introduced by Das *et al.* [142]. It involves the spinning of wheat gluten into nanofibres, followed by carbonisation at temperatures exceeding 700 °C. This process creates a network structure that serves as both the filter medium and reinforcement for masks based on gluten. Another study by Tiliket *et al.* [143] also presented a similar approach utilising wheat gluten biopolymer to produce face masks.

Patil *et al.* [144] developed a 3-ply face mask using biodegradable materials, specifically cotton-PLA-cotton layers. To enhance its properties, they coated the inner nanofibre PLA layer with phytochemicals and electrospun it onto the cotton layers. Their findings showed an increase in the differential pressure of 35.78 $Pa/cm^2$, while achieving a bacterial filtration effectiveness of over 97.9%. In a separate study, Choi *et al.* [145] improved the performance of the mask filter by incorporating two biodegradable microfibre and nanofibre mats into the Janus membrane filter. They further enhanced it by coating the filter with cationically charged chitosan nano whiskers, which resulted in a hydrophobic, highly breathable, and high-performance filter. Their research revealed a reduction in the differential pressure, thereby making it suitable for comfortable breathing.

Wang *et al.* [146] conducted research on the development of a fibrous membrane made of PLA/$TiO_2$. Their findings revealed that the membrane exhibited an impressive antibacterial activity of 99.5% despite containing as little as 1.75% $TiO_2$ by weight. Additionally, the membrane demonstrated excellent particle filtration capability with a rate of 99.996% and maintained a low pressure drop of 128.7 Pa.

The researchers of [147] utilised a PLA nanofibre sheet to print PLA, which resulting in a nano porosity structure that appears translucent. Their argument was that this translucent appearance can lessen the intimidating effect of masks, potentially serving as a method to reduce the social distress caused by the COVID-19 pandemic. Kadam *et al.* [148] developed biodegradable nanofibre mats containing gelatine/β-cyclodextrin. They observed that these nanofibre membranes effectively trapped aerosols (sized between 0.3–5 μm) with a filtering efficiency exceeding 95%. Al Azeem *et al.* [149] introduced a medicinal face mask made from a biopolymer called polyhydroxyalkanoates (PHAs). This biodegradable polymer possesses a high porosity, thus making it highly suitable for medical face masks.

The disposal and waste of personal protective equipment (PPE) can involve various environmental impacts. Some of the potential effects are listed below:

1. Increased landfill waste: PPE, such as disposable masks, gloves, and gowns, contributes to the overall waste generated in landfills. Since PPE items are typically made of synthetic materials that are not easily biodegradable, they can persist in the environment for a long time.

2. Contamination of water bodies: Improper disposal of PPE can lead to littering, where discarded items end up in water bodies like rivers, lakes, and oceans. This can cause pollution and harm aquatic life. Additionally, when PPE breaks down into

smaller particles, known as microplastics, they can further contaminate water sources and affect marine ecosystems.

3. Air pollution: Incineration is sometimes used as a disposal method for PPE. Burning PPE can release harmful pollutants and greenhouse gases into the atmosphere, thereby contributing to air pollution and climate change.

4. Wildlife entanglement and ingestion: Improperly discarded PPE, particularly masks and gloves, can pose risks to wildlife. Animals may become entangled in discarded PPE, which leads to injuries or death. Marine animals, such as turtles and seabirds, may mistake PPE for food and ingest it, thus causing internal injuries or blockages.

5. Resource consumption: PPE production requires the extraction of natural resources, energy, and water. Disposal of PPE after single-use leads to the need for continuous production, subsequently perpetuating the consumption of these resources.

To mitigate the environmental impact of the PPE waste, several steps can be taken:

1. Proper disposal: Individuals should dispose of PPE in designated bins or containers, such as medical waste bins, wherever available. Following the guidelines provided by local authorities for waste disposal is crucial.

2. Recycling and reusing: Wherever feasible, efforts should be made to recycle certain types of PPE, such as plastic face shields. Additionally, reusable PPE options can be considered to reduce waste generation.

3. Education and awareness: Promoting awareness about the environmental impact of PPE waste through educational campaigns can encourage responsible disposal practices.

4. Innovation and sustainable alternatives: Research and development can focus on creating PPE materials that are more environmentally friendly, biodegradable, or easily recyclable. This can help reduce the long-term impact of PPE waste. It is essential for individuals, organisations, and governments to work together to minimise the environmental impact of the PPE disposal and waste through responsible disposal practices and sustainable alternatives.

### 1.8. Summary of Literature Review

The increased usage of disposable personal protective equipment (PPE), especially medical face masks, has resulted in a significant amount of waste being produced, and the use of non-biodegradable materials poses a threat to the environment. The improper disposal of PPE contributes to such issues as landfill waste, water and air pollution, wildlife entanglement, and resource consumption. To tackle these concerns, it is crucial to develop biodegradable and eco-friendly alternatives to the conventional polymers.

To address the disposal and waste problems with non-biodegradable polymers used in PPEs production, we suggest using sustainable and biodegradable polymers instead. *Polyvinyl Alcohol* (PVA) and *Polylactic Acid* (PLA) are two commonly used biodegradable polymers with various sustainable and biodegradable aspects:

Polyvinyl Alcohol (PVA):

1. Biodegradability: PVA is considered biodegradable under specific conditions. Microorganisms, such as bacteria and fungi, can break down PVA in the presence of oxygen and moisture. However, its biodegradation rate can be slow, and it may not readily degrade in certain environments like landfills, which lack these conditions.

2. Renewable Source: PVA can be derived from renewable sources like corn starch or sugarcane, thus making it more sustainable compared to petroleum-based plastics.

3. Water-Solubility: PVA is highly water-soluble, which can be advantageous for applications where the material needs to be dissolved, leaving no waste behind. For instance, it is used in laundry detergent pods.

4. Limited Toxic Byproducts: Unlike some other plastics, the biodegradation of PVA typically results in less harmful byproducts, although it may produce small amounts of acetic acid.

Polylactic Acid (PLA):

1. Biodegradability: PLA is biodegradable and compostable under industrial composting conditions where the presence of specific microorganisms and controlled environmental factors (e.g., temperature, humidity) facilitate its decomposition. In natural environments, PLA can take a longer time to break down compared to PVA.

2. Renewable Source: PLA is made from renewable resources like corn starch or sugarcane, which reduces its reliance on fossil fuels.

3. Reduced Carbon Footprint: PLA production typically results in lower greenhouse gas emissions compared to the traditional petroleum-based plastics.

4. Recyclability: PLA can also be mechanically recycled, although this process may lead to a reduction in the material quality compared to the original PLA.

It is of importance to note that the biodegradability and sustainability of both PVA and PLA depend on various factors, including the specific formulation of the material, environmental conditions, and disposal methods. Proper disposal in industrial composting facilities is crucial to maximise their biodegradability and reduce their environmental impact. Additionally, the sustainability of these materials is also influenced by their production processes, transportation, and end-of-life management.

This dissertation explores the sustainable aspects of PVA and PLA in the context of functionalised nanowebs. Specifically, it aims to investigate their potential for application in medical face masks and devices while considering their environmental impact.

The study involved the development of functionalised nanowebs of PVA by incorporating *Aloe vera* (AV) and zinc oxide (ZnO) nanoparticles. Additionally, carbon nanodots-loaded PLA nanofibres have been developed. These engineered nanowebs were designed to enhance the barrier performance of PVA and PLA, thus making them suitable for use in medical face masks. By harnessing the sustainable properties of PVA and PLA, such as their biodegradability and renewable sourcing

options, the aim is to promote environmentally friendly alternatives to the traditional mask materials.

## 2. MATERIALS AND METHODS

### 2.1. Materials

Zinc oxide (ZnO) nanoparticles in powder form with an acclaimed size less than 200 nm and polyvinyl alcohol (PVA) (MW: 85000–124000) were purchased from the *Sigma-Aldrich Corporation* (St Louis, MO, USA). The herbal leaves of *Aloe vera* were taken from domestic garden from Pakistan.

Polylactic acid 4060D, which is claimed to be a bio polymer, was supplied by *Nature-Works LLC*. PLA was in the form of pellets. It has a melting temperature of 210 °C. Dimethyl formamide was purchased from *Merck*. Glucosamine hydrochloride (98% purity) was purchased from *Thermo Fisher*, Shanghai, China, and 1,3-diaminobenzene (99% purity) was purchased from *Carl Roth*.

### 2.2. Solution Preparation and Electrospinning

#### 2.2.1. Preparation of solution for AV/PVA/ZnO electrospinning

For the formation of AV/PVA/ZnO electrospun fibres, first, the electrospinning solution was prepared. A constant 10% w/v of PVA was taken for all electrospinning solutions, with a varying amount of AV and ZnO in it. The fibre sheets were prepared by using the electrospinning technique. A total of 8 samples were prepared, 4 with varying concentrations of ZnO, and 4 with varying concentrations of AV. For this experiment, a 10% w/v of PVA was dissolved in deionised water and stirred at 450 rpm. The temperature was maintained at 60 °C, and the stirring time was 60 minutes for each sample. After we obtained a homogenous solution of PVA, the required quantity of AV and ZnO NPs was poured in each sample. The detailed composition of all samples of AV/PVA/ZnO is presented in Table 1.

**Table 1**. Design of experiment for the formation of AV/PVA/ZnO electrospun fibres

| Sample Name | PVA (%) | AV (%) | ZnO NPs (%) |
|---|---|---|---|
| AV1/PVA/ZnO0.5 | 10% | 1% | 0.5% |
| AV2/PVA/ZnO0.5 | 10% | 2% | 0.5% |
| AV3/PVA/ZnO0.5 | 10% | 3% | 0.5% |
| AV4/PVA/ZnO0.5 | 10% | 4% | 0.5% |
| AV0.5/PVA/ZnO1 | 10% | 0.5% | 1% |
| AV0.5/PVA/ZnO2 | 10% | 0.5% | 2% |
| AV0.5/PVA/ZnO3 | 10% | 0.5% | 3% |
| AV0.5/PVA/ZnO4 | 10% | 0.5% | 4% |
| AV-0/PVA/ZnO-0 | 10% | 0 | 0 |

Then again, the solutions containing AV/PVA/ZnO were stirred for 60 minutes (without heating), and then the solutions were ready for electrospinning.

Fig. ***20*** depicts the solution formation process for the electrospinning machine.

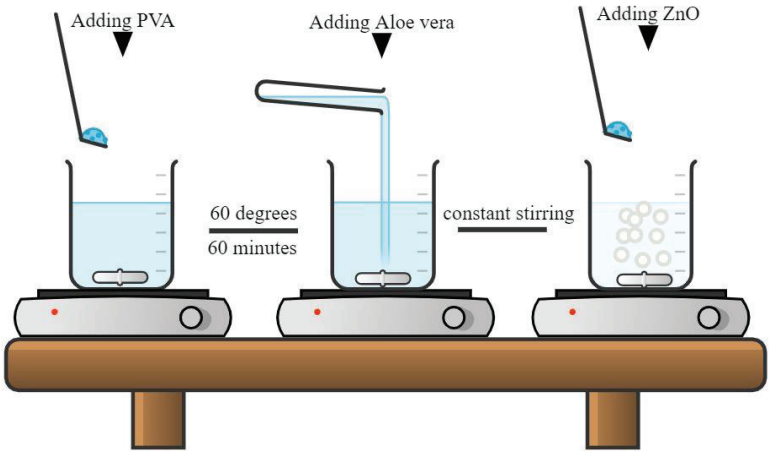


**Fig. 20**. *Aloe vera*/PVA/ZnO solution formation process for electrospinning

### 2.2.2. Electrospinning of AV/PVA/ZnO solution

Needle-based electrospinning was employed to create nanofibres of AV/PVA/ZnO. The desired solution of AV/PVA/ZnO was loaded into a plastic syringe with a metallic needle, which was then connected to a syringe pump for the proper feeding of the electrospinning solution. The metallic needle was connected to the positive electrode of the voltage device, and 20 cm distance was maintained between the needle tip and the collector. A potential difference of 17 kV was applied, which was sufficient for generating fibres from the desired solution. The electrospinning chamber was maintained at a temperature of 25°C and a relative humidity of 65%.

As we had the fibres on the collector, the blended ZnO and AV was embedded in and onto the surface of the fibres. Fig. 21 illustrates the incorporation of AV and ZnO on and into the fibres. The electrospinning process was followed by the characterisation of the formed fibres.

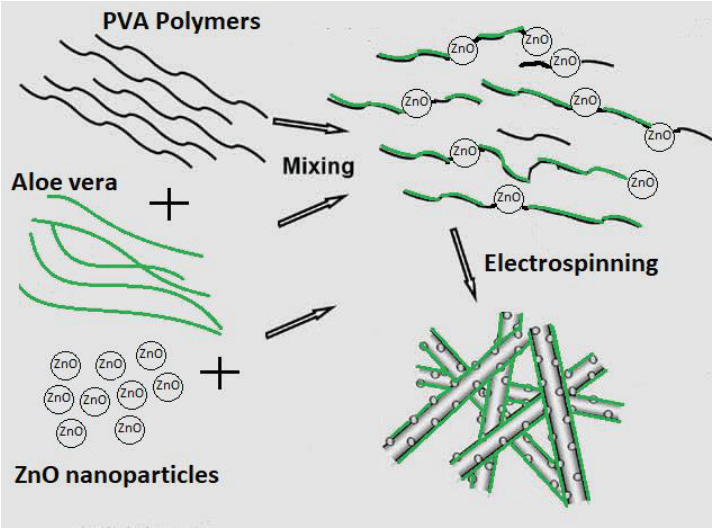


**Fig. 21**. Incorporation of ZnO and *Aloe vera* in electrospun fibres

### 2.2.3. PLA/CNDs solution preparation for electrospinning

To obtain CNDs incorporated PLA electrospun fibres, we first prepared a solution for electrospinning.

First, PLA in pellets form was dissolved in dimethyl formamide with constant stirring for 6 hours to get the proper dissolution of PLA. A schematic diagram for the preparation of the solution for electrospinning is shown in Fig. 22. Following Table 2, 12%, 15%, 17% and 19% PLA was dissolved separately in DMF while stirring at 300 rpm.

**Table 2**. Design of the experiment for the formation of PLA/CNDs electrospun fibres

| Sample # | Concentration of PLA (%, w/v) | Concentration of CNDs (%) |
|---|---|---|
| PLA-12 | 12 | – |
| PLA-15 | 15 | – |
| PLA-17 | 17 | – |
| PLA-17/C1 | 17 | 1 |
| PLA-17/C2 | 17 | 2 |
| PLA-17/C3 | 17 | 3 |
| PLA-17/C4 | 17 | 4 |
| PLA-19 | 19 | – |
| PLA-19/C1 | 19 | 1 |
| PLA-19/C2 | 19 | 2 |
| PLA-19/C3 | 19 | 3 |

| | | |
|---|---|---|
| PLA-19/C4 | 19 | 4 |

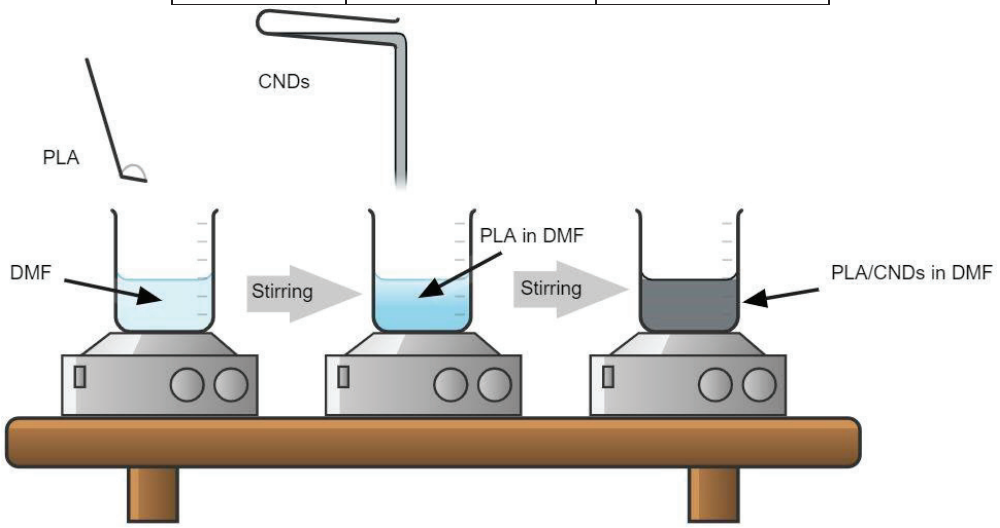


**Fig. 22**. Preparation of solution for electrospinning

### 2.2.4. Electrospinning of PLA/CNDs solutions

The solution preparation was followed by the electrospinning process. After evaluating the morphology of the formed fibres, we selected which one would be more beneficial for further processing. Then we selected the best performance weight percentage of PLA and CNDs, electrospun it, and checked for barrier performance.

The needle electrospinning technique was utilised for the formation of PLA/CNDs fibres. The desired solution (as per Table 2) was filled in a plastic syringe with a metallic needle tip, we placed the syringe on a syringe pump for the proper federate of the solution. The electrospinning machine setup was custom made, with a voltage device, a syringe pump, a collector drum, and a temperature/humidity control device. A schematic illustration of the setup is shown in Fig. 23. The positive terminal from the voltage was connected to the metallic tip, and the collector drum was grounded. The area of the rotating collector drum was 255 $cm^2$, and 17 cm distance was maintained between the tip of the needle and the collector drum. The federate was maintained at 0.4 mL/hour, and a potential difference of 23 kV was applied for the formation of electrospun fibres.

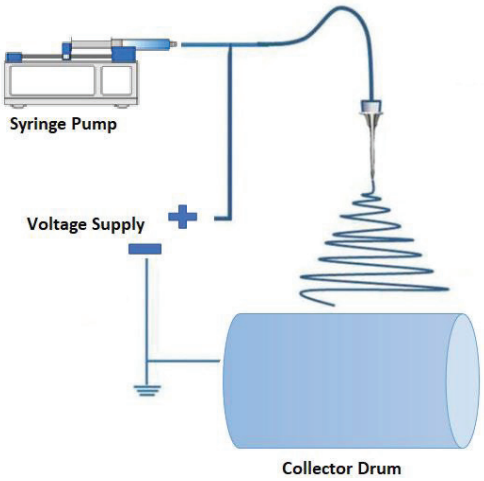


**Fig. 23**. PLA/CNDs electrospinning process

## 2.3. Synthesis of CNDs

For CNDs, we first prepared precursor solutions.

- The 1st solution was prepared by dissolving glucosamine hydrochloride (1.00 g, 4.63 mmol) in 20 mL of deionised water in a 250 mL flask. With proper agitation, we achieved a homogenous solution.
- The 2nd solution was prepared in a separate flask by dissolving 1,3-diaminobenzene (0.55 g, 5.10 mmol) in 10 mL methanol. The flask was placed in a sonicator to achieve the proper dissolution and homogenous solution.

Solution 2 was combined with solution 1 and thoroughly stirred to achieve a uniform solution. The mixture was then placed in a microwave in a well-ventilated area and exposed to irradiation for 3 minutes at 800 W and 90% power. After this irradiation, a thick brown oil-like substance was obtained. It was subsequently dissolved in 10 mL of deionised water and centrifuged at 4000 rpm for 1 hour. The resulting bulk solution was then evaporated under reduced pressure to yield a brown powder. Since the intention was to dissolve PLA in DMF, the obtained CNDs were dispersed in the same DMF solution. Different weight percentages were employed according to the design of the experiments (DOE), as per Table 2.

## 2.4. Preparation of ZnO NPs

Zinc acetate dihydrate Zn $(CH_3COO)_2 \cdot 2H_2O$ (as a zinc source) and sodium hydroxide (NaOH) were used at 7:1 ratio in 200 mL methanol, as precursors for the preparation of ZnO NPs. The solution was prepared in a round bottom flask and then placed in a water bath with stirring at 60 °C for 75 minutes. Then, the resulting solution was centrifuged at 6400 rpm for 30 minutes at 4 °C to obtain the

nanoparticles/nanocrystals of ZnO. Settled-down nanoparticles/nanocrystals were collected and placed in an oven so that no methanol would be left in the particles.
The formation mechanism of ZnO nanostructures is a complex process, and it is mostly considered to include two main steps: the generation of ZnO nuclei, and the subsequent ZnO crystal growth, where the Zn $(OH)_4^{2-}$ complexes serve as the basic growth units for the preparation of ZnO nanostructures. Zinc acetate may convert into $Zn(OH)_2$ colloids firstly under alkali solution, as shown in Reaction 1. During the process, part of $Zn(OH)_2$ colloids dissolves into $Zn^{2+}$ and OH− according to Reaction 2. When the concentration of $Zn^{2+}$ and OH− reaches the supersaturation degree of ZnO, ZnO nuclei will form according to Reaction 4.

### 2.5. Particle Size Analysis of ZnO and CNDs

To check the particle size distribution of ZnO NPs and CNDS in water/DMF, Dynamic *Light Scattering* (DLS) was performed by using a *Zetasizer 1000* apparatus (*Malvern Panalytical Ltd*., Malvern, UK). Fig. 24 presents a schematic diagram of the working principle of the *Zetasizer*.

The principle behind dynamic light scattering is that tiny particles and molecules, which are constantly moving in a random manner due to thermal energy (referred to as Brownian motion), disperse at a speed that is related to their size. Smaller particles diffuse more rapidly compared to larger particles. To determine the diffusion speed, laser-illuminated particles create a speckle pattern, which is then observed. The fluctuation of scattering intensity at a specific angle over time is captured by a sensitive *Avalanche Photodiode Detector* (APD). The changes in intensity are analysed by using a digital autocorrelation, which generates a correlation function. This function can be further analysed to determine the particle size and its distribution.

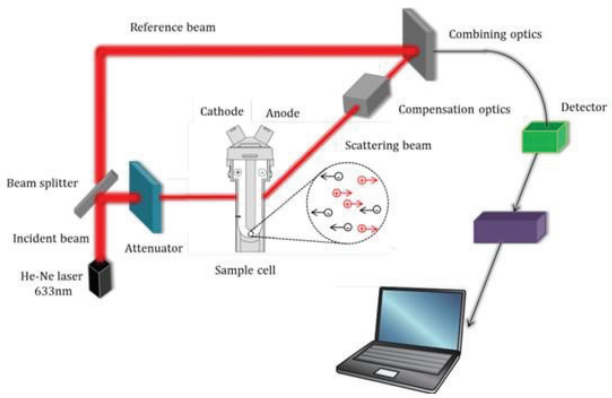


**Fig. 24**. Working principle of the *Zetasizer* instrument [150]

## 2.6. Rheological Properties of Electrospinning Solutions

The rheological properties, such as the viscosity and conductivity of the formed solutions for electrospinning were analysed. The effect of different compositions of solution was checked on the conductivity and viscosity of the solutions.

- The viscosity of the formed solutions was measured with a *Viscometer B-One Plus (Lamy Rheology Instruments)*. First, the instrument was calibrated by making the zero setting. This was done by removing the spindle, and the zero setting was activated; then, the instrument calibrates itself in 60s. After calibration, the R-6 spindle was placed in a stirrer, and the viscosity of all the solutions was measured.
- The electrical conductivity of all electrospinning solutions was checked with a conductivity meter (TDS & EC meter, *PATEA*). The probe was simply placed in the solution, and pressing the hold button simply measures the conductivity of the solution.

### Characterisation of AV/PVA/ZnO electrospun fibres

After electrospinning all the compositions of AV/PVA/ZnO nanofibres from Table 1, the formed electrospun fibres were subjected to the characterisation techniques in order to check the chemical composition and morphology of the formed nanofibres.

- To check the surface morphology and diameter of the formed electrospun fibres, these were subjected to Scanning Electron Microscopy (SEM) *Hitachi* model *S-3400N*. All the morphological studies were carried out at the *Lithuanian Energy Institute*.
- The average diameter from the SEM images was calculated by the *ImageJ* software. 100 measurements were taken to get an average of the fibre diameter.
- As PVA was dissolved with *Aloe vera* and ZnO nanoparticles, just to check any new functional group which may have formed, we subjected them to Fourier transform infrared spectroscopy (*Perkin Elmer* – UK). The FTIR analysis was conducted at NTU, Pakistan.

### Characterisation of PLA/CNDs electrospun fibres

After electrospinning all the compositions of PLA/CNDs nanofibres from Table 1, the formed electrospun fibres were subjected to characterisation techniques to check the chemical composition and morphology of the formed electrospun fibres.

- To check the surface morphology and diameter of the formed electrospun fibres, these were subjected to Scanning Electron Microscopy (SEM) (*Hitachi Model S-3400N, Hitachi High Technologies Europe GmbH*, Tokyo, Japan). All the morphological studies were carried out at DTNW, Germany.

- The average diameter, as determined in the SEM images, was calculated by the *ImageJ* software. 100 measurements were taken to get an average of the fibre diameter.
- As PLA was dissolved with CNDs, just to check the presence of any new functional group which may have formed, we subjected them to Fourier transform infrared spectroscopy (*Shimadzu IRPrestige21*). The FTIR analysis was conducted at DTNW, Germany.
- As we dissolved PLA/CNDs in DMF to check the residual DMF in the electrospun fibres, we subjected them to the thermogravimetric analysis (TGA) (*TA Instrument TGA55*) technique. An aluminium oxide crucible was used to perform TGA with a heating rate of 10 °C/min.

## 2.7. Antibacterial Testing

**ISO 20645:2004**

To assess the effectiveness against microorganisms, the prepared samples underwent antibacterial tests without any additional treatment. The antibacterial tests followed the Plate Count Method ISO 20645:2004 [151]. Qualitative analysis was conducted on AV/PVA/ZnO electrospun fibre against both gram-positive bacteria (*S. aureus*) and gram-negative bacteria (*E. coli*).

**Preparation of the Bacteria Culture**

The sub-culture is initiated by extracting a portion from the agar medium, a nutrient-rich environment where microorganisms can grow. This procedure aims to establish a new agar plate culture for the subsequent analysis. It is essential to note that the initial culture utilised for sub-culturing should not exceed the age of four weeks, as older cultures may display diminished viability and involve contamination risks.

To assess the purity of the culture obtained from the agar sub-culture, streak plates are employed. This technique involves streaking a loop or an inoculating tool across the surface of an agar plate in a pattern which thins out the microbial population. By executing this procedure, we created isolated colonies that can be examined individually. Furthermore, the identity of the microorganisms within the culture is ascertained through microscopic examination, which permits a closer inspection of cellular morphology and characteristics.

To mitigate the potential for contamination during the subsequent transfers, a practice known as ‘liquid-to-liquid’ transfers was carried out for a duration of up to three days. This method involves transferring the culture from one liquid medium to another without exposure to the external environment, thus reducing the risk of foreign microorganisms infiltrating the culture. Each transfer is followed by an incubation period of 24 hours at a constant temperature of 37 °C to encourage microbial growth and the observation of the colony formation.

After each incubation period, the purity of the colonies is re-evaluated by spreading a sample of the culture onto an agar plate. This step allows for the isolation of individual colonies, which can then be scrutinised to ensure their purity and homogeneity. By repeatedly verifying the purity of the culture, researchers can maintain the integrity of the microbial population under investigation and ensure the accuracy of the subsequent scientific experiments and analyses.

**Preparation of the test samples**

The test specimen was cut in circular with a diameter of 25± 5 mm radius. 3 specimens of each sample were checked and were carried out on both sides of the specimens.

**Test Procedure**

For the lower layer, we poured 10 mL into each of the sterilised Petri dishes and let the agar congeal.

For the upper layer, we first prepared the required agar quantity, and then cooled it to 45 ± 2ºC in the water bath. Then, 150 mL of agar was inoculated with bacterial working culture 1–5x$10^8$ cfu/ml. We shook the vessel well for the homogenous dispersion of bacteria. Then, we poured 5 mL into each Petri dish and let the agar congeal. We used the inoculated agar plates for 1 hour.

The prepared samples, taken from the electrospun fibre sheets, were then placed on the agar with the help of sterilised tweezers or with a bent glass rod evenly on the nutrient medium. We made sure that the specimens were in contact with the agar solution.

After placing the specimens, we incubated the plates for 18–24 hours at 37 ºC and then checked the bacterial growth.

**Assessment of tests**

The assessment of the tests is based on the absence or the presence of bacterial growth in the contact zone between agar and the specimen and on the eventual appearance of the zone around the specimens.

The width of the inhibition zone is calculated from the centre of the specimen to the edge of the zone.

**ISO 20743:2013**

To assess the quantitative analysis of the antibacterial activity, adherence to the ISO 20743:2013 [152] Standard was observed. All AV/PVA/ZnO electrospun fibre samples and the selected PLA/CNDs electrospun fibres were subjected to testing against both gram-positive (*S. aureus*) and gram-negative (*E. coli*) bacteria. The procedure for the antibacterial test was as follows.

**Preparation of the bacteria and specimens**

After the incubation of bacteria, we prepared the test inoculum with the bacterial concentration in the range from $1\times10^5$ cfu/ml to $3\times10^5$ cfu/ml.

**Preparation of the test specimens**

We obtained 0.4 grams of test specimens (3 specimens from each sample) from each sample and cut it to a suitable size to be placed in the inoculum.

**Inoculation of the test specimens**

0.2 mL of prepared inoculum was poured at several points on each test specimen, and then 20 ml of neutralising solution was added into each vial. After capping the vials, they were shaken well by hand.

**Incubation of vials**

Then we incubated the vials in the incubator (with the light source turned on) for 18–24 hours at 37 ºC. After the incubation, the vials were shaken well again.

**Quantitative measurement by the plate count method**

After the incubation, 1 mL of the inoculum, which is shake-out bacteria suspension from the specimens, was taken out by using a pipette, and it was poured in a test tube containing 9 mL of peptone-salt solution.

For the lower layer, we poured 10 mL into each of the sterilised Petri dishes and let the agar congeal.

For the upper layer, we first prepared the required agar quantity, and then cooled it to 45 ± ºC in the water bath. Then, 150 mL of agar was inoculated with the bacterial culture obtained from each specimen. We shook the vessel well for the homogenous dispersion of the bacteria. Then, we poured 5 mL into each Petri dish and let the agar congeal. After this, the plates were incubated for 24–48 hours, and then CFUs (colony forming units) were calculated on the Petri dishes.

**2.8. Particulate Filtration Efficiency (PFE) Test**

The filtration efficiency test (also known as PFE) evaluates the effectiveness of filtration by comparing the number of particles in the incoming stream (upstream) with that in the filtered stream (downstream). To produce NaCl aerosols with particle sizes ranging from 0.1 to 0.5 microns, PFE employs clean and dry air passed through HEPA filters. The PFE tester used for this purpose was manufactured by *Lorenz Meßgerätebau GmbH & Co. KG*, Germany. The test procedure followed the guidelines outlined in ASTM F2299 [153]. Each sample was securely clamped in the

fixtures and then mounted onto the machine before initiating the test. The aerosol generated was passed through the sample material, and a photometer detected the upstream and downstream particle counts of the aerosol, thus providing a filtration efficiency report expressed as a percentage for various aerosol sizes.

**Performance requirements with respect to the International Standard**

Particle filtration efficiency requirements for medical face masks and respirators are defined by international standards to ensure their effectiveness in filtering out airborne particles, including viruses and bacteria. Two commonly referenced standards for these requirements are *ASTM F2100* and *ASTM F2299* for medical face masks, and *NIOSH N95* and European *EN 149* for respirators. An overview of the particle filtration efficiency requirements specified by these standards is presented below:

1. **ASTM F2100 (Medical Face Masks)**

*ASTM F2100* [154] is a standard established by the *American Society for Testing and Materials* (ASTM) which outlines the performance requirements for medical face masks. It primarily focuses on surgical masks.
*Particle Filtration Efficiency (PFE):* PFE is often reported alongside BFE. A PFE of ≥95% is commonly expected for high-quality medical face masks.

2. **ASTM F2299 (Submicron Particle Filtration)**

ASTM F2299 is a standard measuring the filtration efficiency of submicron particles (0.1 micron) to assess the mask's ability to filter out smaller particles, such as those carrying viruses. ASTM F2299 requires a filtration efficiency of ≥95% for submicron particles.

3. **NIOSH N95 (Respirators)**

NIOSH (*National Institute for Occupational Safety and Health*) sets the standards for respirators, including N95 respirators, which are widely used in healthcare settings and for the protection against airborne particles.
*N95 Filtration Efficiency*: NIOSH requires an N95 respirator to filter out at least 95% of airborne particles with a diameter of 0.3 microns or larger when properly fitted to the wearer's face.

### 4. European EN 149 (Respiratory Protective Devices)

The EN 149 Standard is used in Europe to assess the filtration efficiency of respiratory protective devices, including FFP1, FFP2, and FFP3 respirators.

*FFP1, FFP2, and FFP3 Filtration Efficiency*: FFP1 respirators must filter at least 80% of particles. FFP2 respirators must filter at least 94%, and FFP3 respirators must filter at least 99% of particles.

The details regarding the particle filtration efficiency of respirators and medical face masks defined by different international standards are defined in Table 3 and Table 4.

**Table 3**. Performance requirements for respirators

| **Respirator** | | | | |
|---|---|---|---|---|
| | **Europe EN 149** | **USA (NIOSH CFR PART 84)** | **China (GB 2626)** | **China (GB 19083)** |
| **PFE (NaCl)** | ≥ 94% (FFP2) | ≥ 95% (N95) | ≥ 95% (KN95) | ≥ 95% (Grade 1) |
| **PFE (Paraffin Oil)** | ≥ 94% (FFP2) | N/A | N/A | N/A |

**Table 4**. Performance requirements for medical face masks

| **Medical face masks** | | |
|---|---|---|
| **PFE (Latex Spheres)** | **ASTM F2100-19** | **EN 14683:2019 Barrier Levels** |
| | ≥ 95% Level 1<br>≥ 98% Level 2 & 3 | Not required |

It is of importance to note that the filtration efficiency requirements may vary for different classes of respirators (e.g., N95, FFP2) and may be subject to updates or modifications over time. Manufacturers must meet these standards to ensure the safety and efficacy of medical face masks and respirators used in healthcare and other settings. Users should also be trained in proper mask or respirator use to maximise their effectiveness.

## 2.9. Differential Pressure

The differential pressure testing machine was employed to measure the differential pressure of the desired samples. This machine gauges the pressure difference necessary to pull air through a specified surface area while maintaining a consistent airflow. To accomplish this, an electric vacuum pump draws air through the test apparatus, and the airflow rate is regulated with a needle valve. The make and model of the differential pressure tester in use was *Qinsun Instruments Co., Ltd.*, model *G285*. The area of the test head was 4.9 $cm^2$, and the machine could measure the readings between 50 to 500 Pascals. The test method EN 14683:2014 [155] was followed, a constant air flow of 8 L/min was maintained through the sample, and the pressure drop was measured in $Pa/cm^2$.

**Performance requirements with respect to international standards**

The differential pressure requirement for medical face masks and respirators is defined by international standards to ensure their effectiveness in providing a barrier against the transmission of respiratory droplets and to ensure breathability for the wearer. One of the key standards addressing this requirement is *ASTM F2100*, which is widely recognised internationally. The *ASTM F2100* Standard specifies several performance requirements for medical face masks, including the differential pressure. Here are the key points related to the differential pressure requirement as per *ASTM F2100*:

*1. Differential Pressure Test*: *ASTM F2100* requires medical face masks to undergo a differential pressure test to measure the breathability of the mask material. This test evaluates how easily air can pass through the mask, which is important for the comfort and prolonged wear.

*2. Differential Pressure Measurement*: The test measures the pressure drop across the mask material, typically expressed in units of mm $H_2O$ (millimetres of water). The lower is the pressure drop, the better is the breathability of the mask.

*3. Performance Levels*: ASTM F2100 categorises masks into different performance levels based on their differential pressure results. These levels are often labelled as Type I, Type II, and Type IIR, with Type I having the lowest differential pressure, and Type IIR conforming to the highest pressure. In general, Type I masks have a lower fluid resistance and are suitable for low-risk situations, while Type IIR masks have a higher fluid resistance and are suitable for high-risk situations, such as surgeries.

4. *Acceptable Differential Pressure Range*: The specific values for differential pressure that masks must meet to achieve each performance level can vary slightly based on the version of the *ASTM F2100* Standard and the regional regulations. The latest version F2100-20 typically specifies that Type I masks should have a differential pressure of < 5.0 mm $H_2O/cm^2$, Type II masks should have a differential pressure of < 6.0 mm $H_2O/cm^2$, and Type IIR masks should have a differential pressure of < 6.0 mm $H_2O/cm^2$. The requirements of EN-14683 and ASTM-F2100-20 are summarised in *Table 5* and *Table 6*.

**Table 5**. EN-14683 performance requirements for medical face masks

| Test | Type I | Type II | Type III |
|---|---|---|---|
| Differential pressure ($Pa/cm^2$) | < 40 | < 40 | < 60 |

**Table 6**. ASTM-F2100-20 medical face mask material requirements by performance level

| Test | Level 1 barrier | Level 2 barrier | Level 3 barrier |
|---|---|---|---|
| Differential pressure, mm $H_2O/cm^2$ | <5.0 | <6.0 | <6.0 |

It is of importance to note that standards and requirements can change over time, and therefore it is advisable to check the latest versions of standards and regulations from such organisations as *ASTM*, the *World Health Organization* (WHO), or the local regulatory authority for the most up-to-date information on differential pressure requirements for medical face masks and respirators. Additionally, the requirements may vary by region or country, and thus the compliance with local regulations is essential.

## 3. RESULTS AND DISCUSSION

### 3.1. Viscosity and Conductivity of Solutions

#### 3.1.1. Viscosity and conductivity of PVA/AV/ZnO solutions:

The viscosity and conductivity of solutions prepared for electrospinning are the important parameters affecting the resultant electrospun fibres and are presented in detail in Table 7.

**Viscosity of pure PVA solution**

Viscosity refers to the resistance a fluid (or solution) offers to flow. In our case, the solution is made of Polyvinyl Alcohol (PVA), which is known for having a high molecular weight (85000–124000). A higher molecular weight means that PVA molecules are larger and longer, which can lead to entanglements of these long molecules. These entanglements create resistance to flow, thus resulting in a higher viscosity. Thus, the pure PVA solution itself is denoted by a high viscosity of 1130 mPa*s due to the large molecular weight of PVA.

**Effect of *Aloe vera* and ZnO nanoparticles on viscosity**

When *Aloe vera* and ZnO nanoparticles were added to the PVA solution, the viscosity increases. This means that the resulting mixture becomes thicker and more resistant to flow. Specifically, when different compositions of *Aloe vera* and ZnO nanoparticles are added, the viscosity changes. For instance, increasing the concentration of *Aloe vera* from 1% to 4% along with 0.5% ZnO nanoparticles increases the viscosity from 1310 to 1490 mPa*s.

Additionally, the conductivity showed a gradual increase as the concentration of *Aloe vera* increased. This significant viscosity increase with higher concentrations of *Aloe vera* has also been observed by other researchers [156, 157].

**Table 7**. Viscosity and Conductivity of AV/PVA/ZnO solutions

| Sample Number | Conc. of polyvinyl alcohol (%, W/V) | Conc. of *Aloe vera* (%) | Conc. of zinc oxide nanoparticles (W/V) | Viscosity (mPa*s) | Conductivity (S/m) |
|---|---|---|---|---|---|
| **AV1/PVA/ZnO0.5** | 10% | 1% | 0.50% | 1310 | 0.0505 |
| **AV2/PVA/ZnO0.5** | 10% | 2% | 0.50% | 1390 | 0.0530 |
| **AV3/PVA/ZnO0.5** | 10% | 3% | 0.50% | 1450 | 0.0542 |
| **AV4/PVA/ZnO0.5** | 10% | 4% | 0.50% | 1490 | 0.0560 |
| **AV0.5/PVA/ZnO1** | 10% | 0.50% | 1% | 1190 | 0.0530 |
| **AV0.5/PVA/ZnO2** | 10% | 0.50% | 2% | 1230 | 0.0570 |

| | | | | | |
|---|---|---|---|---|---|
| **AV0.5/PVA/ZnO3** | 10% | 0.50% | 3% | 1260 | 0.0625 |
| **AV0.5/PVA/ZnO4** | 10% | 0.50% | 4% | 1305 | 0.0657 |
| **AV-0/PVA/ZnO-0** | 10% | 0 | 0 | 1130 | 0.0430 |

**Relationship between *Aloe vera* concentration and conductivity**

As the concentration of *Aloe vera* increases, the solution's conductivity also gradually increases. This means that higher concentrations of *Aloe vera* result in a solution which conducts electrical current more effectively. The text suggests that the relationship between the *Aloe vera* concentration and conductivity is positive, which indicates that *Aloe vera* might have a role in enhancing the solution's electrical conductivity.

**Comparing ZnO nanoparticles and *Aloe vera* effects on viscosity and conductivity**

In comparing the effects of ZnO nanoparticles and *Aloe vera*, it is notable that the impact of ZnO nanoparticles on viscosity is relatively insignificant. This is because *Aloe vera* gel is inherently viscous, and ZnO nanoparticles are at the nanoscale, which means that they do not significantly affect the solution's viscosity. However, as the concentration of ZnO nanoparticles increases, the solution's conductivity notably rises. This is attributed to the fact that a higher quantity of ZnO semiconductor nanoparticles in the solution leads to an enhanced electrical conductivity.
Other researchers have also observed this correlation between an increased ZnO NP concentration and an enhanced conductivity [158, 159].

**Summary**

The results indicate that an increase in the concentration of *Aloe vera* leads to a significant increase in viscosity and a moderate increase in electrical conductivity. Similarly, increasing the concentration of ZnO nanoparticles leads to a significant increase in electrical conductivity while also having a noticeable but less significant impact on viscosity.

### 3.1.2. Viscosity and conductivity of PLA/CNDs solutions

Viscosity and conductivity of all the prepared solutions of PLA and PLA/CNDs are presented in Table 8. The data shows that, as the concentration of PLA in the solvent DMF (dimethylformamide) increases, the viscosity of the solution also increases. Specifically, when the PLA concentration is raised from 12% to 19%, the viscosity rises from 177 millipascal seconds (mPa·s) to 335 mPa·s. This viscosity increase is attributed to the higher concentration of PLA in the solution. However, it is notable that the viscosity increase is not substantial due to the relatively low molecular weight of the PLA used.

Furthermore, we observed that an increase in the concentration of CNDs (carbon nanodots) in the solution also led to an increase in viscosity. However, this increase in viscosity was not as significant. This can be explained by the fact that the particle size of CNDs is very small, around 10–15 nanometres (nm). Because of their small size, they do not contribute as much to the overall viscosity increase as the PLA molecules do.

Both viscosity and conductivity are essential parameters because they have a direct impact on the way the fibres form during the manufacturing process. Higher viscosity solutions tend to have slower flow rates and may affect the processing conditions. Conductivity, on the other hand, can influence the electrostatic interactions and the overall behaviour of the solution during processing.

**Table 8**. Viscosity and conductivity of PLA & PLA/CNDs solutions

| Sample # | Concentration of PLA (%, w/v) | Concentration of CNDs (%) | Viscosity (mPa*s) | Conductivity (S/m) |
|---|---|---|---|---|
| **PLA-12** | 12 | – | 177 | 0.0004 |
| **PLA-15** | 15 | – | 230 | 0.0006 |
| **PLA-17** | 17 | – | 285 | 0.0008 |
| **PLA-17/C1** | 17 | 1 | 288 | 0.0450 |
| **PLA-17/C2** | 17 | 2 | 291 | 0.0666 |
| **PLA-17/C3** | 17 | 3 | 296 | 0.1020 |
| **PLA-17/C4** | 17 | 4 | 305 | 0.1260 |
| **PLA-19** | 19 | – | 335 | 0.0012 |
| **PLA-19/C1** | 19 | 1 | 339 | 0.0465 |
| **PLA-19/C2** | 19 | 2 | 345 | 0.0702 |
| **PLA-19/C3** | 19 | 3 | 351 | 0.1065 |
| **PLA-19/C4** | 19 | 4 | 358 | 0.1290 |

Conductivity refers to the ability of a material to allow the flow of electric current. In this case, we measured how well these PLA solutions can conduct electricity. For the pure 12%, 13%, 15%, and 17% PLA solutions, the conductivity was prominently low, even lower than 0.001 S/m. The results indicate that, as the concentration of PLA in the solution increases, the conductivity decreases. This means that the higher is the concentration of PLA, the less capable the solution is at

conducting electricity. The key reason behind this observation is that PLA is inherently a nonconductive material. It does not easily allow the flow of electrons which are the carriers of electric charge. When we have a solution with a high concentration of PLA, there are more PLA molecules present in the solution. These PLA molecules do not readily allow the movement of charged particles, like ions or electrons. They act as barriers to the flow of the electric current. This resistance to the movement of electrons is analogous to the way a narrow pipe restricts the flow of water.

When considering the insulating properties of PLA (polylactic acid), it is notable that when carbon nanodots (CNDs) are introduced into the solution containing PLA, a noteworthy shift occurs. Rather than acting as an insulator as PLA tends to, the presence of CNDs induces a measure of electrical conductivity. This is simply due to the fact that CNDs are a highly conductive material.

The degree of electrical conductivity exhibited by the PLA/CNDs solutions correlates directly with the concentration of CNDs within the mixture. As the concentration of CNDs increases, so does the electrical conductivity of the solution. For instance, in the case of a solution containing 19% PLA, the electrical conductivity underwent a rise from 0.0465 S/m when 1% CNDs were present, to 0.129 S/m when the concentration of CNDs increased to 4%. This escalation in conductivity can be attributed to the inherent conductivity of CNDs themselves which are known to possess excellent electrical conduction properties.

The presence of CNDs has a marked influence on the electrical conductivity of all PLA solutions. Additionally, the concentration of CNDs also affects the viscosity of the solution. This upsurge in both electrical conductivity and viscosity contributes positively to the process of producing electrospun nanofibres. This suggests that the combination of PLA and CNDs can lead to the creation of nanofibres with enhanced conductive properties and structural stability.

**Summary**

PLA is a non-conductor, and the results indicate that an increase of the concentration of CNDs leads to a significant increase in electrical conductivity of PLA solutions. Also, increasing the concentration of CNDs does not have any significant effect on viscosity as the particle size of CNDs is in tens of nanometres only.

### 3.2. Particle Size Analysis

#### 3.2.1. Particle size analysis of ZnO NPs

The particle size of ZNO NPs was investigated by using the dynamic light scattering technique by using the *Zetasizer* equipment. Fig. 25 shows the size distribution of ZnO NPs, the x-axis shows the size, whereas the y-axis shows the percentage of particles in that specific size. It appears that the average size of ZnO NPs is 50 nm, with a range from 37.8 nm to 68.1 nm. In the SEM images, we could not observe any

visual presence of ZnO NPs on the or embedded into the electrospun fibres due to the large size of electrospun fibres (above 100 nm) and a comparatively small size of ZnO NPs of around 50 nm. Their presence can be verified by the antibacterial results, and it is assumed that ZnO NPs are embedded on the surface and into the core of PVA electrospun fibres.

The investigation of the ZnO nanoparticle (NP) particle size was conducted through the utilisation of the dynamic light scattering technique, while employing the state-of-the-art *Zetasizer* equipment. As depicted in Fig. 25, the resulting data presents a comprehensive size distribution profile of ZnO NPs. On the x-axis, the varying sizes of the nanoparticles are showcased, while the y-axis portrays the corresponding percentage of particles occupying each distinct size range.

Remarkably, the discerned size distribution analysis reveals a prevailing average diameter of approximately 50 nm for ZnO NPs. This value emerges within a size range spanning from 37.8 nm at the lower end to 68.1 nm at the upper end of the spectrum. Such granularity in size statistics affords comprehensive understanding of the dimensions of these nanoparticles and their inherent variability.

Despite the examination conducted under scanning electron microscopy (SEM), the visual detection of ZnO NPs either adhering to the electrospun fibre surfaces or penetrating their structure remained elusive. This observation can be attributed to the relatively substantial dimensions of the electrospun fibres, exceeding 100 nm, in stark contrast to the comparably diminutive size of the ZnO NPs, which are approximately 50 nm in diameter. As a result of this size differential, the direct visualisation of the ZnO NPs within the electrospun fibre matrix was precluded.

However, it is important to emphasise that the absence of visible confirmation through SEM imagery does not negate the presence of ZnO NPs within the electrospun fibre assembly. The validation of their incorporation can be effectively substantiated through the compelling antibacterial outcomes or by EDX analysis. This inference is rooted in the supposition that the ZnO NPs, while not visually apparent, are in fact intricately embedded within both the surface and the core of polyvinyl alcohol (PVA) electrospun fibres.

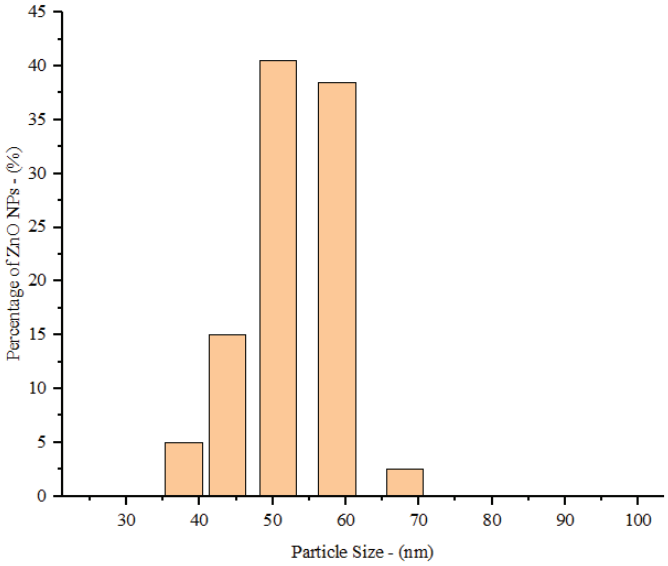


**Fig. 25**. Size distribution of ZnO NPs

As mentioned above, the average size is the 50 nm range, and this would serve a good purpose in exploring the antibacterial properties of the functionalised fibres.

## Summary

In summary, the comprehensive exploration of the ZnO NP particle size distribution, employing the dynamic light scattering technique with the advanced *Zetasizer* apparatus, reveals an average diameter of approximately 50 nm within a range spanning from 37.8 nm to 68.1 nm. While not visually detectable through SEM due to size disparities, the presence of ZnO NPs is effectively affirmed by their antibacterial efficacy and their presumed integration within the structure of PVA electrospun fibres.

### 3.2.2. Particle size analysis of CNDs

In the context of a scientific study, the *Zetasizer* (Dynamic Light Scattering, DLS) was utilised as a measurement tool to examine the hydrodynamic size of Carbon Nanodots (CNDs). The hydrodynamic size refers to the apparent size of particles in a liquid medium due to their interactions with the surrounding molecules. Fig. 26 in the study presents the size distribution analysis of these carbon nanodots. The x-axis of the graph represents the different sizes of the nanodots, while the y-axis represents the percentage of particles which are present in each specific size range. The analysis reveals that the carbon nanodots vary in size, as they range from as small as 7.5 nanometres to as large as 15.7 nanometres.

We found that the mean size of the synthesised carbon nanodots was calculated to be 10.2 nanometres. This indicates that the majority of the nanodots fall within this average size range. Interestingly, when we observed the electrospun fibres under a scanning electron microscope (SEM), we did not visually detect any presence of carbon nanodots on or within the electrospun fibres. This lack of visual detection could be attributed to the significant difference in size between the electrospun fibres and the carbon nanodots. Electrospun fibres were notably larger, with sizes exceeding 100 nanometres, while carbon nanodots were significantly smaller, at around 10 nanometres.

The absence of visual evidence of carbon nanodots on the electrospun fibres does not necessarily mean that they are not present. Instead, researchers propose that the reason for their lack of visibility is the significant size difference between the two materials. The nanodots are suspected to be embedded on the surface and even within the core of the electrospun fibres.

To confirm the presence of carbon nanodots and their effect, the study relied on antibacterial results which likely indicated that the carbon nanodots were indeed present and contributing to the desired properties of the electrospun fibres.

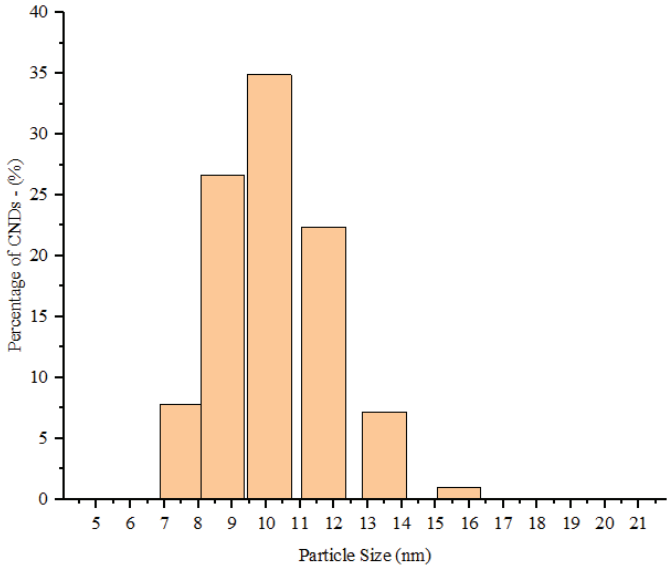


**Fig. 26**. Hydrodynamic size analysis of carbon nanodots

## Summary

In summary, the study employed the Zeta sizer to analyse the hydrodynamic size distribution of carbon nanodots, which reveals a range of sizes with an average of 10.2 nm. While not visible under SEM due to the larger size of the electrospun fibres, the presence of carbon nanodots was suggested to be responsible for certain properties,

as evidenced by antibacterial effects, and they were hypothesised to be embedded within the electrospun fibre structure.

### 3.3. SEM Analysis

#### 3.3.1. SEM analysis of PVA/AV/ZnO electrospun fibres:

To investigate the morphology and diameter of AV/PVA/ZnO electrospun fibres, they were subjected to SEM analysis. Fig. 27 shows the SEM results of AV/PVA/ZnO electrospun fibres with variation in AV in it. The results also indicate that electrospun fibres exhibit slender and seamless diameters with minimal clustering, potentially attributable to the presence of ZnO nanoparticles. The *ImageJ* software was employed to assess the diameter of the electrospun fibres as they were initially formed. A total of 100 measurements, obtained from various locations within the same fibre, as well as from distinct fibres, were averaged.

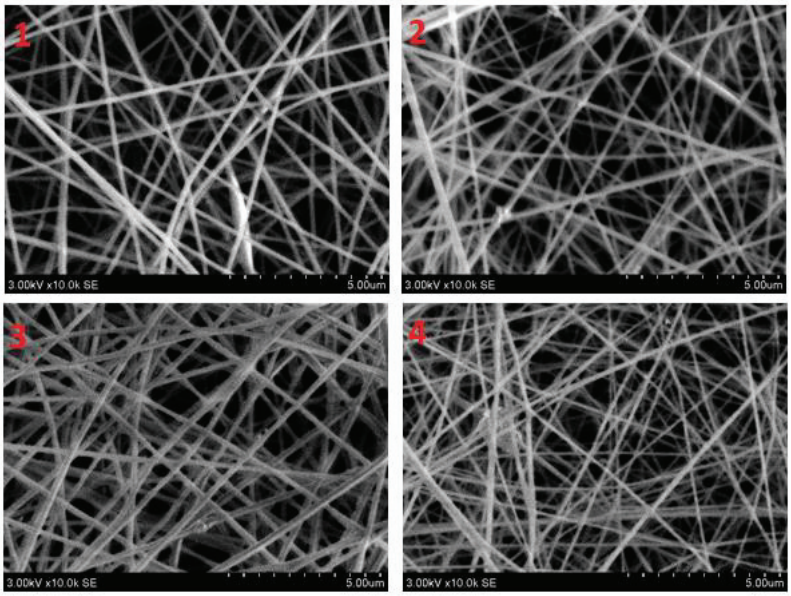


**Fig. 27**. SEM images (×10 mag) of electrospun fibres: (1) 1% AV; (2) 2% AV; (3) 3% AV; and (4) 4% AV

Fig. 28 presents a histogram of the number of fibres per diameter range. Sample AV1/PVA/ZnO-0.5 has an average diameter of 180 nm, AV2/PVA/ZnO-0.5 has an average diameter of 176 nm, AV3/PVA/ZnO-0.5 has an average diameter of 148 nm, whereas AV4/PVA/ZnO-0.5 shows an average diameter of 130 nm.

For the histograms in Fig. 28, it can also be observed that the sample AV4/PVA/ZnO-0.5 has the lowest number of fibres in the 210–270 nm range. It was observed that, with an increase in the concentration of *Aloe vera* from 1% to 4%, the average diameter of the resultant electrospun fibres was decreased, and this can be explained by the fact that electrostatic and columbic repulsive forces increase with an increase in the concentration of *Aloe vera* [160][161]. tα was calculated (tα=68.26) to

check the significance of the decrease in the diameter with an increase in the concentration of *Aloe vera*. The statistical value with a reliability of α=0.95 (tαst=1.98) is much lower than the calculated tα, and it demonstrates the significance of the difference between the average diameters of electrospun fibres formed with different concentrations of *Aloe vera*.

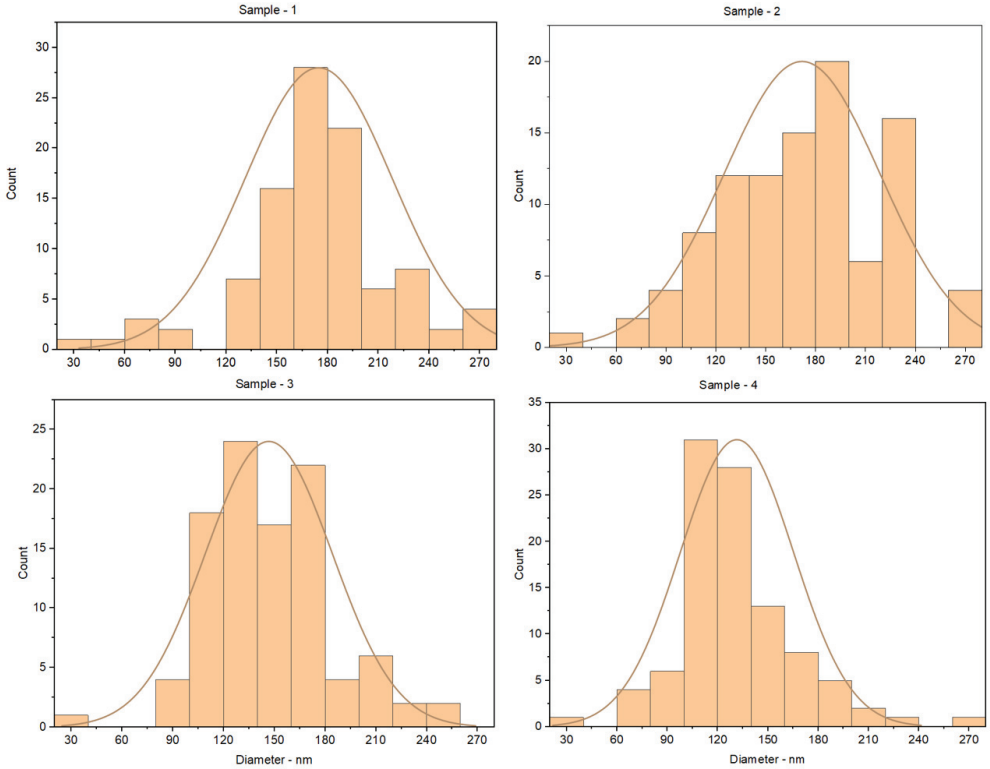


**Fig. 28**. Diameter distribution of electrospun fibres in samples 1, 2, 3 and 4 with 1%, 2%, 3% and 4% AV

SEM images of samples with varying concentration in ZnO NPs are presented in Fig. 29. The images show that the formed electrospun fibres were smooth and regular, just like pure PVA electrospun fibres. But, unlike pure PVA, formation of beads in electrospun fibres was observed, and more beads were formed with a higher concentration of ZnO NPs according to the observations. The point to mention is that rough beads show the presence of ZnO NPs, and smooth beads are merely the polymer itself.

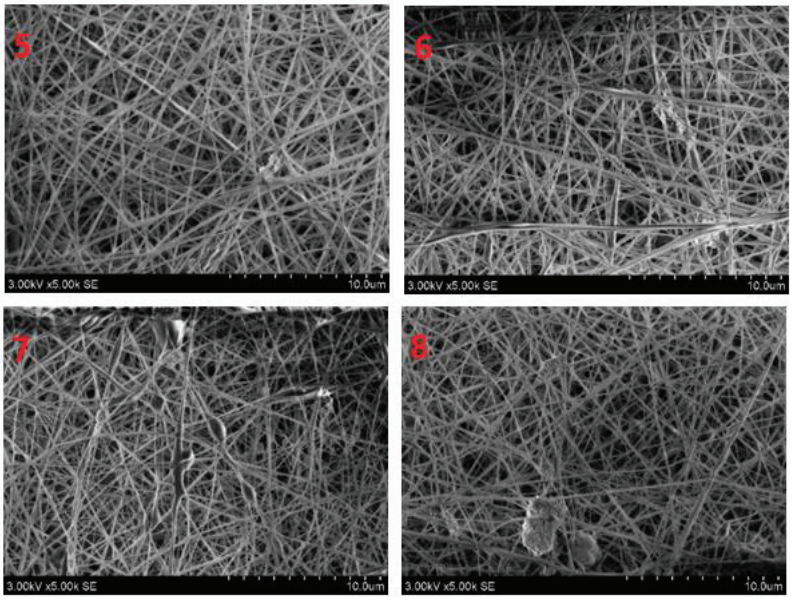


**Fig. 29**. SEM Images (×5 mag) of electrospun fibres: (5) 1% ZnO NPs; (6) 2% ZnO NPs; (7) 3% ZnO NPs; (8) 4% ZnO NPs

It was also observed that the change in the concentration of ZnO nanoparticles exerts some effect on the diameter of the formed fibres, as shown in Fig. 30. With an increase in the concentration of ZnO NPs, the average diameter decreased from 165 nm for 1% ZnO NPs to 145 for 4% ZnO NPs. Furthermore, in order to investigate the significance of the change in concentration to the formed electrospun fibres, when we compared the calculated t-value ($t\alpha=25.27$) with the critical t-value ($t\alpha st=1.98$), we observed that $t\alpha$ is significantly higher than $t\alpha st$. This comparison suggests that the difference between the different concentrations of ZnO NPs is denoted by a very high level of statistical significance. In more accessible terms, our findings suggest that the variation we observed in the electrospun fibre morphology is not a coincidence or a result of random fluctuations. It is highly likely that the different concentrations of ZnO NPs do indeed cause a significant impact on how the electrospun fibres are forming. This result provides strong evidence that the concentration of ZnO NPs is an important factor influencing the morphology of the electrospun fibres.

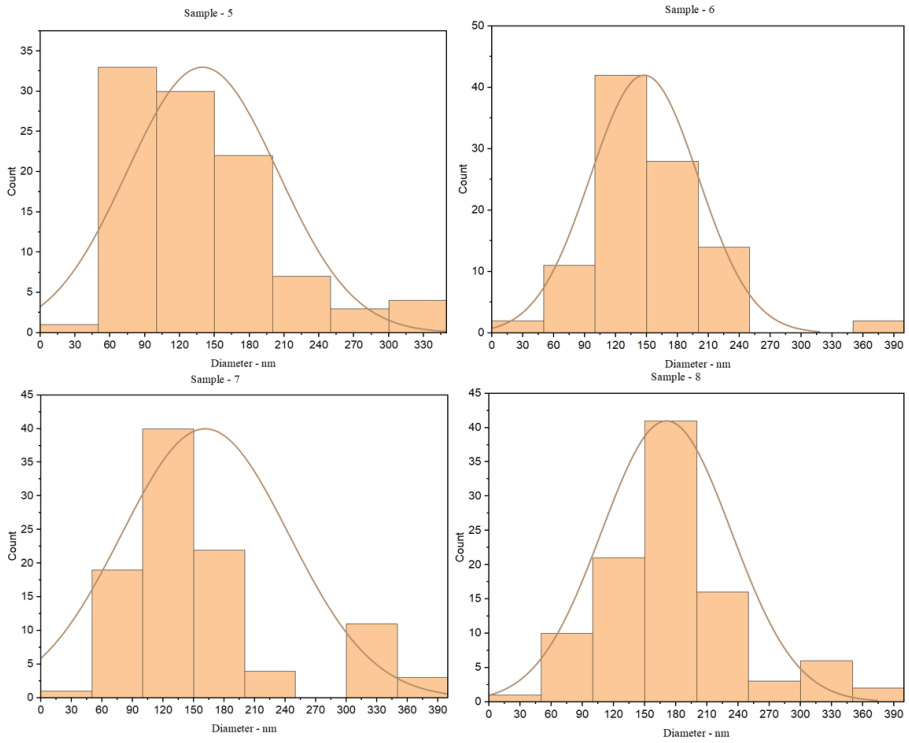


**Fig. 30**. Diameter distribution of electrospun fibre samples 5, 6, 7 and 8 containing 1%, 2%, 3% and 4% ZnO NPs, respectively, with constant amounts of *Aloe vera* and PVA

## Summary

The effect of different concentrations of AV and ZnO NPs on the final diameter has been established. We observed that as we increase the concentration of AV and ZnO NPs in the solution, the average diameter also increases, which is due to the fact that electrostatic and columbic repulsive forces increase with an increase in the concentration of *Aloe vera* and ZnO NPs.

### 3.3.2. SEM analysis of PLA/CNDs electrospun fibres

In this section, the focus is on discussing the results of the *Scanning Electron Microscopy* (SEM) analysis conducted on electrospun fibres made from two different materials: pure *PolyLactic Acid* (PLA), and a composite of PLA with *Carbon NanoDots* (CNDs). SEM analysis is a powerful technique used to examine the surface and structure of materials at the microscopic level. It helps in understanding the characteristics and dimensions of the electrospun fibres.

To perform this analysis, all the samples, both PLA and PLA/CNDs, were carefully prepared and then subjected to SEM examination. During the examination, the diameter of the electrospun fibres was a critical parameter of interest. To determine this diameter, measurements were taken at multiple locations on different fibres as well as at different spots along the same fibre. To ensure accuracy and consistency in these measurements, *ImageJ* software was employed. This software assists in processing the SEM images and provides a means to quantify the dimensions of the electrospun fibres.

In total, 100 readings were collected from the SEM images for each type of electrospun fibre (PLA and PLA/CNDs) to calculate the average diameter. This approach helps in obtaining a representative measurement, by considering any variations in the fibre size that may exist within the samples. Additionally, it is important to note that the formation of electrospun fibres is influenced by various factors which were briefly mentioned above. These factors include the properties of the solution used to create electrospun fibres, as well as the specific process parameters employed during their fabrication. Parameters such as the potential difference (the voltage applied), the distance between electrodes, and other conditions during the electrospinning process play a crucial role in determining the characteristics of the resulting electrospun fibres. Understanding how these factors affect electrospun fibre formation is essential for optimising their properties for various applications [162].

Further we explored the parameters that are crucial for the successful electrospinning of polymer electrospun fibres. One of the key factors we investigated was the concentration of PLA (Polylactic Acid) in DMF (Dimethylformamide). Initially, we began with a low concentration of PLA i.e., 12% in DMF, and carried out experiments to see how this concentration behaved under defined process conditions. During the electrospinning process, with this low concentration of PLA (12% in DMF), we noticed that, instead of forming electrospun fibres, the solution was producing droplets. This unexpected behaviour was attributed to the fact that PLA with a lower molecular weight, even at a 12% weight percentage, did not provide enough viscosity to the solution. This lack of viscosity was preventing the formation of electrospun fibres, as a certain level of viscosity is required to promote the formation of these fine-scale structures.

To understand this phenomenon better, we decided to investigate higher concentrations of PLA in DMF, notably, 15%, 17%, and 19%. What we found was that an increase in the concentration of PLA in the DMF solution had a positive impact on the formation of electrospun fibres. As the PLA concentration increased, the solution became more viscous, which favoured the successful creation of electrospun fibres.

We also included SEM (Scanning Electron Microscopy) images, shown in Fig. 31, to visually illustrate the differences in the electrospun fibre morphology at various PLA concentrations. This helped us visualise how the concentration of PLA influenced the resulting electrospun fibre structures. It is worth noting that our findings align with the previous research conducted by Fong and colleagues who also

highlighted the significance of viscosity in electrospinning. They observed that higher viscosity not only prevents the formation of bead-like structures in the fibres, but also encourages the production of thinner, more desirable electrospun fibres. In summary, our study emphasised the critical role of polymer concentration and viscosity in the electrospinning process, thereby shedding light on the factors influencing the formation of electrospun fibres for various applications [163].

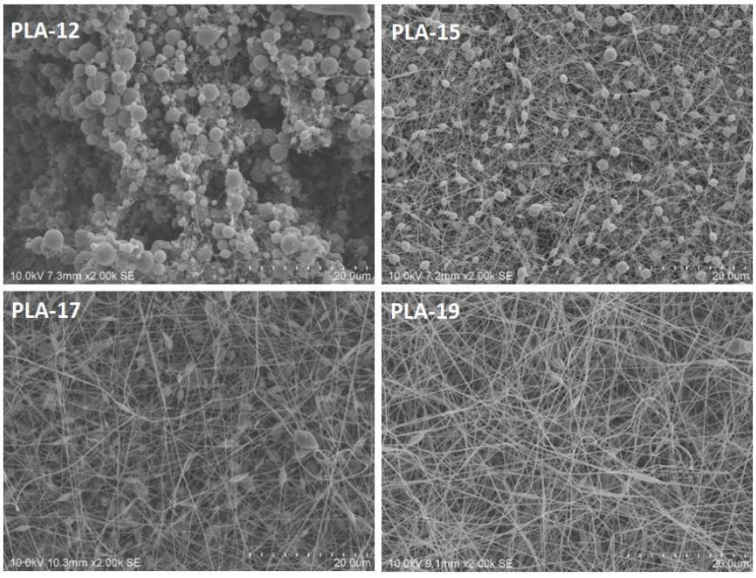


**Fig. 31**. SEM images (×2 mag) of pure PLA electrospun fibres with concentrations of 12%, 15%, 17%, and 19% (scale – 20 μm)

The formation of fibres with a thinner diameter was observed with 17% and 19% PLA in DMF; therefore, we selected these concentrations for further research. To enhance the functionality of these PLA electrospun fibres, we aimed to incorporate antibacterial properties. To achieve this, we introduced photoactive carbon nanodots (CNDs) into the electrospinning solution. Our research included varying the concentration of CNDs within the PLA electrospun fibres. We employed *Scanning Electron Microscopy* (SEM) to examine the electrospun fibres produced with 17% PLA and different quantities of CNDs.

The SEM analysis revealed an interesting trend which is shown in Fig. 32. As the concentration of CNDs increased within the PLA-17 solution, we observed a reduction in the average diameter of the resulting electrospun fibres. For instance, in the case of PLA-17/C1, we obtained fibres with an average diameter of approximately 178 ± 37 nanometres, while, for PLA-17/C4, the diameter reduced further to 98 ± 25 nanometres. This reduction in the diameter is significant because it suggests that the addition of CNDs had a substantial impact on the electrospun fibre structure. This change in behaviour can be attributed to the fact that PLA, in its pure form, is not conductive. However, when CNDs were introduced into the solution, they increased its conductivity. This increase in conductivity played a crucial role in favouring the

formation of finer electrospun fibres. This observation aligns with findings presented by other researchers who also noted similar improvements in the electrospun fibre formation when incorporating conductive additives into nonconductive polymer solutions [164].

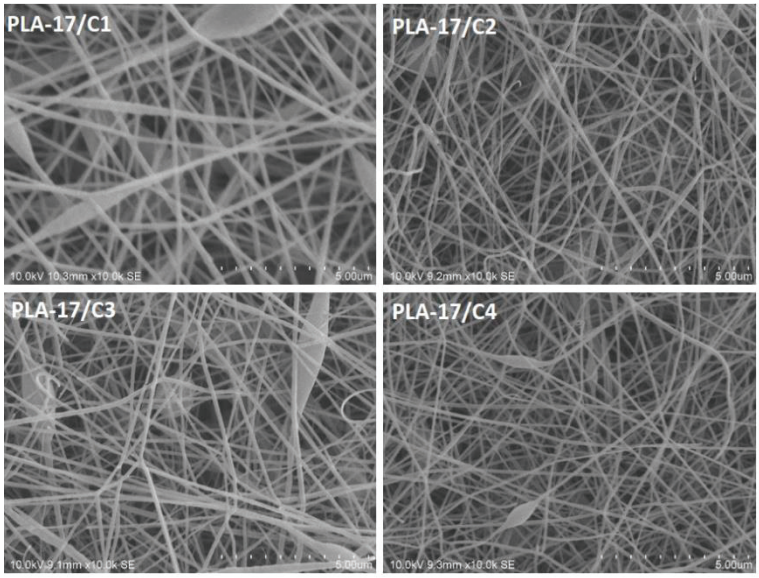


**Fig. 32**. SEM images (×10 mag) of 17% PLA electrospun fibres with a variation of the CNDs 1%, 2%, 3%, and 4% (scale – 5 μm)

In samples containing 19% polylactic acid (PLA) and different quantities of carbon nanodots (CNDs), a similar pattern of behaviour was observed. The SEM analysis, as highlighted in Fig. 33, was conducted on these fibres. It was noted that, as the concentration of CNDs in the PLA increased, there was a reduction in the diameter of the fibres. Specifically, the diameter decreased from an initial measurement of 150 ± 40 nm in the case of PLA-19/C1 to 88 ± 25 nm in the case of PLA-19/C4. This trend indicates that the presence of a higher concentration of CNDs within the PLA matrix results in a significant reduction in the fibre diameter, as evidenced by the SEM analysis [164].

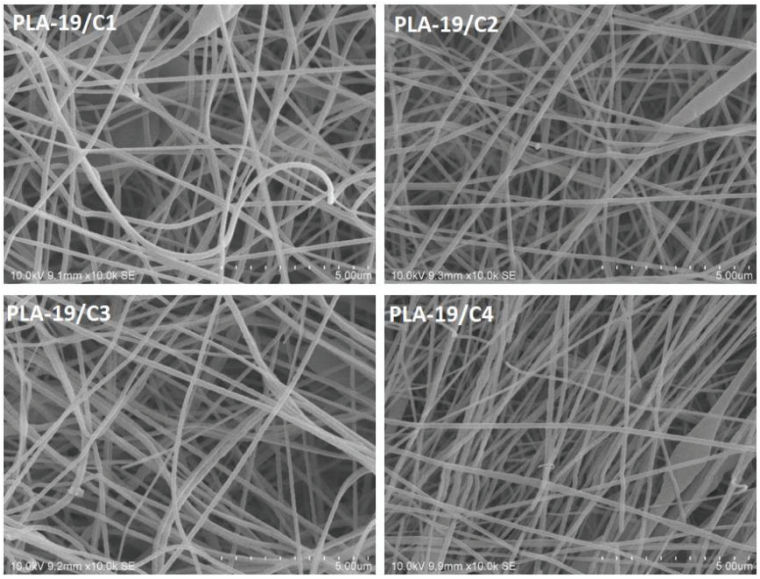


**Fig. 33**. SEM images (×10 mag) of 19% PLA electrospun fibres with a variation of CNDs 1%, 2%, 3%, and 4% (scale – 5 μm)

## Summary

The overall impact of an increase in the concentration of PLA in DMF was very significant, as this shifts the electrospraying process at 12% concentration to the electrospinning process at 19% concentration. Also, an increase in conductivity by incorporating CNDs played a significant role in the morphology of electrospun fibres.

### 3.4. EDX Analysis of AV/PVA/ZnO Fibres

EDX analysis, also known as *Energy-Dispersive X-ray Spectroscopy*, was employed in the examination of electrospun fibres in order to ascertain the presence of ZnO nanoparticles.

During the analysis, the electrospun fibres were subjected to a focused electron beam causing the emission of characteristic X-rays from the sample. These emitted X-rays were collected by an X-ray detector and then processed to generate an elemental spectrum. By examining the spectral data, the presence of specific peaks (Fig. 34, Fig. 35, Fig. 36, Fig. 37) corresponding to zinc (Zn) and oxygen (O) could be ascertained. The presence of these elements indicated the existence of ZnO nanoparticles within the electrospun fibres.

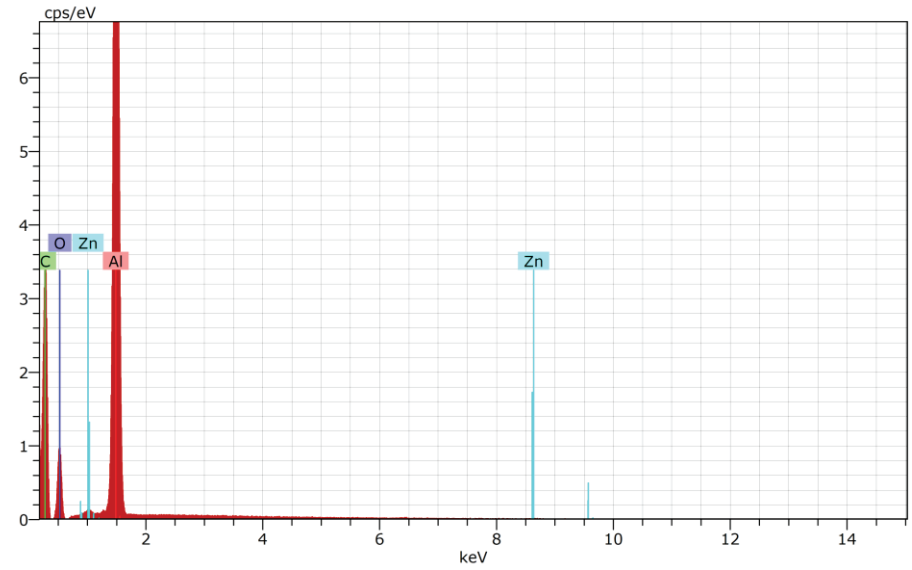


**Fig. 34**. EDX analysis of electrospun nanofibers with 1% ZnO

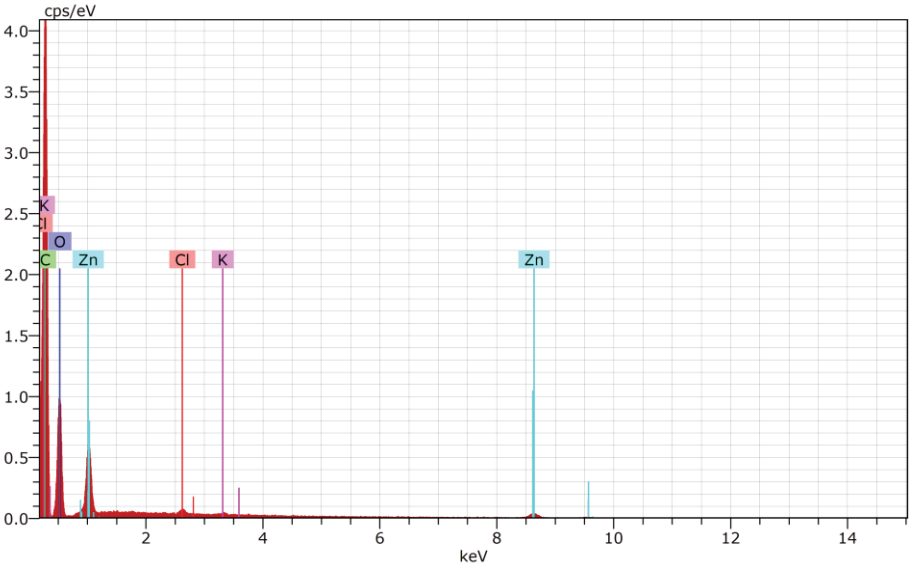


**Fig. 35**. EDX analysis of electrospun fibres with 2% ZnO

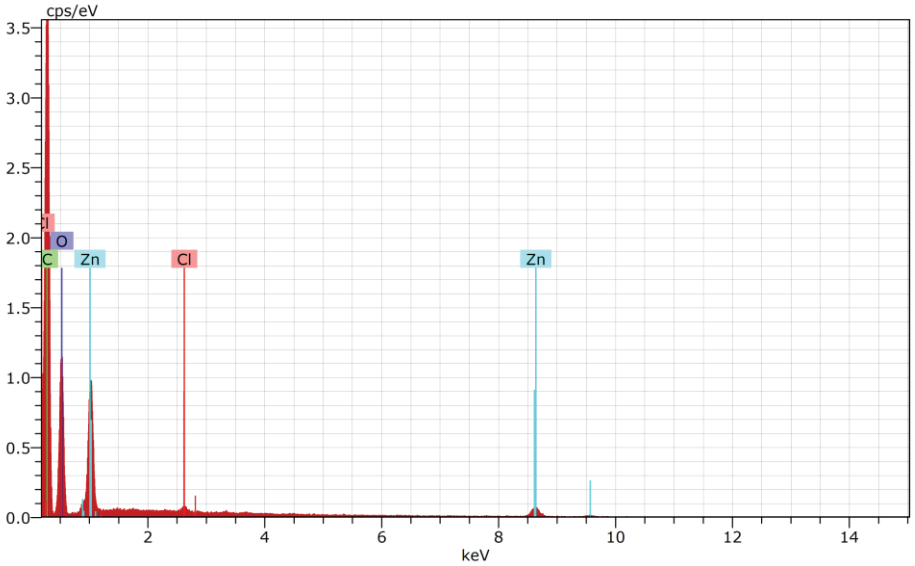


**Fig. 36**. EDX analysis of electrospun fibres with 3% ZnO

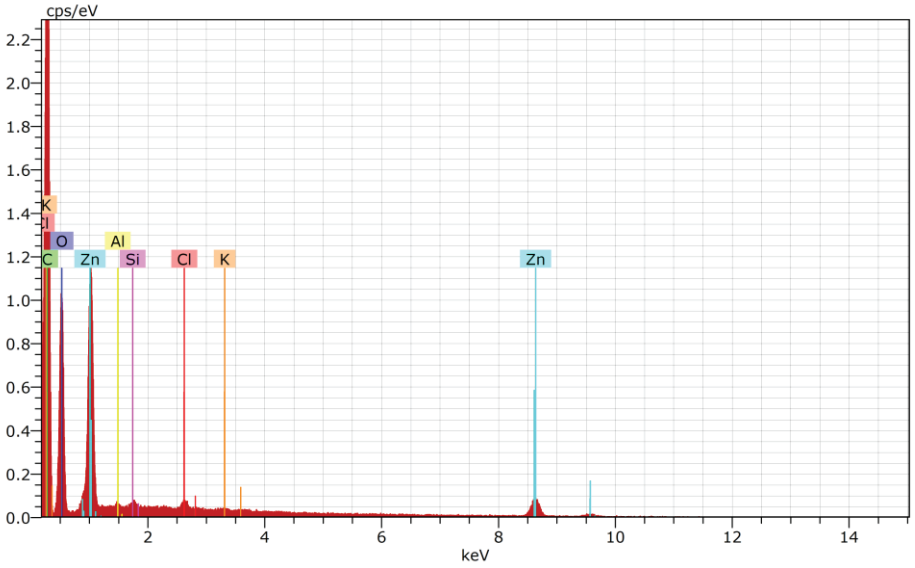


**Fig. 37**. EDX analysis of electrospun fibres with 4% ZnO

It is of importance to note that EDX analysis is a non-destructive technique, allowing for the characterisation of samples without altering their structural integrity. This feature is particularly advantageous when investigating nanomaterials like ZnO nanoparticles embedded in electrospun fibres, as it enables a thorough examination while preserving the sample's composition and morphology.

**Summary**

EDX analysis was solely done to check the presence of ZnO NPs and also to check the increase in concentration of ZnO NPs in different samples. The results depict the same outcome.

### 3.5. Antibacterial Activity

#### 3.5.1. Antibacterial activity of AV/PVA/ZnO electrospun fibres

The focus of this study was to assess the antibacterial activity of the prepared samples of AV/PVA/ZnO. Studies show that AV gel contains anthraquinones which are responsible for imparting antibacterial properties to AV. Furthermore, cinnamic acid, a constituent found in AV, plays a crucial role in inhibiting bacterial growth. This inhibition occurs by actively resisting the uptake of glucose by resting bacteria. The cumulative effect of these antibacterial components within the AV/PVA/ZnO samples was evaluated according to *ISO 20645:2004* guidelines so that to determine their effectiveness in preventing bacterial growth. This research underscores the potential of AV-based materials as effective agents in combatting microbial activity, while also shedding light on their promising applications in various industries, such as healthcare and hygiene. [165]. ZnO nanoparticles (NPs) are characterised as semiconductors, and their antibacterial activity is attributed to their semiconductive behaviour when exposed to incident light with energy greater than their band gap. The various beneficial properties of ZnO NPs, such as UV resistance, photocatalysis, and antibacterial effects, are all linked to their inherent semiconducting properties. When ZnO NPs absorb incident light with energy exceeding their band gap of roughly 3.31 eV, electrons in their valence shells become excited and transmitted to the conduction band, subsequently leaving behind electron holes in the valence shell. This shift of electrons into the conduction band initiates a reaction with the adjacent moisture molecules generating *Reactive Oxygen Species* (ROS). These ROS molecules subsequently engage with the cell walls of microorganisms, thus causing disruption and rupture, and ultimately leading to the killing of the bacteria. In summary, the antibacterial action of ZnO NPs hinges on their semiconductor nature, due to enabling them to harness the incident light energy to create ROS, which, in turn, disrupts and destroys bacterial cell walls [166].

After preparing agar plates with uniform bacteria in them, AV/PVA/ZnO samples were placed on the surface and pressed for uniform and firm attachment, the samples tended to shrink. The reason behind this phenomenon can be explained by the fact that PVA is hydrophilic, and, as soon as it meets the wet surface, it shrinks – this is a common behaviour among hydrophilic nonwoven fabrics [167]. The antibacterial activity of all samples was calculated by measuring the zone of inhibition from the edge of the samples. Fig. 38 shows the zone of inhibition of AV/PVA/ZnO and pure PVA samples.

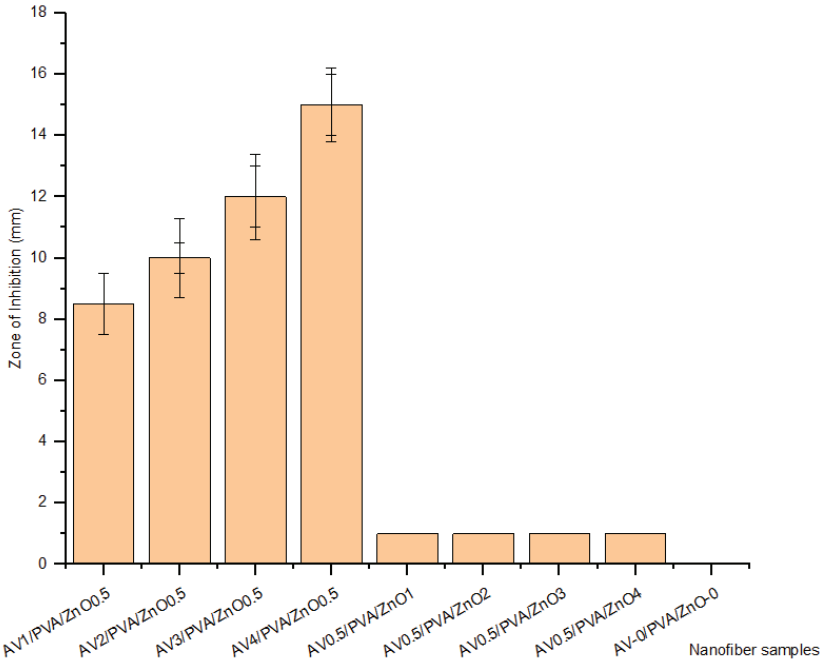


**Fig. 38**. Qualitative analysis – zone of inhibition of all electrospun samples against *S. aureus*

From Fig. 38, it is apparent that, in the case of samples exhibiting variation in the AV content (ranging from 1% to 4%), an observable increase in the zone of inhibition is noted as the concentration of AV increases. Specifically, the zone of inhibition exhibited a noticeable expansion, extending from 8.5 to 15 mm as the AV concentration increased from 1% to 4%. For samples with varying ZnO NPs concentration, it was observed that augmenting the ZnO NPs concentration from 1% to 4% did not result in any discernible visual growth in the zone of inhibition. In fact, the zone of inhibition remained consistently below 1 mm from the sample's edge. Intriguingly, there was a conspicuous absence of bacterial growth on the surface of these samples.

This behaviour can be elucidated by the fact that ZnO NPs are incorporated within both the core and surface of PVA electrospun fibres. Consequently, they do not undergo release into the surrounding moisture or liquid; instead, they only exert their antibacterial effects on bacteria which come into close proximity with these samples. In stark contrast to this ZnO behaviour, AV gel is released from the surface of PVA electrospun fibres, after which, it actively targets and eliminates bacteria coming into contact with it. Consequently, a notable and prominent increase in the zone of inhibition, from 8.5 to 15 mm, was conspicuously observed for these samples.

The qualitative antibacterial activity, as defined in *ISO 20645:2004*, did not serve the full purpose to check the activity of ZnO NPs, there we moved to quantitative analysis of antibacterial activity, as defined in ISO 20743:2013. Again, the

antibacterial activity of the prepared AV/PVA/ZnO electrospun fibres was analysed by this method. The graphical results of antibacterial activity are presented in Fig. 39.

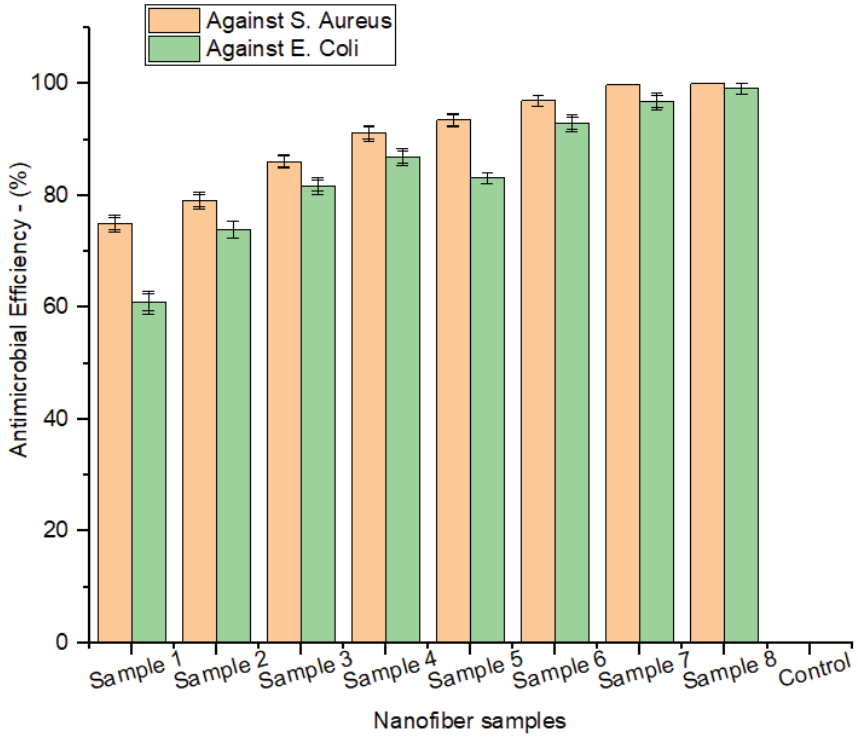


**Fig. 39**. Antibacterial activity of all electrospun samples with variation in *Aloe vera* and ZnO NPs against *S. aureus* and *E. coli*

In all the samples, variations in ZnO NPs, as well as samples with varying concentrations of AV gel, we observed an increase in the antibacterial activity against both gram-positive and gram-negative bacteria when the antibacterial agent was increased. The growth inhibition of *S. aureus*, in particular, was notable in samples with varying AV concentrations. These samples were found to inhibit bacterial growth by a range of percentages, from 75% when containing 1% AV to 91% when containing 4% AV. Similarly, when dealing with *E. coli*, an escalation in antibacterial activity was evident, with percentages rising from 61% to 87% as the concentration of the antibacterial agent increased.

The reduction in the *Colony Forming Units* (cfu) against both *S. aureus* and *E. coli* is visually represented in Fig. 40 and Fig. 41, thus highlighting the effectiveness of the antibacterial agent in reducing the bacterial growth. These findings illustrate the impact of varying concentrations of antibacterial agents in combatting bacterial infections, with implications for potential applications in medical and pharmaceutical fields.

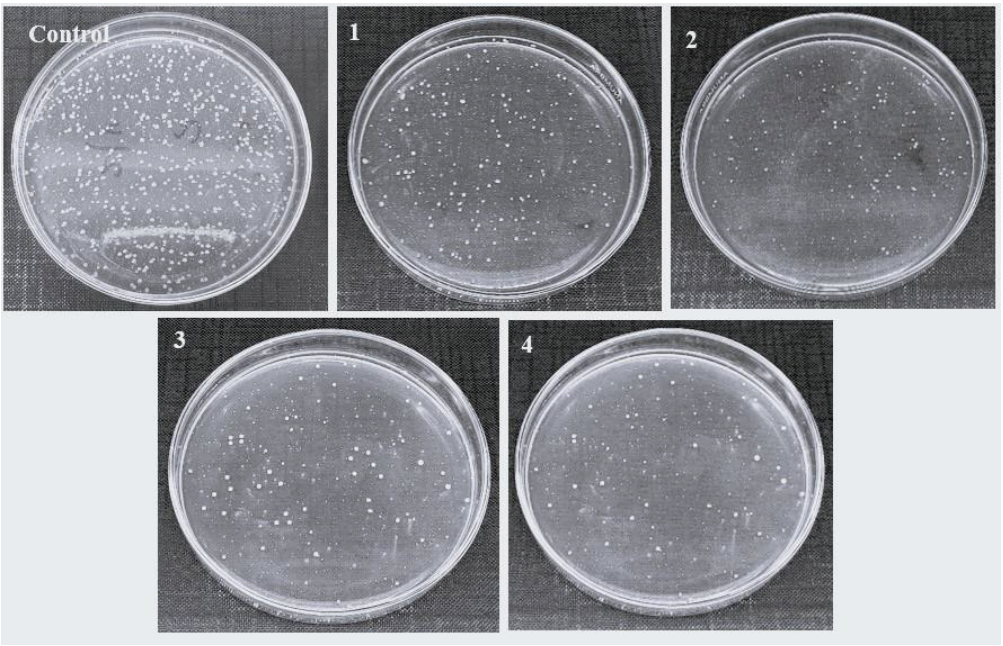


**Fig. 40**. Antibacterial activity of electrospun fibres samples against *S. aureus*: (1) 1% AV; (2) 2% AV; (3) 3% AV; and (4) 4% AV

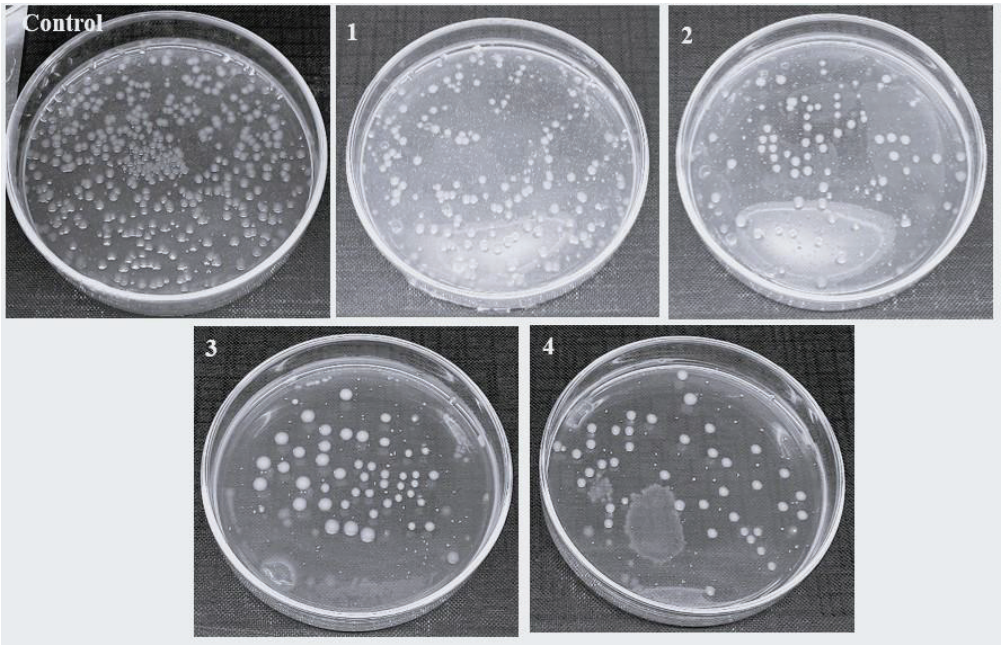


**Fig. 41**. Antibacterial activity of electrospun fibres samples against *E. coli*: (1) 1% AV (2) 2% AV; (3) 3% AV; and (4) 4% AV

It can be observed from Fig. 39 that the antibacterial activity of these samples against *E. coli* is greater than their activity against *S. aureus*. The reason for this can be attributed to the absence of an outer phospholipid bilayer in the cell wall of the gram-positive bacteria *S. aureus*, whereas gram-negative *E. coli* possesses a cell wall which is surrounded by two phospholipid bilayers. Consequently, the task of eradicating *E. coli*, which has a bi-layered structure, becomes challenging, which leads to reduced antibacterial effectiveness [166][168].

Fig. 39 also demonstrates the antibacterial activity of electrospun fibres with a variation in the concentration of ZnO NPs in it. Against *S. aureus*, the samples having a variation in ZnO NPs inhibited the growth of bacteria by killing 94% with 1% ZnO NPs in it to 100% with 4% ZnO NPs in it. Whereas, against *E. coli*, the antibacterial activity got increased from 83% to 99%. A visual representation of a decrease in the *Colony Forming Units* (cfu) against *S. aureus* and *E. coli* is shown in Fig. 42 and Fig. 43. The antibacterial activity against *E. coli* was lower compared to its activity against *S. aureus*. This difference can be attributed to the structural disparity between the two bacteria. *E. coli*, being a gram-negative bacterium, has its cell wall protected by two layers of phospholipids. On the other hand, *S. aureus*, as a gram-positive bacterium, lacks an external phospholipid bilayer to shield its cell membrane. Consequently, the outer lipid layers of *E. coli* hinder the **e** and $h^+$ movements, thereby reducing the effectiveness of redox reactions at the outer layer of ZnO nanoparticles. As a result, the antibacterial activity is less effective in eliminating *E. coli*.

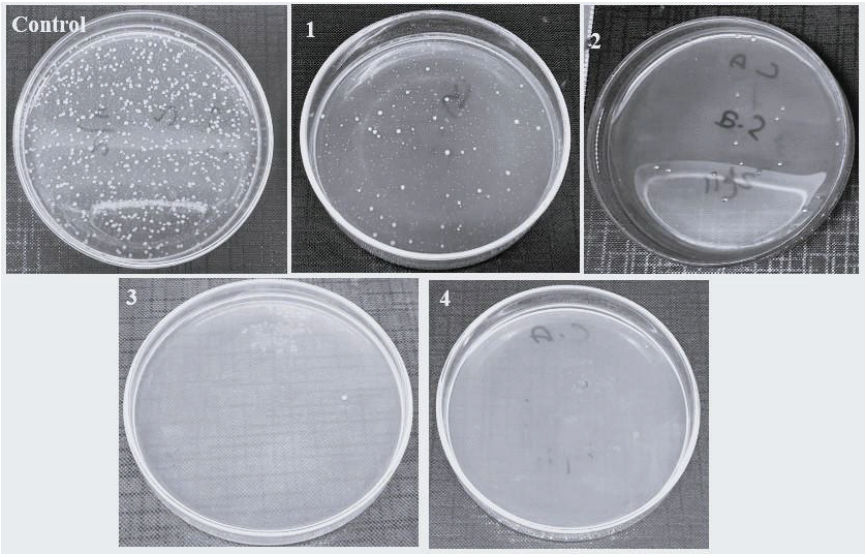


**Fig. 42**. Antibacterial activity of electrospun fibres samples against *S. aureus* (5) 10% PVA/0.5% *Aloe vera*/1% ZnO NPs; (6) 10% PVA/0.5% *Aloe vera*/2% ZnO NPs; (7) 10% PVA/0.5% *Aloe vera*/3% ZnO NPs; (8) 10% PVA/0.5% *Aloe vera*/4% ZnO NPs

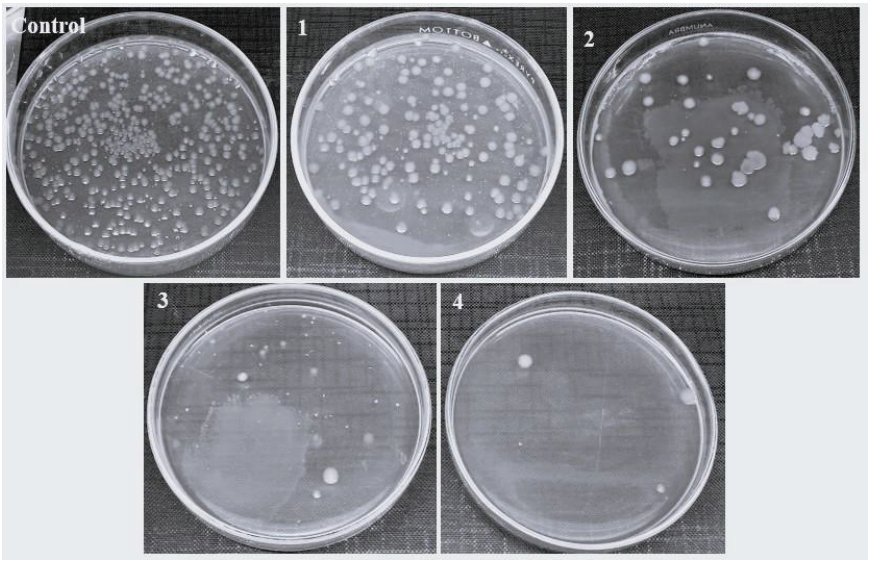


**Fig. 43**. Antibacterial activity of electrospun fibres samples against *E. coli* (5) 10% PVA/0.5% *Aloe vera*/1% ZnO NPs; (6) 10% PVA/0.5% Aloe vera/2% ZnO NPs; (7) 10% PVA/0.5% *Aloe vera*/3% ZnO NPs; (8) 10% PVA/0.5% *Aloe vera*/4% ZnO NPs

**Summary**

The overall impact of increase in concertation of both ZnO and *Aloe vera* to the antibacterial activity was very significant. The point to notice is that AV gel is a natural product, and its antibacterial activity can be observed in all conditions, irrespective of the incident light. Meanwhile, ZnO is a semiconductor, and its photocatalytic and antibacterial activity is dependent on incident light.

### 3.5.2. Antibacterial activity of PLA/CNDs electrospun fibres

As stated in Section 3.3.2, it was concluded that 19% PLA in DMF produces fibres with good morphology, so we selected this concentration and checked the antibacterial activity of the following samples: PLA-19, PLA-19/C1, PLA-19/C2, PLA-19/C3, and PLA-19/C4. Fig. 44 shows a comparison of antibacterial activity against *S. aureus* and *E. coli*. It can be observed that PLA-19 with no CNDs in it showed no antibacterial properties, whereas all other samples showed antibacterial activity due to the addition of CNDs in it. It was also observed that, with the increase in concentration of CNDs in PLA electrospun fibres, the antibacterial activity against both types of bacteria – gram-positive and gram-negative – was observed.

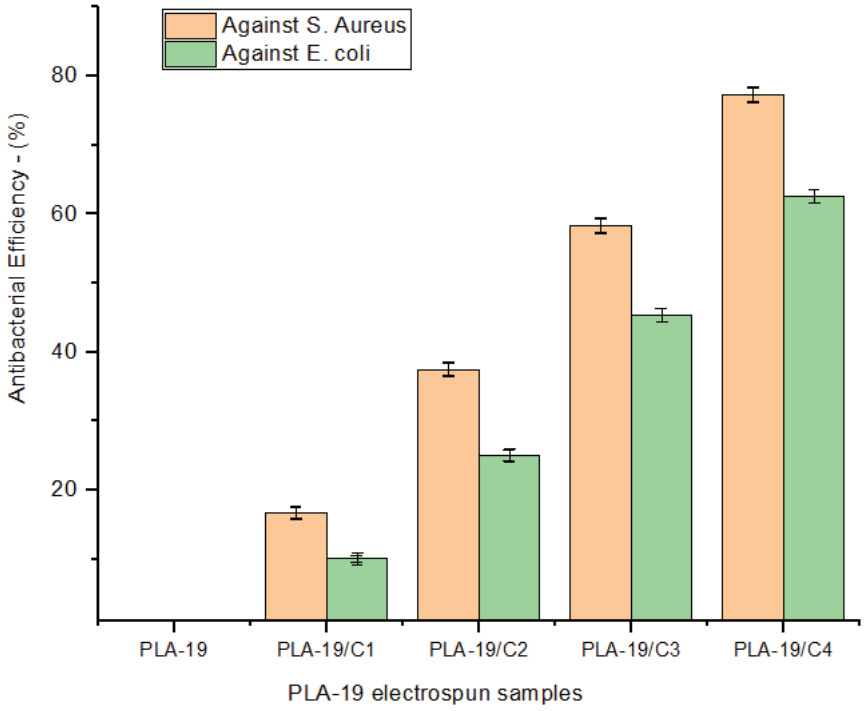


**Fig. 44**. Antibacterial activity against *S. aureus* and *E. coli*

Against *S. aureus*, all the samples having CNDS inhibited the growth of bacteria by killing 16% with 1% CNDs in it up to 77% with 4% CNDs in it. Whereas, against *E. coli*, the antibacterial activity got increased from 10% to 62%. A visual representation of the decrease in the *Colony Forming Unit* (cfu) against *S. aureus* and *E. coli* is shown Fig. 45 and Fig. 46.

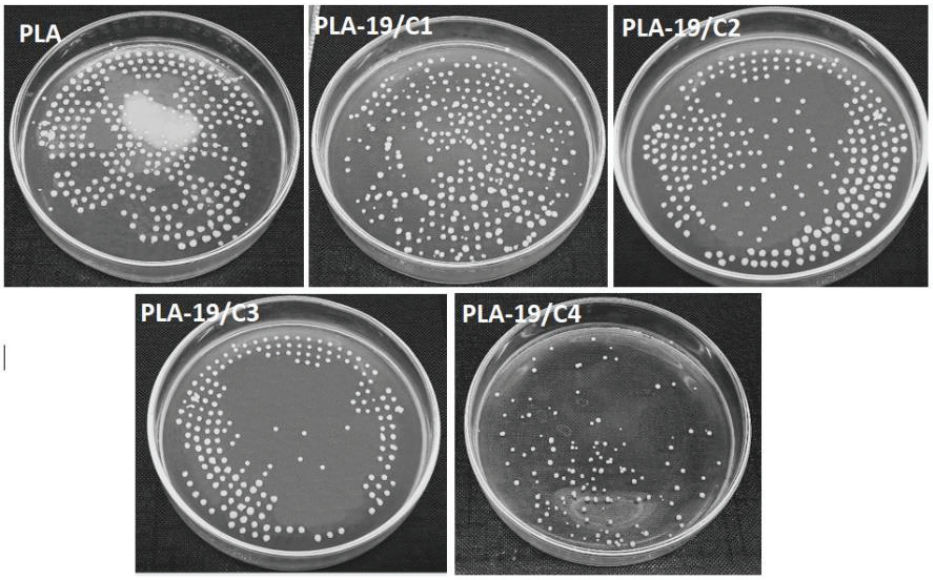


**Fig. 45**. Quantitative measurement of antibacterial activity of 19% PLA electrospun fibres with different CNDs concentration against *E. coli* bacteria

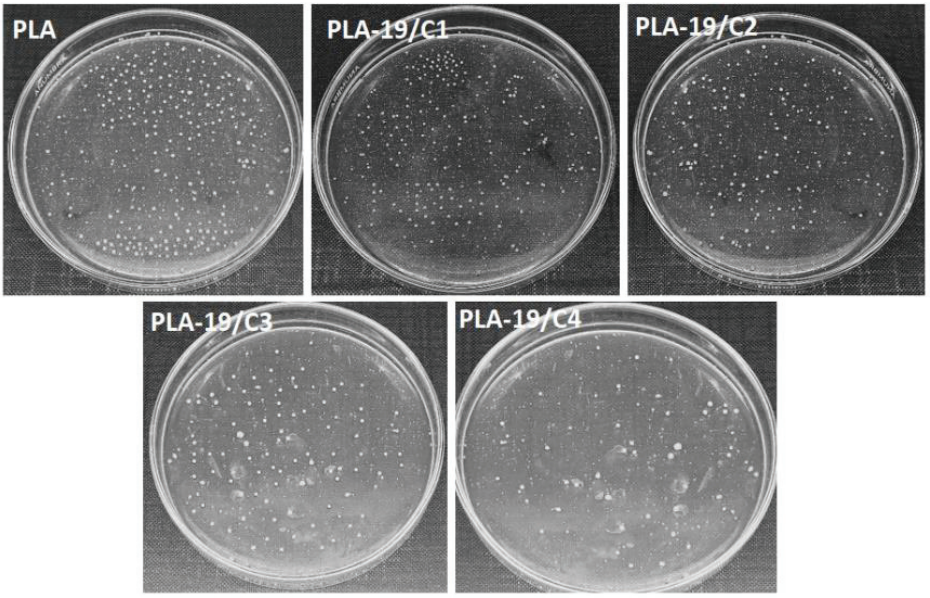


**Fig. 46**. Quantitative measurement of antibacterial activity of 19% PLA electrospun fibres with different CNDs concentration against *S. aureus* bacteria

## Summary

It was noted that, on equal weight basis of CNDs in PLA, the antibacterial effectiveness against *S. aureus* was greater in comparison to *E. coli*. This discrepancy can be elucidated by the fact that *E. coli*, due to being a gram-negative bacterium, possesses a cell wall structure enveloped by two phospholipid layers, which provides added protection. Consequently, the outer lipid layer exhibits resistance towards reactive oxygen species, and this leads to a diminished antibacterial activity.

## 3.6. FTIR Analysis

### 3.6.1. FTIR of AV/PVA/ZnO electrospun fibres

The FTIR analysis was conducted on all the prepared samples of AV/PVA/ZnO in order to ascertain whether the electrospinning process led to the formation of any new functional groups. The FTIR spectra of the electrospun fibres, varying in AV content, were examined, and the findings are presented in Fig. 47. The y-axis in the graph depicts transmittance, while the x-axis represents the wavenumber. It is worth noting that each material possesses a distinctive fingerprint region spanning from 600 to 1400 $cm^{-1}$.

In the case of pure PVA electrospun fibres, the fingerprint region exhibits unique spectral characteristics differentiating it from the other electrospun fibre samples. However, when considering the samples containing 1%, 2%, 3%, and 4% AV, a noteworthy alteration is observed in the –OH peak which becomes notably broadened. This phenomenon can be attributed to the presence of AV within these electrospun fibres, which causes modifications in the spectral signature of the –OH functional group. It is of importance to note that, aside from this broadening of the –OH peak, no additional peaks were observed in any of the samples. This indicates the absence of any new functional groups resulting from the electrospinning process.

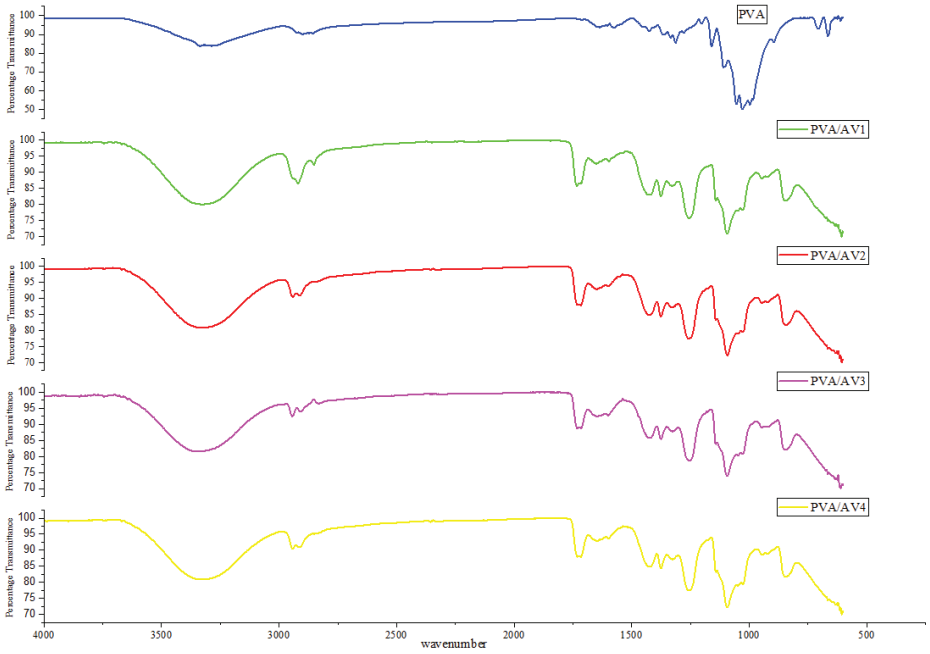


**Fig. 47**. FTIR analysis of samples with 1%, 2%, 3%, and 4% AV

In order to investigate the potential formation of new functional groups, samples with variation in ZnO NPs were also subjected to *Fourier-Transform InfraRed* (FTIR) analysis. The results of this FTIR analysis are presented in Fig. 48. On the graph, the y-axis represents transmittance, while the x-axis denotes the wavenumber. It is important to note that each material possesses a unique fingerprint region within the range of 600 to 1400 $cm^{-1}$.

In this context, the fingerprint region of pure PVA (polyvinyl alcohol) exhibits distinct characteristics differing from those observed in the electrospun fibres containing AV/PVA/ZnO composites. Specifically, when comparing the samples containing 1%, 2%, 3%, and 4% ZnO NPs, their FTIR spectra display remarkable similarities. These spectra do not exhibit any additional peaks or distinctive features, thereby suggesting that no new chemical bonds formed during the electrospinning process.

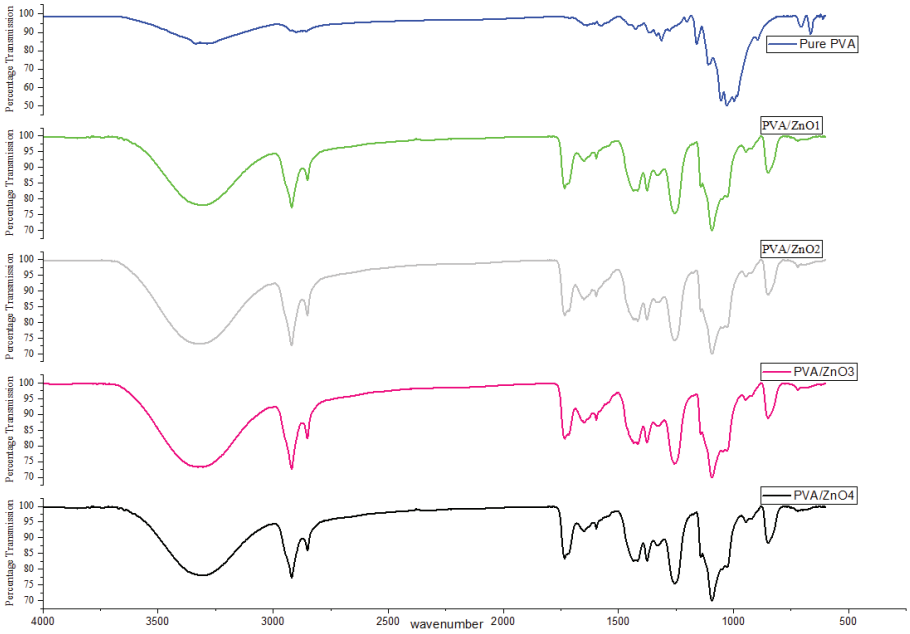


**Fig. 48**. FTIR analysis of samples with 1%, 2%, 3%, and 4% ZnO NPs

## Summary

The incorporation of various concentrations of ZnO NPs into the AV/PVA electrospun fibres does not lead to any discernible alterations in the chemical composition or the formation of novel functional groups. Consequently, the electrospinning process appears to retain the chemical integrity of the AV/PVA/ZnO composite, as evidenced by the absence of new chemical bonds in the FTIR spectra.

### 3.6.2. FTIR of PLA/CNDs electrospun fibres

After the electrospinning process had been carried out by using *PLA-19/C4* on PLA nonwoven fabric, an extensive FTIR (Fourier-transform infrared) analysis was conducted on the resultant samples. The FTIR analysis was performed on the samples in their as-is state, following a post-electrospinning resting period of 24 hours. Electrospinning was conducted for varying durations, specifically, 30, 60, 90, and 120 minutes, while using a feedrate of 0.4 mL for the electrospinning solution. It is remarkable that the collected electrospun fibres displayed a notably low weight addition.

To gain comprehensive understanding of the chemical composition of the electrospun fibres, FTIR spectra were collected and subsequently compared to those of the nonwoven PLA fabric. This comparison, as depicted in Fig. 49, aimed to determine any discernible variations in the peak patterns or additional peaks within the samples. The primary focus of this analysis was to ascertain the presence of any residual dimethylformamide (DMF) in the electrospun fibres.

The outcomes of this comparison revealed the absence of any supplementary peaks in the FTIR spectra of the *PLA-19/C4* electrospun fibres when compared with the nonwoven PLA fabric.

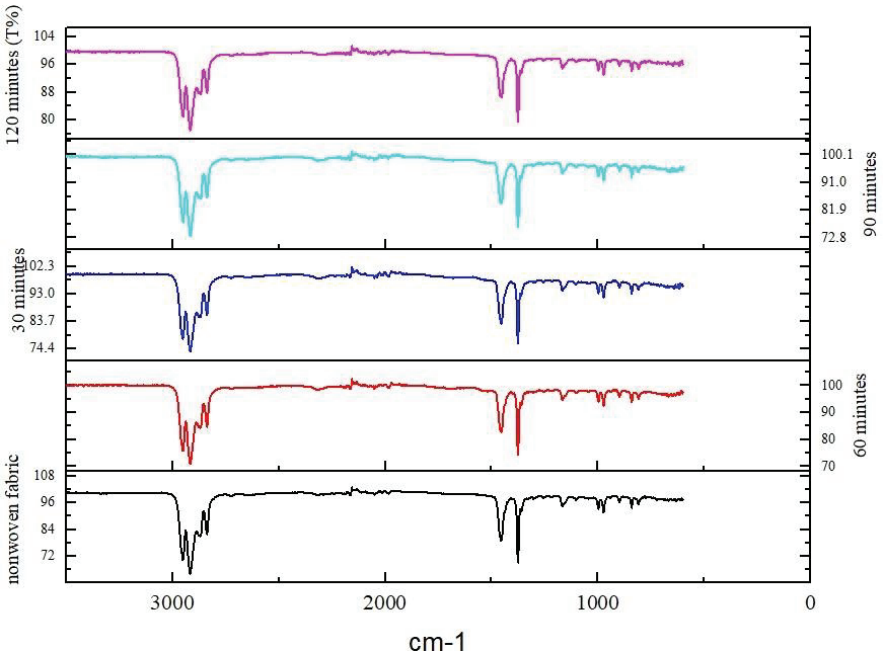


**Fig. 49**. FTIR spectra of PLA-19/C4 samples at different electrospinning times: 30, 60, 90, and 120 min

## Summary

No additional functional groups or substances other than PLA were detected within the electrospun fibre structures. Consequently, the absence of additional peaks in the FTIR spectra strongly suggests the absence of DMF residues in the electrospun fibres. This finding underscores the purity and integrity of the *PLA-19/C4* electrospun fibres, thereby confirming their suitability for applications in the medical filed.

### 3.7. TGA of PLA/CNDs

*ThermoGravimetric Analysis* (TGA) was conducted in order to assess the thermal stability and the potential presence of volatile components within the sample. The sample in question, consisting of electrospun fibres, underwent heating, during which, changes in weight, or any weight losses were being closely monitored. This TGA procedure was executed on electrospun fibres in their as-produced state, approximately 24 hours after their production. Fig. 50 illustrates the TGA curves pertaining to PLA-19 electrospun fibres, encompassing all compositions of *Carbon NanoDots* (CNDs). Interestingly, these curves exhibited analogous behaviours across all four samples. Initially, a linear weight retention trend was observed up to a

temperature of 240 °C. However, as the temperature surpassed this point, decomposition and the subsequent weight loss occurred, commencing at around 250°C and continuing until approximately 270–280 °C.

Remarkably, the TGA curves did not exhibit any distinctive spikes or irregularities suggesting the absence of other volatile compounds or solvents, particularly Dimethylformamide (DMF), which was utilised in the electrospinning process of PLA electrospun fibres.

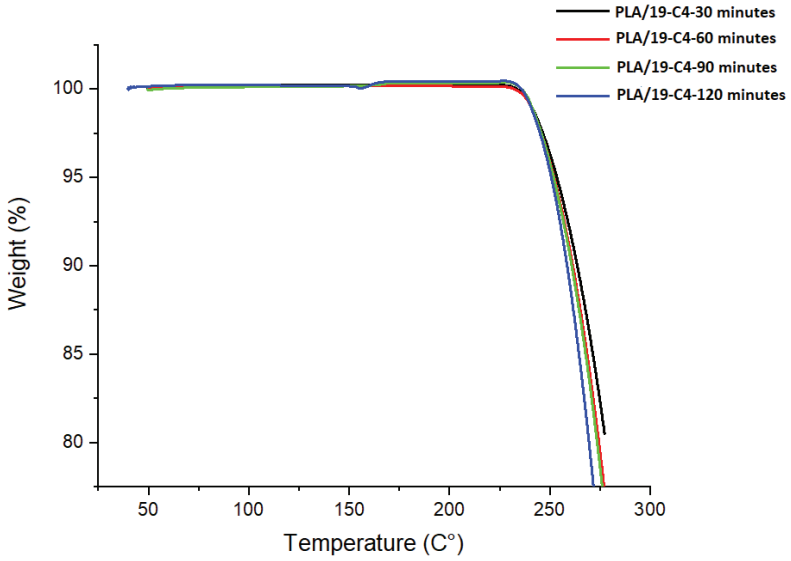


**Fig. 50**. TGA Analysis of PLA-19/C4 electrospun fibres

**Summary**

The primary motivation for conducting this TGA analysis on PLA/CNDs electrospun fibres stemmed from their intended use in medical devices. It was imperative to ascertain whether any residual traces of DMF were present within the electrospun fibres, as its presence could potentially have adverse implications for their suitability in medical applications. Therefore, the TGA results provided valuable insight into the thermal behaviour and purity of these electrospun fibres, thereby instilling confidence in their applicability for medical device fabrication.

### 3.8. Particle Filtration Efficiency Test

#### 3.8.1. Particle filtration efficiency of AV/PVA/ZnO

Particle filtration efficiency of AV/PVA/ZnO electrospun fibres formed with 4% of ZnO was performed to check their filtration to 0.1 microns of particles. This is one of the important requirements of medical face masks. The 4% ZnO loaded PVA was electrospun with different production time rates, specifically, 30, 60, 90, and 120 minutes. The effect of the weight add-on to the particle filtration efficiency was observed. Table 9 represents the PFE results of PVA/$ZnO_4$ electrospun fibres.

**Table 9**. Particle filtration efficiency of 4% ZnO loaded PVA electrospun fibres: various weight add-ons

| Sample # | % ZnO | Electrospinning time (min) | Weight add-on ($g/m^2$) | Particle filtration efficiency (%) |
|---|---|---|---|---|
| PVA/ZnO4 | 4 | 30 | 0.88 | 71.5 |
| | | 60 | 1.78 | 80.7 |
| | | 90 | 2.64 | 84.3 |
| | | 120 | 3.52 | 92.5 |
| Meltblown nonwoven sheet | | | 17.8 | 95.5 |

Table 9 shows the weight add-on and the effect of weight add-on to the PFE of the formed electrospun fibres. With an increase in the electrospinning time, the weight add-on was also increased, and it was calculated in $g/m^2$. With an increase in the weight add-on from 0.88 $g/m^2$ to 1.78 $g/m^2$, the particle filtration efficiency of electrospun fibres also increased from 71.5% to 92.5%.

The PFE of all PVA samples is below the minimum acceptance limit, as compared to a nonwoven meltblown sheet which is typically used in medical face masks. The PFE of a meltblown sheet weighing 1.78 $g/m^2$, when sandwiched between spunbond sheets, is around 95.5%. Contrarily, the PFE of all PVA electrospun fibres weighing 0.88, 1.78, 2.64, and 3.52 $g/m^2$ is below the minimum acceptance range of 95%. Therefore, none of the above PVA samples is feasible for use in medical face masks.

### 3.8.2. Particle filtration efficiency of PLA/CNDs

Particle filtration efficiency of PLA/CNDs electrospun fibres formed with 4% of CNDs was performed to check their filtration to 0.1 microns of particles. This is one of the important requirements of medical face masks. PLA-19/C4 was electrospun with different production time rates, specifically, 30, 60, 90 and 120 minutes. The effect of the weight add-on to the particle filtration efficiency was observed. Table 10 shows the weight add-on along with the effect of the weight add-on to the PFE of the formed electrospun fibres.

**Table 10**. PFE of PLA-19/C4 electrospun fibres with different weight add-ons

| Sample # | PLA % | CNDs % | Electrospinning time (min) | Weight add-on ($g/m^2$) | Particle filtration efficiency (%) |
|---|---|---|---|---|---|
| PLA-19/C4 | 19 | 4% | 30 | 1.49 | 80.0 |

| | | | | | |
|---|---|---|---|---|---|
| | | | 60 | 2.98 | 85.3 |
| | | | 90 | 4.47 | 96.5 |
| | | | 120 | 5.96 | 100 |
| Meltblown nonwoven sheet | | | | 17.8 | 95.0 |

With an increase in the electrospinning time of PLA-19/CNDs, the weight add-on was also increased, and it was thus calculated in g/m$^2$. With an increase in the weight add-on from 1.49 g/m$^2$ to 5.96 g/m$^2$, the particle filtration efficiency of electrospun fibres was also increased from 80% to 100%.

The PFE of all PLA samples with the weight add-on of 4.47 and 5.96 g/m$^2$ fell into the acceptable range, within ca. 96.5% and 100%. As compared to nonwoven meltblown sheet (17.8 g/m$^2$), which is typically used in a medical face mask, the PLA electrospun fibre sheet electrospun at 90 and 120 minutes is more suitable as they provide more PFE with less weight (g/m$^2$) of the material used. It follows that these sustainable, biodegradable nanosheets are suitable to be used in medical face masks. 100% PFE is perfect, yet we must check if it also provides good differential pressure results with the same parameters.

### 3.9. Differential Pressure Test

#### 3.9.1. Differential pressure of AV/PVA/ZnO

Table 11 indicates that an increased accumulation of electrospun fibres on the surface of a nonwoven sheet could have a detrimental effect on the breathability of face masks. To assess this, we examined the differential pressure and observed that electrospinning for 30 and 60 minutes resulted in measurements exceeding the minimum requirements.

However, the pressure values recorded for electrospinning durations of 90 and 120 minutes were 28.5 and 34.6 Pa/cm$^2$, respectively. These values comply with the standards set by EN 14683 and ASTM-F2100-20 for Type I and Type II medical face masks. However, we must also consider the PFE values from Section 3.8.1, and we can thus conclude that even the DF value is within the acceptable range, but these PVA nanosheets cannot be used in medical face masks as they fail to fulfil the minimum requirement of 95% PFE.

**Table 11**. Differential pressure of 4% loaded ZnO electrospun fibres: with weight add-ons

| **Sample #** | **% ZnO** | **Electrospinning time (min)** | **Weight add-on (g/m$^2$)** | **Differential pressure (Pa/cm$^2$)** |
|---|---|---|---|---|
| PVA/ZnO4 | 4 | 30 | 0.88 | Over range |
| | | 60 | 1.78 | Over range |

| | | | | |
|---|---|---|---|---|
| | | 90 | 2.64 | 28.5 |
| | | 120 | 3.52 | 34.6 |
| Meltblown nonwoven sheet | | | 17.8 | 38.5 |

### 3.9.2. Differential pressure of PLA/CNDs

Table 12 indicates the DP values of PLA/CNDs, and it can be observed that an increase in the accumulation of electrospun fibres on the surface of a nonwoven sheet can exert a negative impact on the breathability of face masks. In order to assess this impact, we measured the differential pressure and observed that PLA-19/C4 electrospinning for 30 and 120 minutes resulted in differential pressures below and above the limits. This suggests that the differential pressure is too low for a 30-minute electrospinning process and too high for a 120-minute electrospinning process when using PLA-19/C4. However, the samples obtained at 60 and 90 minutes exhibited differential pressures of 33.6 and 39.0 Pa/cm$^2$, respectively, which falls within the suitable range for ASTM-F2100-20 Type I medical face masks.

Keeping in account the performance of nano sheets as compared to meltblown nonwoven sheets, it can be concluded that the 4.47 g/m$^2$ nano sheet provides more efficiency than the 17.8 g/m$^2$ nonwoven sheet. Thus, these sustainable and biodegradable, CNDs loaded PLA nanosheets can serve as a good alternative to the conventional nonbiodegradable meltblown sheets.

**Table 12**. Differential Pressure of PLA-19/C4 electrospun fibres with different weight add-ons

| **Sample #** | **% PLA** | **% CNDs** | **Electrospinning time (min)** | **Weight add-on (m/m$^2$)** | **Differential pressure (Pa/cm$^2$)** |
|---|---|---|---|---|---|
| PLA-19/C4 | 19 | 4% | 30 | 1.49 | Over range |
| | | | 60 | 2.98 | 33.6 |
| | | | 90 | 4.47 | 39.0 |
| | | | 120 | 5.96 | Over range |
| Meltblown nonwoven sheet | | | | 17.8 | 38.5 |

## 3.10. 3-Ply Prototype with an Electrospun Layer

Sustainable electrospun fibres are the way forward, since we can offer solid scientific grounds to propose them to be used in the filtration layer of medical face mask or respirators. They would combine the benefits of multiple layers for effective filtration with the advanced properties of nanofibres. Here is how we structure our proposal:

Nanofibres should be directly incorporated onto the nonwoven sheet or fabric. To align with the sustainability principles, the nonwoven sheet should also be made from environmentally friendly and biodegradable polymers. This involves covering the collector drum or plate with a sustainable nonwoven fabric. When a potential difference is applied, nanofibres are deposited onto the surface of the nonwoven sheet. This method is recommended due to the considerable difficulty in separating the nanofibre layer from the collector drum or the aluminium foil covering the drum. Additionally, an attempt to peel it off results in immediate breakage, which subsequently leads to the loss of the web structure.
After collecting the electrospun fibres on the nonwoven sheet, there are two potential approaches for utilising this combination in the production of medical face masks. These shall be discussed below:

**Spunbond-nanofibre-spunbond structure**

In this approach, the collected nanofibres are situated on the spunbond sheet; they form a two-layer structure. The upper layer consists of nanofibres, while the other side comprises the spunbond sheet. By adding an additional layer of spunbond sheet on top of the nanofibre layer, a three-layered structure is created, known as the spunbond-nanofibre-spunbond assembly.

This structure is ideal for use in medical face masks. The outer spunbond layers provide mechanical support and stability, while the nanofibre layer in the middle offers exceptional filtration capabilities, by virtue of efficiently capturing particles and viruses.

**Spunbond-nanofibre-nanofibre-spunbond structure**

In this alternative configuration, the nanofibres collected on the spunbond sheet also form a two-layer structure, with nanofibres in the upper layer and the spunbond sheet on the opposite side. By folding this two-layer structure in a manner which positions the spunbond layer as the outermost layers, a unique assembly is created: the spunbond-nanofibre-nanofibre-spunbond structure.

This assembly is advantageous not only for medical face masks but also for respirators. It offers the benefits of two nanofibre layers, due to doubling the filtration efficiency for particles and viruses. The outer spunbond layers provide structural integrity and ensure that the nanofibre layers remain intact and functional.

## 4. CONCLUSIONS

1. PVA and PLA electrospun fibres have been successfully formed with optimised solution parameters. It has been found that 10% PVA in water was enough to obtain electrospun fibres, while, with 12% PLA in DMF, there was only electrospraying, and no fibres were formed. This happened due to the fact that PVA has a much higher molecular weight as compared to PLA. For PLA, it was 19% (w/v in DMF), whereas, for PVA, it was 10% (w/v in water) which came out to be the perfect solution percentages for their electrospinning.
   It has also been found that the solution viscosity and conductivity play their part in electrospinning as well as in the morphology of electrospun fibres:
   - For PVA electrospun fibres, the thinner diameter of electrospun fibres was obtained by 0.056 S/m conductivity and 1490 mPa·s viscosity.
   - For PLA electrospun fibres, good morphology of electrospun fibres was obtained by 0.129 S/m conductivity and 358 mPa·s viscosity.

2. Analysis of the surface morphology of electrospun fibres, functionalised with antibacterial agents, and their chemical composition has been concluded with the following points:

   AV/PVA/ZnO electrospun fibres:
   - For samples with varying concentrations of AV, it has been found that 4% AV in PVA produced thinner electrospun fibres; with an average diameter in the 130 nm range. It has also been found that 4% ZnO produced thinner electrospun fibres with an average of 145 nm.
   - The FTIR analysis of all samples has shown that there are no additional peaks after the formation of electrospun fibres, and it can thus be concluded that no other chemical reaction is ta\king place while producing these electrospun fibres.
   - It has been concluded that 4% AV in PVA and 4% ZnO in PVA are the optimum concentration values for the formation of functionalised PVA electrospun fibres.

   PLA/CNDs electrospun fibres:
   - It has been found that a low concentration of PLA (12%) in DMF results in droplet formation instead of fibre formation during electrospinning. Whereas, 19% PLA in DMF with 4% CNDs produced electrospun fibres with an average of a fibre diameter of 88 nm.
   - FTIR analysis seems to have revealed no additional peaks as compared to PLA which shows that no residual DMF is present in these electrospun fibres. Therefore, it can be concluded that these fibres are safe to be used in medical face masks.

- It has also been found that 19% PLA with 4% CNDs in it produces electrospun fibres with a thinner diameter, and this combination is concluded to be the best option amongst all the alternatives.

3. Functionalisation of PVA with such antibacterial agents as AV and ZnO NPs, and functionalisation of PLA with photoactive material CNDs has proven to impart antibacterial activity against gram-positive and gram-negative bacteria too. The following points have been concluded with respect to their antibacterial activity:
    - 4% AV in PVA provided the highest antibacterial activity of 91.2% against *S. aureus* and 86.9% against *E. coli*.
    - In case of ZnO, 4% of it in PVA provided excellent antibacterial properties with 100% killing of *S. aureus* and 99.2% killing of *E. coli*.
    - With PLA electrospun fibres, it has been found that 4% CNDs provided the highest antibacterial activity, by killing 77.3% of *S. aureus* and 62.5% of *E. coli*.
    - It has also been found that, on the basis of equal weight, the overall antibacterial activity of CNDs was lower as compared to that of AV and ZnO, and the reason behind this phenomenon can be attributed to the fact that CNDs were embedded in and onto the surface of hydrophobic PLA, whereas AV and ZnO were embedded in and onto hydrophilic PVA.
4. Regarding the barrier performance, particulate filtration efficiency (PFE) and differential pressure, it has been concluded that the nanowebs formed with PLA/CNDs showed a better performance as compared to the nanowebs of AV/PVA/ZnO. It has been found that, when PVA/$ZnO_4$ was electrospun for 90 minutes, PFE came out to be 84.3%, whereas, when PLA/CNDs was electrospun for 90 minutes, its PFE was 96.5%. This PLA/CNDs electrospun fibre sheet is perfect to be used in medical face masks, as it offers the minimum barrier performance for particulate filtration efficiency, i.e., 96.5%, while providing acceptable differential pressure, i.e., 39 Pa/$cm^2$.
5. Nanowebs, when compared to the conventional nonwoven webs, exhibit superior filtration properties on an equal weight basis. A PLA nanoweb weighing 4.47 g/$m^2$ demonstrates a higher efficiency in particulate filtration and differential pressure in comparison to a meltblown sheet weighing 17.8 g/$m^2$. Consequently, the utilisation of PLA nanowebs allows for a 75% reduction in the material costs compared to the conventional meltblown sheets. Furthermore, the use of PLA and PVA electrospun fibres can effectively address the issues of disposal and waste associated with face masks since both PLA and PVA are sustainable and biodegradable polymers.

# 5. SANTRAUKA

## ĮVADAS

2019 m. gruodį pasaulis susidūrė su pirmuoju SARS-CoV-2 atveju. Šis virusas buvo labai užkrečiamas ir netrukus išplito visame pasaulyje [1]. Vos per 3 mėnesius užsikrėtimų skaičius taip išaugo, kad 2020 m. kovo 11 d. PSO turėjo paskelbti pasaulinę pandemiją [2] . Dėl šio staigaus SARS-CoV-2 protrūkio ir užkrečiamumo žmonės pirmiausia turėjo imtis atsargumo priemonių, pavyzdžiui, laikytis saugaus atstumo ir naudoti asmenines apsaugos priemones. Šis virusas daugiausia pažeidžia žmogaus kvėpavimo sistemą [3]. Tai sukėlė neįprastai didelį AAP naudojimą ir paklausą. 2020 m. dėl šio SARS-CoV-2 viruso asmeninių apsaugos priemonių rinkos dydis, palyginti su 2019 m., padidėjo 17 %. Pasaulinės AAP rinkos dydis 2022 m. buvo 80 mlrd., ir prognozuojama, kad iki 2029 m. ji padidės iki 111 mlrd. [5].

Kaip ir gripas bei sunkus ūminis kvėpavimo sindromas (SARS), SARS-CoV-2 dažniausiai perduodamas pacientui kosint ar čiaudint lašeliais. Vidutinis kosint, čiaudint, kalbant ar atsidusus iškvepiamų lašelių dydis yra 5 mikronai, o diapazonas, iki kurio pacientas gali platinti virusą, – 1–2 metrai, todėl žmonių buvo prašoma laikytis saugaus bent 2 metrų atstumo vienas nuo kito, taip sumažinant užsikrėtimo virusu galimybę [6]. Prastas vėdinimas vykstant ilgiems užsiėmimamskambaryje taip pat yra viena pagrindinių priežasčių, dėl kurios SARS-CoV-2 žiemą plinta greičiau nei vasarą. Kaip ir vasarą, langai ir durys turi būti atveriami, kad patalpos būtų tinkamai vėdinamos [6]. 2020 m., kol vakcina nuo šio mirtino viruso nebuvo plačiai prieinama, vienintelis būdas sumažinti viruso plitimą buvo laikytis atstumo ir naudoti tinkamas AAP, ypač veido kaukes. Medicininės veido kaukės gali būti labai naudingos, nes uždengia vartotojo nosį ir burną ir yra kliūtis bet kokiems viruso lašeliams plisti kosint, čiaudint ar kalbant [7].

Tradiciškai medicininėms veido kaukėms ir respiratoriams naudojama trijų sluoksnių struktūra iš filjerinės neaustinės medžiagos ir lydymo-pūtimo būdu pagamintos neaustinės medžiagos [8]. Žinoma, kad mikropluoštinė tekstilė, ypač nanopluoštai, pasižymi geresnėmis savybėmis, palyginti su makropluoštinėmis medžiagomis. Taip yra dėl to, kad nanopluoštų skersmuo yra nanometrų diapazone ir sudaro tankų neaustinį tinklelį, kuris taip pat efektyviai gali filtruoti nano- ir mikrodydžio daleles [9].

Yra įvairių būdų gauti šiuos nanopluoštus. Vienas iš plačiai naudojamų nanopluoštų gavimo būdų yra elektrinis verpimas. 1900 m. Johnas Francis Cooley'us pateikė pirmąjį elektrinio verpimo patentą. Tada 1964 m. seras Geoffrey'us Ingramas Tayloras pasiūlė matematinį kūgio formavimosi iš lašelių paviršiaus elektrinėje dėžutėje modelį. Jis yra žinomas kaip Taylore'o kūgis pagal Geoffrey'ų Ingramą Taylorą. Nuo 1995 m. nanopluoštų formavimas elektrinio verpimo būdu tapo svarbia mokslinių tyrimų sritimi [10] .

Elektrinio verpimo būdu paruošti nanopluošto tinkleliai pasižymi puikiomis savybėmis, todėl gali būti naudojami kaip filtravimo sluoksnis medicininėse veido kaukėse ir respiratorių filtruose. Vienkartinių veido kaukių tvarumas ir poveikis aplinkai vis dar yra problema, todėl polimerinės nanomembranos buvo paruoštos

naudojant skirtingus tvarius polimerus. Šie polimerai buvo funkcionalizuoti antimikrobinėmis medžiagomis, efektyviai kovojančiomis su bakterijomis.

**Daktaro darbo tikslas:**

Tyrimo tikslas – elektrinio verpimo būdu sukurti medicininėms veido kaukėms skirtus tvarius, antibakterinėmis medžiagomis funkcionalizuotus pluoštus ir nustatyti šių funkcionalizuotų pluoštinių dangų barjerines savybes.

**Šiam tikslui pasiekti buvo nustatyti šie tikslai:**

- Optimizuoti tirpalo parametrus tvarių polimerų, tokių kaip PVA ir PLA, elektriniam verpimui.
- Išanalizuoti gautų pluoštų paviršiaus morfologiją ir cheminę sudėtį bei nustatyti optimalią polimerų masės procentinę sudėtį elektriniam verpimui.
- Įvertinti nanopluoštų, funkcionalizuotų alavijais, cinko oksidu ir anglies nanodalelėmis, antimikrobines savybes.
- Įvertinti sukurtų prototipų ir medicinoje naudojamų veido kaukių barjerines savybes.

**Mokslinis naujumas**

Doktorantūros tyrimus apibendrinančiame darbe pristatomi tvarių ir labai funkcionalių elektrinio verpimo pluoštų kūrimo metodai, naudojant pažangiausią elektrinio verpimo techniką. Buvo atlikti išsamūs tyrimai, siekiant ištirti puikias natūralių ir fotoaktyvių medžiagų, tokių kaip alavijas, ZnO ir anglies nanodalelės, antibakterines galimybes, todėl buvo atliktas išsamus ir įtikinamas jų veikimo palyginimas.

Ypatingą dėmesį reikia atkreipti į anglies nanodalelių priedus PLA nanopluoštuose, kurie pasižymi ne tik tvarumu ir biologiniu skaidumu, bet ir išskirtinėmis funkcinėmis savybėmis matomoje šviesoje, atsižvelgiant į CND būdingą fotoaktyvų elgesį. Šie nanopluoštai yra proveržis, suderinantis aplinkosauginį sąmoningumą ir patobulintą funkcionalumą, nustatantis naują tvarių medžiagų standartą įvairiose srityse.

Be to, tiriant sukurtus medicininės paskirties prototipus, tiek PVA, tiek PLA nanopluoštai pasižymėjo geresnėmis barjerinėmis savybėmis, palyginti su įprastinėmis neaustinėmis medžiagomis. Šių tyrimų rezultatai turi didžiulį potencialą pakeisti apsaugines medicinos priemones, pasiūlant sustiprintą apsaugą ir užtikrinant aukščiausius saugos standartus.

**Praktinė darbo vertė**

Šis tyrimas parodė, kad funkcionalizuoti elektrinio verpimo būdu gauti pluoštai gali būti naudojami kaip filtravimo sluoksnis medicinos priemonėse. Siūlomas daugiasluoksnis modelis: vidurinis sluoksnis, sudarytas iš nanopluoštų, ir išoriniai sluoksniai, sudaryti iš filjerinės neaustinės medžiagos; tai taip pat gali būti naudojama respiratoriuose ir neaustiniuose chirurginiuose chalatuose. Šiame tyrime pateiktas modelis atitinka tarptautinius I tipo/1 lygio medicininių veido kaukių reikalavimus.

Tokių apsauginių sluoksnių pramoninis naudojimas taip pat yra labai paprastas ir įmanomas, be to, tai sumažintų išlaidas, palyginti su įprastomis lydalo pūtimo būdu pagamintomis neaustinėmis medžiagomis, įprastai naudojamomis medicininėse veido kaukėse.

**Autoriaus indėlis**

Šioje daktaro disertacijoje pateikiami autoriaus surinkti ir išanalizuoti rezultatai. Autorius rūpinosi šios daktaro disertacijos rezultatų paskelbimu.

Kai kurie doktorantūros tyrimai buvo atlikti bendradarbiaujant su Nanotechnologijų tyrimų laboratorija Nacionaliniame tekstilės universitete Pakistane. Autorius dirbo kuriant ekologiškas alavijo/PVA/ZnO nanomembranas ir patarė, kaip jas pritaikyti tekstilėje. Autorius suplanavo ir atliko visus AV/PVA/ZnO nanopluoštų gamybos tirpalo elektrinio verpimo technika eksperimentus.

Kita didelė dalis doktorantūros tyrimų buvo atlikta bendradarbiaujant su dr. Thomas Mayer-Gall laboratorija DTNW, Vokietijoje. Autorius suplanavo ir atliko visą PLA/CND pluoštų gamybą elektrinio verpimo būdu.

## 5.1. Literatūros apžvalgos santrauka

**Medicinos prietaisai**

Pagal ISO 13485:2016(E) standarto, kuris susijęs su medicinos prietaisų kokybės valdymo sistemomis, 3 skirsnį, medicinos prietaisas apibrėžiamas kaip bet koks instrumentas, aparatas, įrenginys, mašina, prietaisas, implantas, reagentas, skirtas naudoti *in vitro*, programinė įranga, medžiaga ar panašus gaminys. Šiuos prietaisus galima naudoti atskirai arba kartu įvairiais medicininiais tikslais, įskaitant:

1. Ligos diagnostiką, prevenciją, stebėseną, gydymą arba priežiūrą.
2. Traumų diagnostiką, stebėjimą, gydymą, priežiūrą ar kompensavimą.
3. Anatomijos ar fiziologinio proceso tyrimus, pakeitimus, modifikavimus arba priežiūrą.
4. Gyvybės palaikymą arba priežiūrą.
5. Pastojimo kontrolę.
6. Medicinos prietaisų dezinfekciją.
7. Informacijos teikimą atliekant mėginių, paimtų iš žmogaus kūno, tyrimą *in vitro*.

Remiantis šiuo aprašymu, veido kaukės, barjerinės veido dangos, chirurginės kaukės ir respiratoriai, naudojami COVID-19 profilaktikai ir kontrolei, laikomi medicinos prietaisais. Šią klasifikaciją patvirtino JAV maisto ir vaistų administracija (FDA), kuri reguliuoja šiuos prietaisus, įskaitant medžiaginius veido apdangalus ir chirurgines kaukes, kai jie skirti medicininiams tikslams, pavyzdžiui, siekiant užkirsti kelią COVID-19 plitimui. Pasaulio sveikatos organizacija (PSO) taip pat palaiko šį apibrėžimą ir pateikia pasaulinę pavyzdinę medicinos prietaisų, įskaitant *in vitro* diagnostikos medicinos prietaisus, reguliavimo sistemą, skatindama valstybes nares

kurti ir įgyvendinti reguliavimo kontrolę ir regionines gaires, siekiant užtikrinti medicinos prietaisų kokybę, saugą ir veiksmingumą savo šalyse.

**Bendra medicininių veido kaukių ir respiratorių struktūra**

Veido kaukė yra medicinos prietaisas, dengiantis nosį ir burną ir veikiantis kaip fizinė kliūtis, filtruojanti įeinantį ir išeinantį oro srautą. Kai vartotojas čiaudi, kosėja ar kalba, kaukė filtruoja lašelius ir neleidžia jiems išplisti aplinkoje. Panašiai įkvėpimo metu kaukė išfiltruoja lašelius iš išorės, suteikdama apsaugą dėvėtojui. Medicininės veido kaukės paprastai gaminamos iš trijų neaustinių medžiagų sluoksnių: dviejų išorinių sluoksnių formai palaikyti ir vidinio filtravimo sluoksnio. Nors jie tam tikru mastu gali filtruoti virusus, bakterijas, daleles ir lašelius, dėl laisvo tvirtinimo ant veido gali patekti šiek tiek nefiltruoto oro.

**Nanopluoštai medicininėje tekstilėje**

Elektrinio verpimo procesas yra universalus būdas sukurti nanopluoštus iš įvairių polimerų, įskaitant natūralias ir sintetines medžiagas, taip pat biologiškai skaidžius ir biologiškai neskaidžius variantus. Šis universalumas pastaraisiais metais įgavo augančią svarbą, nes vis daugiau dėmesio skiriama tvariems ir biologiškai skaidiems polimerams, ką lėmė aplinkos ir sveikatos problemos. Tokių polimerų pavyzdžiai yra kolagenas, alginatas, chitozanas, celiuliozės acetatas, želatina, polietilenglikolis ir kt.

Kai kurie natūralūs polimerai turi jiems natūraliai būdingų antimikrobinių savybių, o kiti gali būti modifikuoti, kad į juos būtų įterptos antimikrobinės medžiagos. Šie nanopluoštai, turintys antimikrobinių savybių, yra labai pageidaujami įvairioms reikmėms dėl jų biologinio suderinamumo, netoksiškumo ir biologinio skaidumo. Pavyzdžiui, chitozanas, natūralus polisacharidas, pasižymi antimikrobinėmis savybėmis dėl savo unikalaus teigiamo krūvio, kuris leidžia sąveikauti su bakterijų ląstelių sienelėmis ir sutrikdyti esminius jų procesus. Be to, nanopluoštai gali būti įmirkomi biologiškai aktyviomis medžiagomis iš žolelių, tokių kaip *Centella asiatica* ir žaliosios arbatos ekstraktas, taip sustiprinant jų antimikrobines ir žaizdų gydymo savybes. *Aloe vera* gelis, žinomas dėl savo minkštumo ir antimikrobinių savybių, taip pat gali būti įterptas į nanopluoštus, pagamintus iš tokių medžiagų, kaip PCL, PVA ir chitozanas, taip dar labiau sustiprinant jų antimikrobines savybes.

Svarbu pažymėti, kad šių natūralių medžiagų veiksmingumas, suteikiant nanopluoštams antimikrobines savybes, gali skirtis atsižvelgiant į tokius veiksnius, kaip augalų rūšys, apdorojimo metodai ir laikymo sąlygos. Tyrėjai nustatė šių medžiagų išsiskyrimo nanopluoštuose kinetiką ir optimizavo jų įterpimo į skirtingas polimerines matricas sąlygas. Apibendrinant galima pasakyti, kad natūralių antimikrobinių savybių turinčių nanopluoštų panaudojimas yra daug žadantis kelias įvairioms reikmėms, siūlantis funkcionalumo, biologinio suderinamumo ir tvarumo derinį.

**Nanopluoštai, papildyti sintetinėmis antimikrobinėmis medžiagomis**

Mokslininkai sukūrė sintetinius nanoskalės dydžių antimikrobinius agentus, kurie pasižymi geresnėmis savybėmis, palyginti su didesnių dydžių medžiagomis. Šios nanodalelės gali būti įterptos į nanopluoštus elektrinio verpimo būdu, todėl jos yra tinkamos nanopluoštų gamybai. Šios nanomedžiagos turi skirtingus antimikrobinius mechanizmus, kai kurios slopina augimą dėl savo krūvio pobūdžio, o kitos sukuria reaktyviąsias deguonies rūšis. Sidabro nanodalelės (Ag NP) buvo plačiai naudojamos kaip antimikrobinės medžiagos ir pasižymėjo dideliu antibakteriniu aktyvumu, biologiniu suderinamumu ir minimaliu toksiškumu. Tyrimai parodė, kad Ag nanodalelės veiksmingai veikia SARS-CoV-2, tiek slopinant virusą, tiek mažinant užsikrėtimo dažnį.

Varis ir jo junginiai, įskaitant vario (I) jodidą, taip pat pasižymi stipriomis antivirusinėmis ir antibakterinėmis savybėmis. Vario nanodalelės ir vario oksidai buvo panaudoti respiratoriuose ir veido kaukėse, pasižyminčiose dideliu antivirusiniu veiksmingumu. Tačiau svarbu atsižvelgti į galimą riziką ir neigiamą poveikį, susijusį su vario nanodalelėmis.

Įrodyta, kad cinko oksido nanodalelės (ZnO NP) veiksmingai veikia įvairius patogenus, ypač bakterijas, ir yra laikomos saugiomis sąlyčiui su žmonėmis. ZnO NP antivirusinės veiklos tyrimai yra riboti, tačiau jie parodė poveikį SARS-CoV-2. Nustatyta, kad sudėtiniai nanotinkleliai, kuriuose yra ZnO nanodalelių, pasižymi puikiomis antibakterinėmis savybėmis ir gali būti naudojami veido kaukėse.

Titano dioksido nanodalelės (TiO2 NP) turi minimalų toksiškumą žmogui ir turi antibakterinį bei antivirusinį poveikį fotokataliziniu būdu generuojant reaktyviąsias deguonies rūšis. TiO2 nanopluoštai pasižymi dideliu filtravimo efektyvumu ir gali būti naudojami veido kaukėse ir respiratoriuose.

Geležies oksido nanodalelės (IONP) pasižymi biologiniu suderinamumu ir magnetinėmis savybėmis, todėl yra tinkamos naudoti medicinoje. Jos pasižymi ir antivirusinėmis bei antimikrobinėmis savybėmis įvairiais mechanizmais ir gali būti padengtos polimerais, kad sustiprėtų jų aktyvumas.

Anglies pagrindu pagamintos nanomedžiagos, įskaitant grafeną ir anglies nanovamzdelius, įrodė, kad slopina SARS-CoV-2 užkrečiamumą. Šių medžiagų naudojimas gali apriboti virusų ir bakterijų užkrečiamumą. Anglies nanodalelės arba anglies kvantiniai taškai atsirado kaip medžiagos, turinčios fotokatalizinių ir antibakterinių savybių, siūlančios tokių pranašumų, kaip matomos šviesos aktyvavimas ir reaktyviųjų deguonies rūšių generavimas.

Apskritai, nanodydžio sintetinės antimikrobinės medžiagos pasirodė turinčios didelį potencialą kovojant su patogenais, įskaitant SARS-CoV-2, ir gali būti naudojamos įvairiose srityse, tarp jų veido kaukėse ir respiratoriuose.

**Aplinkosauginiai AAP šalinimo aspektai**

Dėl staigaus vienkartinių asmeninių apsaugos priemonių (AAP), ypač medicininių veido kaukių, naudojimo padidėjimo visame pasaulyje susidaro nemažas kiekis atliekų, kasdien ne mažiau kaip 7200 tonų. Medicininės veido kaukės labai prisideda prie šių atliekų kiekių augimo. Šios AAP paprastai gaminamos iš biologiškai

neskaidžių medžiagų, pvz., neaustinių polipropileno medžiagų arba sintetinių pluoštų / polimerų, keliančių didelę grėsmę sausumos ir jūros organizmams. Remiantis JT aplinkosaugos programa, maždaug 75 % išmestų veido kaukių patenka į sąvartynus arba į vandenyną. Reaguodami į šias aplinkosaugos problemas, mokslininkai sutelkė dėmesį į biologiškai skaidžių ir ekologiškų medicininių veido kaukių kūrimą.

Asmeninių apsaugos priemonių (AAP) atliekos gali sukelti įvairius poveikius aplinkai, įskaitant šiuos:

1. Padidėjęs atliekų kiekis sąvartynuose: AAP, pavyzdžiui, vienkartinės kaukės, pirštinės ir chalatai, prisideda prie bendro atliekų kiekio sąvartynuose. Kadangi AAP gaminiai paprastai gaminami iš biologiškai neskaidžių sintetinių medžiagų, jie ilgą laiką išlieka aplinkoje.

2. Vandens telkinių užteršimas: netinkamai šalinant AAP gali atsirasti šiukšlių, kurios pateks į vandens telkinius, pavyzdžiui, upes, ežerus ir vandenynus. Ši tarša kenkia vandens gyvybei. Be to, kai AAP skyla į mikroplastiką, jos dar labiau užteršia vandens šaltinius ir paveikia jūrų ekosistemas.

3. Oro tarša: AAP naikinti kartais naudojamas deginimas. Deginant AAP į atmosferą išskiriami kenksmingi teršalai ir šiltnamio efektą sukeliančios dujos, o tai prisideda prie oro taršos ir klimato kaitos.

4. Laukinių gyvūnų įsipainiojimas ir nurijimas: netinkamai išmestos AAP, ypač kaukės ir pirštinės, kelia pavojų laukinei gamtai. Gyvūnai gali įsipainioti į išmestas AAP ir susižaloti arba mirti. Jūrų gyvūnai, tokie kaip vėžliai ir jūros paukščiai, gali supainioti AAP su maistu ir jį nuryti, tai gali sukelti vidinius sužalojimus arba užsikimšimus.

5. Išteklių švaistymas: AAP gamybai reikia išgauti gamtos išteklius, energiją ir vandenį. Išmetus AAP po vienkartinio naudojimo, šie ištekliai naudojami nuolat.

Siekiant sumažinti AAP atliekų poveikį aplinkai, galima imtis veiksmų, kurie gali būti:

1. Tinkamas šalinimas: asmenys turėtų išmesti AAP į tam skirtas dėžes arba konteinerius, pavyzdžiui, medicininių atliekų konteinerius, vadovaudamiesi vietinių valdžios institucijų pateiktomis atliekų šalinimo gairėmis.

2. Perdirbimas ir pakartotinis naudojimas: kai tik įmanoma, reikia stengtis perdirbti tam tinkamas AAP rūšis, pavyzdžiui, plastikinius veido skydelius. Be to, siekiant sumažinti atliekų susidarymą, galima apsvarstyti daugkartinio AAP naudojimo galimybes.

3. Švietimas ir informuotumas: informuotumo apie AAP atliekų poveikį aplinkai skatinimas per šviečiamąsias kampanijas gali paskatinti atsakingą atliekų šalinimą.

4. Inovacijos ir tvarios alternatyvos: moksliniai tyrimai ir plėtra gali būti sutelkti į aplinkai nekenksmingų, biologiškai skaidomų arba lengvai perdirbamų AAP medžiagų kūrimą. Tai gali padėti sumažinti ilgalaikį AAP atliekų poveikį.

Labai svarbu, kad asmenys, organizacijos ir vyriausybės bendradarbiautų mažinant AAP šalinimo ir atliekų poveikį aplinkai, taikydamos atsakingą šalinimo praktiką ir tvarias alternatyvas.

**Tvarūs sprendimai**

Padidėjęs vienkartinių asmeninių apsaugos priemonių (AAP), ypač medicininių veido kaukių, naudojimas lemia didelius atliekų kiekius. Šios atliekos, sudarytos iš biologiškai neskaidžių medžiagų, kelia grėsmę aplinkai. Netinkamas AAP šalinimas prisideda prie tokių problemų, kaip vandens ir oro tarša, laukinės gamtos įsipainiojimas ir apsinuodijimas, pernelyg didelis išteklių naudojimas. Siekiant išspręsti šias problemas, labai svarbu sukurti aplinkai nekenksmingas alternatyvas tradiciniams polimerams, kurie būtų biologiškai skaidūs.

Polivinilo alkoholis (PVA) turi pranašumų, palyginti su biologiškai neskaidžiais polimerais. Pirma, PVA yra biologiškai skaidi medžiaga, kurią gali skaidyti aplinkoje esantys mikroorganizmai, taip sumažinant jos ilgalaikį poveikį aplinkai. Skirtingai nuo biologiškai neskaidžių polimerų, PVA nesikaupia sąvartynuose ar vandenynuose, o tai padeda sumažinti taršą. Be to, PVA pasižymi puikiomis plėvelę formuojančiomis savybėmis, todėl tinka tokiems procesams, kaip elektrinis verpimas, taip pat gali būti naudojamas medicinos prietaisuose. Be to, PVA yra mažai toksiškas ir laikomas saugiu tiek žmonėms, tiek gyvūnams. Papildžius tinkamomis antimikrobinėmis medžiagomis, PVA gali būti paverstas nanopluoštais / nanotinkleliais, kurie gali būti panaudoti medicininėse veido kaukėse.

Kitas polimeras, galintis sumažinti poveikį aplinkai, yra polipieno rūgštis (PLA). PLA turi didelių pranašumų, palyginti su biologiškai neskaidžiais polimerais. Pirma, PLA gaunama iš atsinaujinančių išteklių, pavyzdžiui, kukurūzų ar cukranendrių, todėl tai yra tvaresnis pasirinkimas. Tai sumažina priklausomybę nuo iškastinio kuro ir prisideda prie mažesnio anglies pėdsako. Antra, PLA yra biologiškai skaidus, tai reiškia, kad jis gali natūraliai suskilti aplinkoje, įskaitant pramoninius kompostavimo įrenginius, sumažindamas atliekų kaupimąsi. Be to, PLA tinka elektriniam verpimui, todėl galima gaminti nanotinklelius, kurie gali būti naudojami medicininėse veido kaukėse, taip sumažinant atliekų šalinimo ir aplinkosaugos problemas.

## 5.2. Medžiagos ir metodai

**Medžiagos**

Cinko oksido (ZnO) nanodalelės miltelių pavidalu, kurių dydis mažesnis nei 200 nm, ir polivinilo alkoholis (PVA) (MW: 85000–124000) buvo nupirkti iš „Sigma-Aldrich Corporation“ (St Louis MO, JAV). Alavijų lapai buvo paimti iš Pakistano namų sodo.

Polilakto rūgštis 4060D įsigyta iš „Nature-Works LLC“. PLA buvo granulių pavidalo, jo lydymosi temperatūra 210 $^{o}$C. Dimetilformamidas buvo nupirktas iš „Merck“. Gliukozamino hidrochloridas (98 % grynumo) buvo įsigytas iš „Thermos Fischer“ (Šanchajus, Kinija), o 1,3-diaminobenzenas (99 % grynumo) – iš „Carl Roth“.

**Tirpalų ruošimas elektriniam verpimui**

Norint suformuoti AV/PVA/ZnO elektrinio verpimo pluoštus, visam elektrinio verpimo tirpalui buvo paimtas pastovus 10 % PVA kiekis tirpale, o jame naudotas kintamas AV ir ZnO kiekis. Pagal 5.2.1 13 **lentelė**. buvo paruošti 8 mėginiai, 4 su skirtingomis ZnO koncentracijomis ir 4 su skirtingomis AV koncentracijomis.

**13 lentelė**. Eksperimento, skirto AV/PVA/ZnO elektrinio verpimo pluoštams formuoti, planas

| Pavadinimo pavyzdys | PVA (%, w/v) | AV (%, w/v) | ZnO NPs (%, w/v) |
|---|---|---|---|
| AV1/PVA/ZnO0.5 | 10% | 1% | 0,5% |
| AV2/PVA/ZnO0.5 | 10% | 2% | 0,5% |
| AV3/PVA/ZnO0.5 | 10% | 3% | 0,5% |
| AV4/PVA/ZnO0.5 | 10% | 4% | 0,5% |
| AV0.5/PVA/ZnO1 | 10% | 0,5% | 1% |
| AV0.5/PVA/ZnO2 | 10% | 0,5% | 2% |
| AV0.5/PVA/ZnO3 | 10% | 0,5% | 3% |
| AV0.5/PVA/ZnO4 | 10% | 0,5% | 4% |
| AV-0/PVA/ZnO-0 | 10% | 0 | 0 |

AV / PVA / ZnO pluoštams sukurti buvo naudojamas adatinio elektrinio verpimo būdas. Norimas AV / PVA / ZnO tirpalas buvo įdėtas į plastikinį švirkštą su metaline adata, kuris vėliau buvo prijungtas prie siurblio, kad būtų tinkamai tiekiamas elektrinio verpimo tirpalas. Metalinė adata buvo prijungta prie teigiamo įtampos įtaiso elektrodo, o tarp adatos galo ir kolektoriaus buvo išlaikytas 20 cm atstumas. Taikyta 17 kV elektros įtampa, kurios pakako pluoštams iš tirpalo generuoti. Elektrinio verpimo kameroje buvo palaikoma 25°C temperatūra ir 65 % santykinė drėgmė.

Norėdami gauti PLA elektrinio verpimo pluoštą su CND, vadovaudamiesi 5.2.2.14 **lentelė**., pirmiausia paruošėme elektrinio verpimo tirpalą.

**14 lentelė**. Eksperimento, skirto PLA/CNDs elektrinio verpimo pluoštams formuoti, planas

| Sample # | PLA koncentracija (%, w/v) | CND koncentracija (%, w/v) |
|---|---|---|
| PLA-12 | 12 | – |
| PLA-15 | 15 | – |
| PLA-17 | 17 | – |
| PLA-17/C1 | 17 | 1 |
| PLA-17/C2 | 17 | 2 |
| PLA-17/C3 | 17 | 3 |
| PLA-17/C4 | 17 | 4 |
| PLA-19 | 19 | – |

| | | |
|---|---|---|
| PLA-19/C1 | 19 | 1 |
| PLA-19/C2 | 19 | 2 |
| PLA-19/C3 | 19 | 3 |
| PLA-19/C4 | 19 | 4 |

PLA buvo ištirpintas dimetilformamide, nuolat maišant 6 valandas, kad PLA ištirptų tinkamai. PLA / CND pluoštams formuoti buvo panaudota adatinė elektrinio verpimo technika. Norimas tirpalas buvo pilamas į plastikinį švirkštą su metaliniu adatos antgaliu, uždedant švirkštą ant švirkštinės pompos. Besisukančio kolektoriaus būgno plotas buvo 255 $cm^2$, o tarp adatos galiuko ir kolektoriaus būgno išlaikytas 17 cm atstumas, naudota 23 kV elektros įtampa. Elektrinio verpimo kameroje buvo palaikoma 25°C temperatūra ir 65 % santykinė drėgmė. Elektrinio verpimo mašinos schema pateikta 5.2.1 51 **pav**.

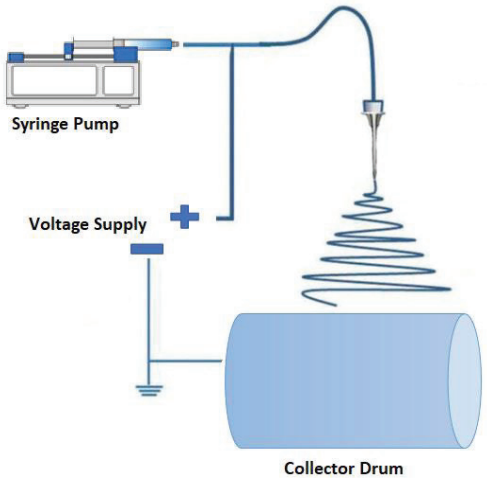


**51 pav**. Elektrospiningo sąrankos iliustracija

**CND sintezė**

CND paruošti pirmiausia buvo pagaminti du tirpalai. Pirmasis tirpalas buvo paruoštas ištirpinant gliukozamino hidrochloridą (1,00 g, 4,63 mmol) 20 ml dejonizuoto vandens 250 ml kolboje. Maišant gautas homogeninis tirpalas. Antrasis tirpalas buvo paruoštas atskiroje kolboje, ištirpinant 1,3-diaminobenzeną (0,55 g, 5,10 mmol) 10 ml metanolio. Kolba buvo įdėta į ultragarsinį aparatą, kad būtų gautas homogeniškas tirpalas. Abu tirpalai kruopščiai sumaišyti, tada mišinys įdėtas į mikrobangų krosnelę gerai vėdinamoje vietoje ir 3 minutes švitintas 800 W ir 90 % galia. Po šio švitinimo buvo gauta tiršta rudos spalvos į aliejų panaši medžiaga. Ji buvo ištirpinta 10 ml dejonizuoto vandens ir centrifuguojama 4000 aps/min 1 valandą. Kadangi buvo siekiama ištirpinti PLA DMF, gauti CND buvo disperguoti tame pačiame DMF tirpale.

**ZnO NP sintezė**

Cinko acetato dihidratas Zn (CH3COO)2.2H2O (kaip cinko šaltinis) ir natrio hidroksidas (NaOH) buvo naudojami santykiu 7:1 200 ml metanolyje, kaip pirmtakai

gaminant ZnO NP. Tirpalas ruošiamas apvaliadugnėje kolboje, maišant 75 minutes. Gautas tirpalas centrifuguotas 6400 aps/min. greičiu 30 minučių 4 $^{o}$C temperatūroje, kad būtų gautos ZnO nanodalelės.

**Charakterizavimo būdai**

Norint įvertinti elektrinio verpimo būdu pagamintų pluoštų paviršiaus morfologiją ir skersmenį, buvo atlikta skenuojamoji elektroninė mikroskopija (SEM) (Hitachi Model S-3400N, „Hitachi High Technologies Europe GmbH“, Tokijas, Japonija). Vidutinis skersmuo iš SEM vaizdų buvo apskaičiuotas naudojant „ImageJ“ programinę įrangą. Norint gauti vidutinį pluošto skersmenį, buvo atlikta 100 matavimų.

*Antibakterinis tyrimas*

Antibakterinis elektrinio verpimo būdu pagamintų pluoštų aktyvumas nustatytas pagal ISO 20645:2004 standartą. Kiekybinei antibakterinio aktyvumo analizei įvertinti buvo naudotas ISO 20743:2013 standartas.

*Fizinio barjero veikimo bandymas*

Filtravimo efektyvumo bandymo procedūra buvo atlikta pagal ASTM F2299 standartą. Dalelių filtravimo efektyvumo reikalavimai medicininėms veido kaukėms ir respiratoriams yra apibrėžti tarptautiniais standartais, siekiant užtikrinti jų efektyvumą filtruojant ore esančias daleles, įskaitant virusus ir bakterijas. Du dažniausiai naudojami standartai yra ASTM F2100 ir ASTM F2299 medicininėms veido kaukėms ir EN 149 respiratoriams.

Bandinių slėgio skirtumui matuoti buvo panaudota diferencinio slėgio bandymo mašina „Qinsun Instruments Co.“, Ltd, modelis G285 pagal standartą EN 14683:2014.

## 5.3. Rezultatai ir jų aptarimas

**Elektrinio verpimo tirpalų klampa ir laidumas**

Elektrinio verpimo metu naudojamų tirpalų klampumas ir laidumas vaidina lemiamą vaidmenį nustatant gautų nanopluoštų charakteristikas. 5.3.1 lentelėje pateikiamas išsamus šių parametrų aprašymas. Grynas PVA tirpalas pasižymi didele klampa – 1130 mPa·s, nes jo molekulinė masė svyruoja nuo 85000 iki 124000. Didėjant molekulinei masei, didėja ir klampa, kas lemia ilgų grandinių susipynimus.

**15 lentelė**. AV/PVA/ZnO tirpalų klampa ir laidumas

| **Bandinio kodas** | **Konc. polivinilo alkoholio (%, g/ml)** | **Konc. alavijų (AV) (%)** | **Konc. cinko oksido nanodalelių (g/ml)** | **Klampa (mPa·s)** | **Laidumas (S/m)** |
|---|---|---|---|---|---|
| AV1/PVA/ZnO0.5 | 10 % | 1 % | 0,50 % | 1310 | 0,0505 |

| | | | | | |
|---|---|---|---|---|---|
| AV2/PVA/ZnO0.5 | 10 % | 2 % | 0,50 % | 1390 | 0,0530 |
| AV3/PVA/ZnO0.5 | 10 % | 3 % | 0,50 % | 1450 | 0,0542 |
| AV4/PVA/ZnO0.5 | 10 % | 4 % | 0,50 % | 1490 | 0,0560 |
| AV0.5/PVA/ZnO1 | 10 % | 0,50 % | 1 % | 1190 | 0,0530 |
| AV0.5/PVA/ZnO2 | 10 % | 0,50 % | 2 % | 1230 | 0,0570 |
| AV0.5/PVA/ZnO3 | 10 % | 0,50 % | 3 % | 1260 | 0,0625 |
| AV0.5/PVA/ZnO4 | 10 % | 0,50 % | 4 % | 1305 | 0,0657 |
| AV-0/PVA/ZnO-0 | 10 % | 0 | 0 | 1130 | 0,0430 |

Klampos matavimai buvo atlikti 27 °C temperatūroje standartinėmis laboratorinėmis sąlygomis. Kai į PVA tirpalą buvo pridėta alavijo ir ZnO nanodalelių, klampumas padidėjo nuo 1310 iki 1490 mPa·s, nes tirpalo sudėtis pasikeitė nuo 1 % alavijų ir 0,5 % ZnO nanodalelių iki 4 % alavijų ir 0,5 % ZnO nanodalelių. Be to, didėjant alavijų koncentracijai, laipsniškai didėjo ir laidumas. Šis klampumo padidėjimas esant didesnei alavijų koncentracijai sutampa su kitų tyrėjų išvadomis. Kita vertus, tiriant skirtingas ZnO nanodalelių koncentracijas, klampa padidėjo nuo 1190 iki 1305 mPa·s, kai koncentracija pakito nuo 1 % iki 4 %. Tačiau ZnO nanodalelių įtaka klampai buvo palyginti nereikšminga. Be to, pastebimai padidėjo tirpalo laidumas esant didesnei ZnO nanodalelių koncentracijai, o tai gali būti siejama su padidėjusiu laidumu, susijusiu su didesniu ZnO puslaidininkinių nanodalelių kiekiu – koreliaciją taip pat pastebėjo kiti tyrėjai.

16 lentelė. pateikta visų paruoštų PLA ir PLA/CND tirpalų klampa ir laidumas. Šie parametrai yra labai svarbūs, nes jie turi įtakos gautų pluoštų morfologijai. Padidėjus PLA koncentracijai DMF, klampumas padidėjo nuo 177 mPa·s 12 % iki 335 mPa·s 19 %. Tačiau klampumo padidėjimas nebuvo reikšmingas dėl mažesnės PLA molekulinės masės. Taip pat buvo pastebėtas klampumo padidėjimas didėjant CND koncentracijai, nors jis buvo palyginti mažas, nes CND dalelių dydis buvo apie 10–15 nm.

**16 lentelė**. PLA ir PLA/CNDs tirpalų klampa ir laidumas

| **Bandinio numeris** | **PLA koncentracija (%, mol/l)** | **CND koncentracija (%)** | **Klampa (mPa·s)** | **Laidumas (S/m)** |
|---|---|---|---|---|
| PLA-12 | 12 | – | 177 | 0,0004 |
| PLA-15 | 15 | – | 230 | 0,0006 |
| PLA-17 | 17 | – | 285 | 0,0008 |
| PLA-17/C1 | 17 | 1 | 288 | 0,0450 |
| PLA-17/C2 | 17 | 2 | 291 | 0,0666 |
| PLA-17/C3 | 17 | 3 | 296 | 0,1020 |
| PLA-17/C4 | 17 | 4 | 305 | 0,1260 |
| PLA-19 | 19 | – | 335 | 0,0012 |

| | | | | |
|---|---|---|---|---|
| PLA-19/C1 | 19 | 1 | 339 | 0,0465 |
| PLA-19/C2 | 19 | 2 | 345 | 0,0702 |
| PLA-19/C3 | 19 | 3 | 351 | 0,1065 |
| PLA-19/C4 | 19 | 4 | 358 | 0,1290 |

Gryni PLA tirpalai, kurių koncentracija buvo 12 %, 13 %, 15 % ir 17 %, pasižymėjo mažu laidumu, net mažesniu nei 0,001 S/m. Tai galima paaiškinti tuo, kad PLA yra nelaidi medžiaga. Į tirpalą pridėjus CND, atsirado elektros laidumas. Visų PLA / CND tirpalų elektrinis laidumas padidėjo didėjant CND koncentracijai. 19 % PLA tirpalo laidumas padidėjo nuo 0,0465 S/m su 1 % CND iki 0,129 S/m su 4 % CND. Tai gali būti siejama su dideliu CND, kaip medžiagos, laidumu.

**Dalelių dydžio analizė**

Tyrėjai naudojo Zeta sizemer, dinaminio šviesos sklaidos metodą, norėdami ištirti ZnO nanodalelių (NP) dalelių dydį. 5.3.1 52 pav. parodytas ZnO NP dydžio pasiskirstymas. Analizė atskleidžia, kad vidutinis ZnO NP dydis yra 50 nm, svyruoja nuo 37, 8 nm iki 68, 1 nm. Nagrinėjant skenuojamojo elektroninio mikroskopo (SEM) vaizdus, nebuvo matomų ZnO nanodalelių ant nanopluoštų ar jų viduje dėl didesnio nanopluošto dydžio (daugiau nei 100 nm), palyginti su santykinai mažesnėmis ZnO nanodalėmis, maždaug 50 nm. Nepaisant to, ZnO NP buvimą galima patvirtinti antimikrobiniais rezultatais, o tai rodo, kad jie yra įterpti į PVA nanopluošto paviršių ir šerdį.

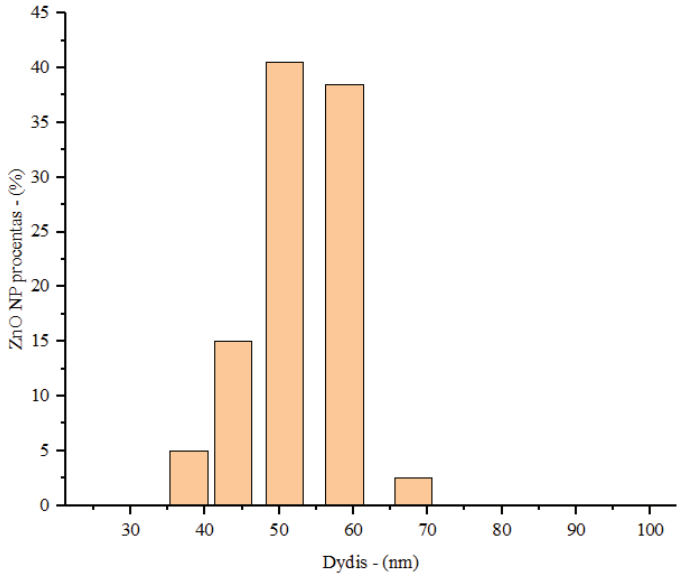


**52 pav**. ZnO nanodalelių dydžio pasiskirstymas

Anglies nanodotų (CND) hidrodinaminis dydis buvo įvertintas naudojant Zeta sizemer (DLS). 5.3.2 pav. parodytas anglies nanodalelių dydžio pasiskirstymas.

Nustatyta, kad anglies nanodalelės yra gana mažos – nuo 7,5 nm iki 15,7 nm, o vidutinis dydis – 10,2 nm. Nors dėl didesnio nanopluošto dydžio (daugiau nei 100 nm) ir labai mažo anglies nanodalelių dydžio (vidutiniškai apie 10 nm) SEM vaizduose ant nanopluošto ar jų viduje nebuvo matomų anglies nanodalelių, jų buvimą galima patvirtinti antimikrobiniais rezultatais.

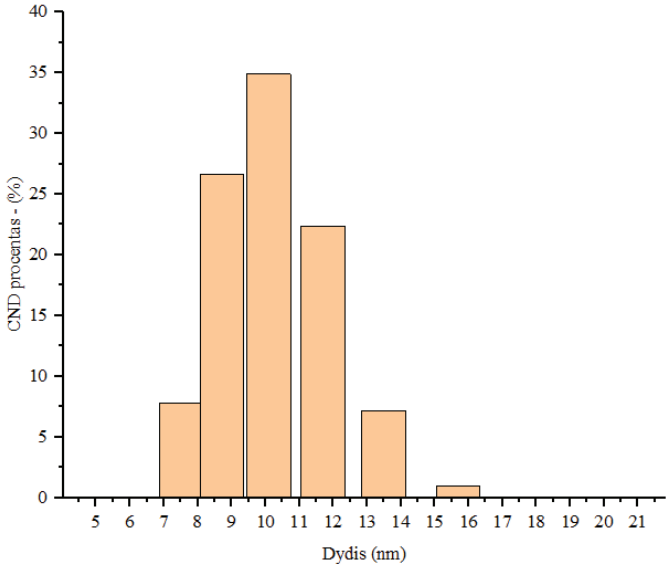


**53 pav**. Anglies nanodalelių dydžio analizė

**SEM analizė**

**AV/PVA/ZnO nanopluoštų SEM analizė**

AV/PVA/ZnO nanopluoštų morfologija ir skersmuo buvo analizuojami naudojant skenuojamąją elektroninę mikroskopiją (SEM). SEM rezultatai 5.3.3 54 pav. rodo nanopluoštus su skirtingu alijošiaus (AV) kiekiu. Nanopluoštai pasižymi plonu ir vientisu skersmeniu su minimaliu klasterizavimu, greičiausiai dėl ZnO nanodalelių. Pradiniam nanopluoštų skersmeniui matuoti buvo naudojama „ImageJ“ programinė įranga. Buvo apskaičiuojamas 100 matavimų vidurkis, paimtas iš skirtingų to paties pluošto vietų ir iš skirtingų pluoštų.

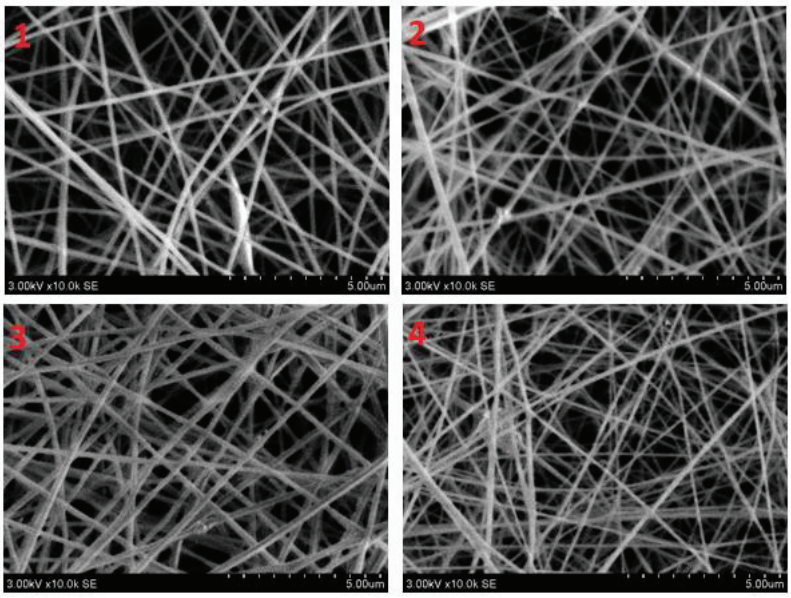


**54 pav**. Elektrinio verpimo pluošto SEM vaizdai: (1) 1 % AV; (2) 2 % AV; (3) 3 % AV; (4) 4 % AV

SEM vaizdai 5.3.4 55 pav.iliustruoja gijines dangas su skirtingomis ZnO nanodalelių koncentracijomis. Pluoštai atrodo lygūs ir taisyklingi, panašūs į grynus PVA pluoštus. Tačiau matomas dėmių susidarymas nanopluoštuose, o didesnė ZnO nanodalelių koncentracija lemia daugiau dėmių.

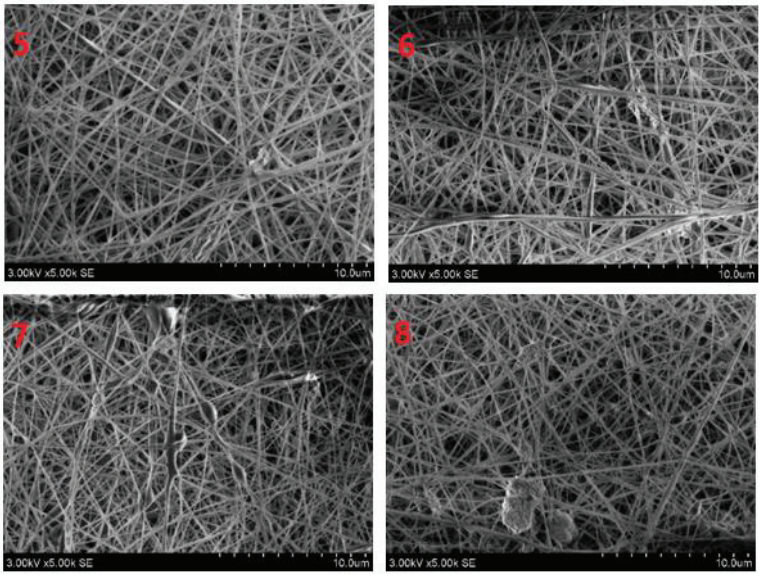


**55 pav**. Elektrinio verpimo pluoštų SEM vaizdai: (5) 1 % ZnO NPs; (6) 2 % ZnO NPs; (7) 3 % ZnO NPs; (8) 4 % ZnO NPs

ZnO nanodalelių koncentracijos pokytis turi pastebimą, bet ne ryškų poveikį gijų skersmeniui. Padidinus ZnO nanodalelių koncentraciją nuo 1 % iki 4 %, vidutinis skersmuo sumažėjo nuo 165 nm iki 145 nm. Šio koncentracijos pokyčio reikšmingumui nustatyti atliktas statistinis palyginimas, naudojant apskaičiuotą *tα* reikšmę (25,27) ir statistinę reikšmę (*tαst* = 1,98), kurių patikimumas *α* = 0,95. Didesnė apskaičiuota *tα* reikšmė rodo aiškią skirtingų ZnO nanodalelių koncentracijų įtaką susidariusių nanopluoštų morfologijai.

**PLA/CND nanopluoštų SEM analizė**

Atlikta pluoštų, pagamintų iš PLA (polipieno rūgšties) ir PLA/CND (anglies nanodalelių, SEM analizė. Visi mėginiai buvo analizuojami naudojant SEM, o pluoštų skersmuo buvo apskaičiuotas matuojant skirtingas gijas ir skirtingas to paties pluošto vietas. Tirpalo parametrai, įskaitant polimero koncentraciją, buvo tiriami pradedant nuo mažos koncentracijos PLA (12 % DMF) be CND, siekiant nustatyti jų tinkamumą elektriniam verpimui pagal apibrėžtus proceso parametrus. PLA-12 atveju buvo pastebėtas lašelių susidarymas, o ne gijų dėl mažos PLA molekulinės masės, kuri neužtikrina pakankamo klampumo, kad susidarytų nanopluoštas. Buvo ištirtas PLA-15, 17 ir 19 % DMF (be CND), o PLA koncentracijos padidėjimas paskatino nanopluoštų susidarymą. Skirtingų koncentracijų grynų PLA nanopluoštų SEM vaizdai pateikti 5.3.5 56 pav.

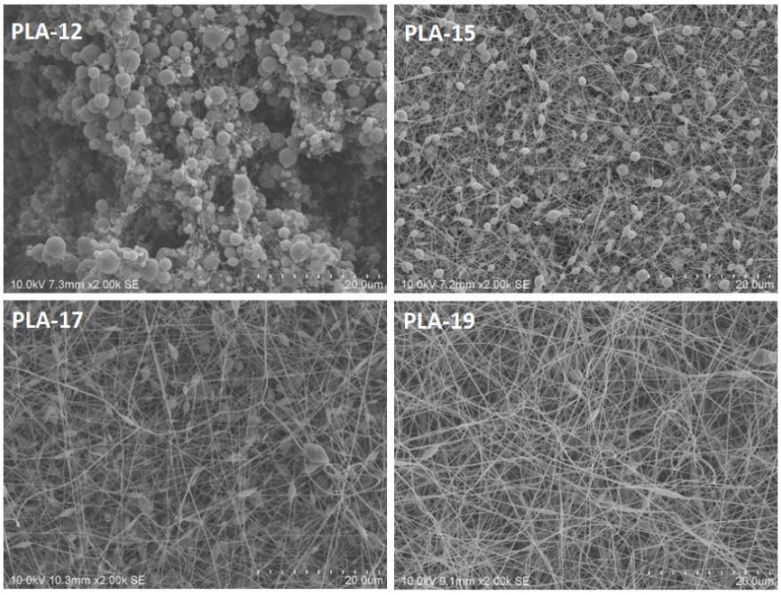


**56 pav**. Gryno 12, 15, 17 ir 19 % koncentracijos PLA elektrinio verpimo pluošto SEM vaizdai (mastelis – 20 μm)

Remiantis pastebėtu geru gijų susidarymu, tolesniems tyrimams buvo parinktos 17 % ir 19 % PLA koncentracijos DMF. Kad PLA nanopluoštams būtų suteiktas antimikrobinis aktyvumas, į elektrinio verpimo tirpalą buvo pridėta fotoaktyvių CND. SEM analizė (5.3.6 56 **pav**. ) pluoštų, turinčių 17 % PLA ir skirtingos koncentracijos CND, parodė, kad, padidinus CND koncentraciją, skersmuo gautas mažesnis. PLA-

17/C1 vidutinis skersmuo buvo maždaug 178 ± 37 nm, o PLA-17/C4 skersmuo buvo 98 ± 25 nm. CND pridėjimas padidino PLA tirpalo laidumą. Panašus elgesys buvo pastebėtas 19 % PLA ir skirtingomis CND koncentracijomis pluoštuose. Šių gijų SEM analizė parodyta 5.3.7 57 *pav*. Nustatyta, kad, padidinus CND koncentraciją PLA, skersmuo sumažėjo nuo 150 ± 40 nm (PLA-19/C1) iki 88 ± 25 nm (PLA-19/C4).

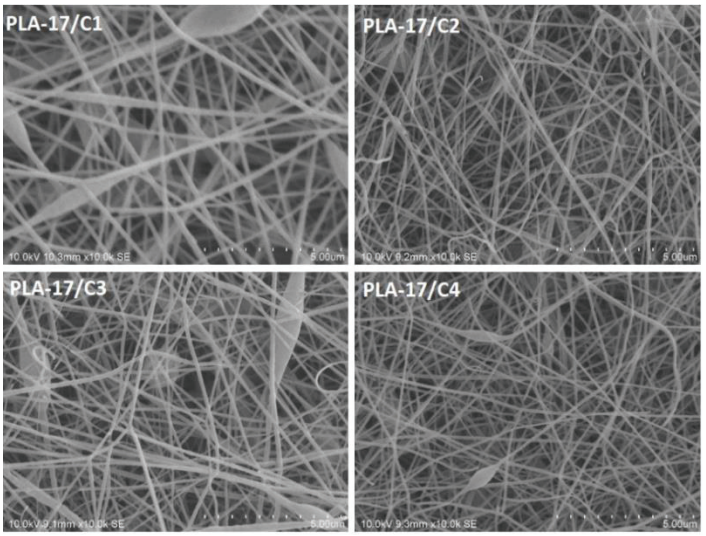


**56 pav**. 17 % PLA su kintamu CND kiekiu – 1, 2, 3 ir 4% elektrinio verpimo pluoštų SEM vaizdai (mastelis – 5 μm)

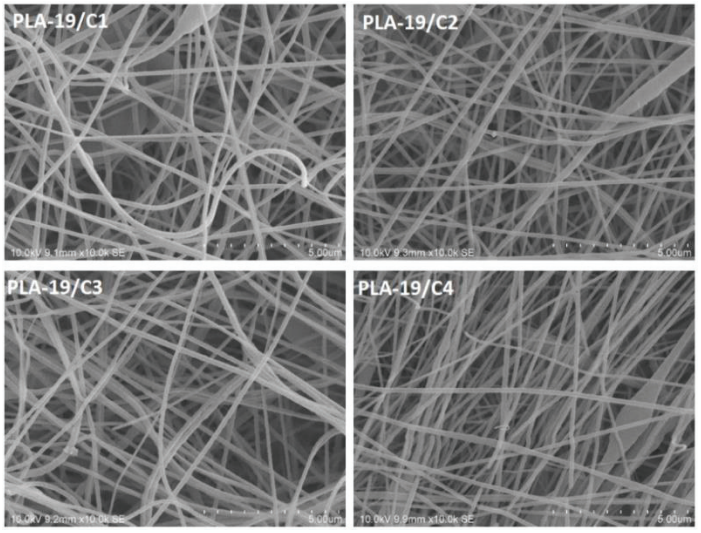


**57 pav**. 19% PLA su kintamu CND kiekiu – 1, 2, 3 ir 4 % elektrinio verpimo pluoštų SEM vaizdai (mastelis – 5 μm)

**AV/PVA/ZnO pluoštų EDX analizė**

Elektrinio verpimo būdu pagamintų pluoštų EDX analizė atlikta siekiant nustatyti ZnO nanodalelių egzistavimą. Ištyrus spektrinius duomenis, nustatyta specifinių smailių, atitinkančių cinką (Zn) ir deguonį (O). Šių elementų buvimas parodė, kad elektrinio verpimo pluoštuose yra ZnO nanodalelių.

**FTIR analizė**

**AV/PVA/ZnO pluošto FTIR analizė**

FTIR analizė buvo atlikta su visais paruoštais AV / PVA / ZnO pavyzdžiais, siekiant išsiaiškinti, ar elektrinio verpimo procesas paskatino naujų funkcinių grupių susidarymą. Mėginiams su skirtinga ZnO NP koncentracija buvo atlikta Furjė transformacijos infraraudonųjų spindulių (FTIR) analizė. Nustatyta, kad įvairių koncentracijų ZnO NP įterpimas į AV/PVA elektrinio verpimo pluoštus nesukelia jokių pastebimų cheminės sudėties pakitimų ar naujų funkcinių grupių susidarymo. Elektrinio verpimo procesas išlaiko cheminį AV/PVA/ZnO kompozito vientisumą, ką rodo naujų cheminių jungčių nebuvimas FTIR spektruose.

**PLA/CNDs pluošto FTIR analizė**

Po PLA-19/C4 elektrinio verpimo proceso gautiems bandiniams buvo atlikta išsami FTIR (Furjė transformacijos infraraudonųjų spindulių) analizė. Šio tyrimo rezultatai atskleidė, kad PLA-19/C4 pluoštų FTIR spektruose nėra jokių papildomų smailių, palyginti su PLA medžiaga. Tai reiškia, kad elektrinio verpimo pluošto struktūrose nebuvo aptikta jokių papildomų cheminių junginių ar medžiagų, išskyrus PLA. Vadinasi, papildomų smailių nebuvimas FTIR spektruose rodo, kad pluoštuose nėra DMF likučių. Tai rodo PLA-19/C4 pluošto grynumą ir vientisumą.

**Antimikrobinis aktyvumas**

**AV/PVA/ZnO nanopluoštų antimikrobinis aktyvumas**

Antimikrobinės medžiagos, įskaitant AV ir ZnO nanodaleles (NP) skirtingomis proporcijomis, buvo tirtos pagal ISO 20645:2004. Buvo ištirtas AV/PVA/ZnO bandinių antimikrobinis aktyvumas ir nustatyta, kad AV gelyje yra antrachinonų, kurie suteikia antimikrobinį poveikį. Cinamo rūgštis, kita AV sudedamoji dalis, slopina bakterijų augimą, priešindamasi gliukozės įsisavinimui. ZnO NP pasižymi antimikrobinėmis savybėmis dėl jų puslaidininkinio elgesio. Bandinių antimikrobiniam aktyvumui nustatyti buvo paruoštos agaro plokštelės su bakterijomis, o mėginiai išdėlioti ant paviršiaus. Siekiant įvertinti jų antimikrobinį veiksmingumą, buvo išmatuota slopinimo zona aplink mėginius. Rezultatai parodė, kad, padidinus AV koncentraciją, slopinimo zona padidėjo, o ZnO NP koncentracija reikšmingos įtakos slopinimo zonai neturėjo. Tačiau mėginių su ZnO NP paviršiuje nebuvo matomo augimo, o tai rodo jų veiksmingumą naikinant bakterijas. Antibakterinių bandymų rezultatų santrauka pateikta 5.3.8 58 **pav.**

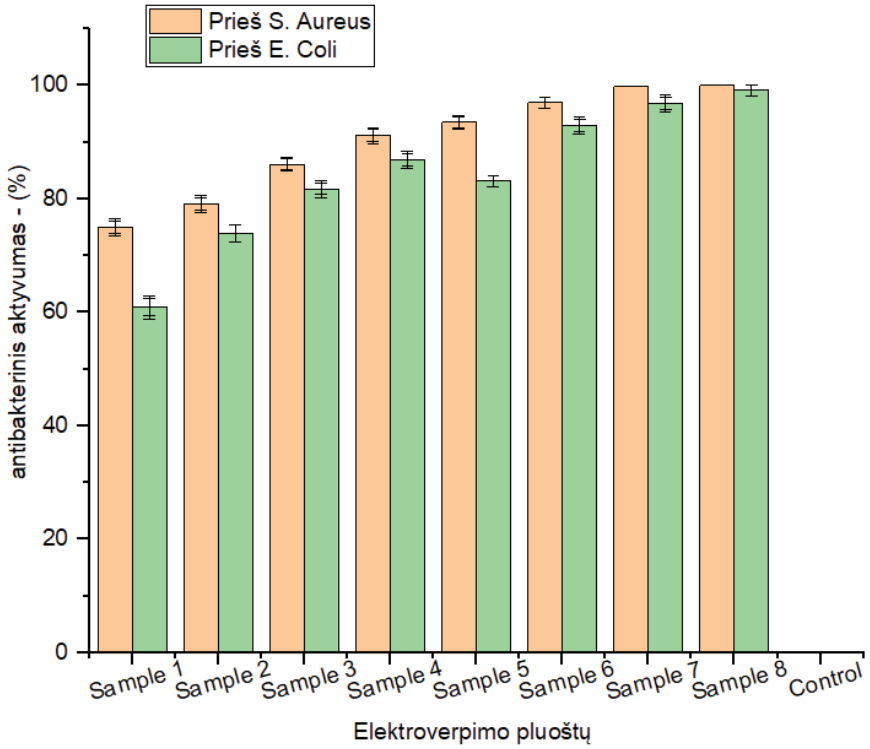


**58 pav.** Elektrinio verpimo pluoštų su kintamu ZnO NPs kiekiu antibakterinis poveikis *S. Aureus* ir *E. Coli*

Atlikta tolesnė kiekybinė antimikrobinio aktyvumo analizė pagal ISO 20743:2013 standartą, rezultatai pateikti 5.3.8 paveiksle. Rezultatai parodė, kad tiek AV, tiek ZnO NP koncentracijos didinimas sustiprino antimikrobinį poveikį tiek gramteigiamoms (*S. aureus*), tiek gramneigiamoms (*E. coli*) bakterijoms. Antimikrobinis poveikis *E. coli* buvo didesnis nei *S. aureus*, o tai gali būti siejama su struktūriniais dviejų bakterijų skirtumais. Gramneigiamos bakterijos turi išorinį fosfolipidinį dvigubą sluoksnį, kuris trukdo antimikrobinių medžiagų veiksmingumui, palyginti su gramteigiamomis bakterijomis.

**PLA/CND nanopluoštų antimikrobinis aktyvumas**

5.3.9 59 *pav***.** parodytas PLA-19, PLA-19/C1, PLA-19/C2 , PLA-19/C3 ir PLA-19/C4 pluoštų antimikrobinio poveikio *S. Aureus* ir *E. Coli* palyginimas. Galima pastebėti, kad PLA-19, kuriame nėra CND, nepasižymėjo antimikrobinėmis savybėmis, o visi kiti mėginiai turėjo antimikrobinį aktyvumą dėl CND. Taip pat pastebėta, kad, didėjant CND koncentracijai PLA nanopluoštuose, antimikrobinis poveikis abiejų tipų bakterijoms – gramteigiamoms ir gramneigiamoms – didėja.

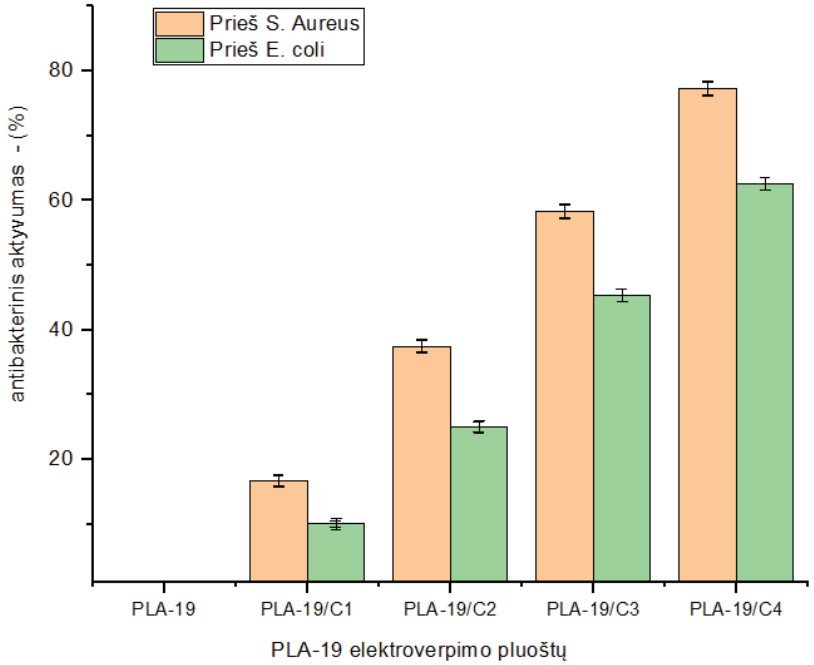


**59 pav.** PLA-19, PLA-19/C1, PLA-19/C2 , PLA-19/C3 ir PLA-19/C4 elektrinio verpimo pluoštų antibakterinis poveikis *S. Aureus* ir *E. Coli*

**Dalelių filtravimo efektyvumo testas**

**AV/PVA/ZnO dalelių filtravimo efektyvumas**

Elektrinis verpimas buvo atliktas naudojant 4 % ZnO skirtingu gamybos laiku (30, 60, 90 ir 120 minučių), o gautas papildomas svoris buvo matuojamas mg / $cm^2$. PFE rezultatai (5.3.3 17 **lentelė.*1***) parodė, kad filtravimo efektyvumas padidėjo nuo 71,5 % iki 92,5 %, padidėjus svoriui.

Lyginamoji analizė su standartiniu neaustiniu lydytu pūstu lakštu, naudojamu medicininėse kaukėse (95,5 % PFE), parodė, kad visi PVA pluoštai (0,88, 1,78, 2,64 ir 3,52 g/$m^2$) nukrito žemiau 95 % minimalaus priimtinumo diapazono. Todėl nė vienas PVA mėginys nebuvo laikomas tinkamu medicininėms veido kaukėms.

**17 lentelė.1** 4 % ZnO pripildytų PVA elektrinio verpimo pluoštų skaidulų dalelių filtravimo efektyvumas – elektrinis verpimas 30, 60, 90 ir 120 min

| **Pavyzdys Nr.** | **% ZnO** | **Elektrinio sukimosi laikas (min.)** | **Papildomas svoris (g/$m^2$)** | **Dalelių filtravimo efektyvumas (%)** |
|---|---|---|---|---|
| PVA/ZnO4 | 4 | 30 | 0,88 | 71,5 |
| | | 60 | 1,78 | 80,7 |
| | | 90 | 2,64 | 84,3 |

| | | | | |
|---|---|---|---|---|
| | | 120 | 3,52 | 92,5 |
| Lydytas pūstas neaustinis lakštas | | | 17,8 | 95,5 |

**PLA/CND dalelių filtravimo efektyvumas**

Buvo įvertintas PFE iki 0,1 mikrono dalelių, atskleidžiant ryšį tarp pailgėjusio elektrinio verpimo laiko, didesnio svorio priedo (nuo 1,49 g/m$^2$ iki 5,96 g/m$^2$) ir pagerėjusio PFE (nuo 80 % iki 100 %). Mėginiai su svorio priedais 4,47 ir 5,96 g/m$^2$ parodė, kad PFE yra priimtiname diapazone nuo 96,5% iki 100%. Palyginti su įprastu neaustiniu lydytu pūstu lakštu, naudojamu medicininėse veido kaukėse, PLA elektrinio verpimo pluoštai, ypač pagaminti 90 ir 120 minučių, turėjo didesnį PFE ir mažesnį medžiagos svorį. Tyrimas rodo, kad šie tvarūs, biologiškai skaidūs nanoskopai yra perspektyvūs naudoti medicininėse veido kaukėse, pabrėžiant tolesnio jų diferencinio slėgio rezultatų tyrimo svarbą. Dalelių filtravimo efektyvumo rezultatai pateikti 5.3.4 lentelėje.

**18 lentelė.** PLA-19/C4 elektrinio verpimo pluoštų PFE su skirtingu elektrinio verpimo laiku

| **Pavyzdys Nr.** | **PLA %** | **CNDs %** | **Elektrinio sukimosi laikas (min)** | **Papildomas svoris (g/m$^2$)** | **Dalelių filtravimo efektyvumas (%)** |
|---|---|---|---|---|---|
| PLA-19/C4 | 19 | 4% | 30 | 1,49 | 80,0 |
| | | | 60 | 2,98 | 85,3 |
| | | | 90 | 4,47 | 96,5 |
| | | | 120 | 5,96 | 100 |
| Lydytas pūstas neaustinis lakštas | | | | 17,8 | 95,0 |

**Diferencinio slėgio bandymas**

**AV/PVA/ZnO slėgio skirtumas**

Padidėjęs elektrinio verpimo pluoštų susikaupimas neaustinio lakšto paviršiuje neigiamai veikia veido kaukės pralaidumą orui, kaip nurodyta 5.3.5 lentelėje. Slėgių skirtumo matavimai, kai elektrinio verpimo trukmė yra 30 ir 60 minučių, viršija minimalius reikalavimus, o 90 ir 120 minučių atitinka minimalius I ir II tipo medicininių veido kaukių reikalavimus.. Tačiau, atsižvelgiant į PFE vertes, PVA nanosluoksniai neatitinka minimalaus 95 % reikalavimo, todėl jie netinkami medicininėms veido kaukėms, nepaisant priimtino slėgio skirtumo.

**19 lentelė.** 4 % apkrautų ZnO elektrinio verpimo pluoštų diferencinis slėgis – 30, 60, 90 ir 120 min

| **Pavyzdys Nr.** | **% ZnO** | **Elektrinio sukimosi laikas (min)** | **Papildomas svoris (g/m$^2$)** | **diferencinis slėgis (Pa/cm$^2$)** |
|---|---|---|---|---|
| PVA/ZnO4 | 4 | 30 | 0,88 | virš diapazono |
| | | 60 | 1,78 | virš diapazono |
| | | 90 | 2,64 | 28,5 |
| | | 120 | 3,52 | 34,6 |
| Lydytas pūstas neaustinis lakštas | | | 17,8 | 38,5 |

**PLA/CND diferencinis slėgis**

PLA-19/C4 elektrinio verpimo atveju 30 minučių ir 120 minučių DP vertės atitinkamai yra mažesnės ir didesnės už priimtinas ribas. Tačiau 60 ir 90 minučių procesai duoda tinkamas medicininių veido kaukių DP vertes. Be to, 4.47 g/m$^2$ nanolakštai pranoksta 17,8 g/m$^2$ neaustinius lakštus, o tai rodo, kad CND įtaisyti PLA nanosluoksniai yra perspektyvi, tvari alternatyva įprastiems biologiškai neskaidomiems lydant pūstiems lakštams. Slėgio skirtumo rezultatai pateikti 5.3.6 20 *lentelė***.** .

**20 lentelė.** Skirtingas elektrinio verpimo PLA-19/C4 pluoštų slėgis su skirtingu elektrinio verpimo laiku

| **Pavyzdys Nr.** | **% PLA** | **% CNDs** | **Elektrinio sukimosi laikas (min)** | **Papildomas svoris (g/m$^2$)** | **diferencinis slėgis (Pa/cm$^2$)** |
|---|---|---|---|---|---|
| PLA-19/C4 | 19 | 4% | 30 | 1,49 | virš diapazono |
| | | | 60 | 2,98 | 33,6 |
| | | | 90 | 4,47 | 39,0 |
| | | | 120 | 5,96 | virš diapazono |
| Lydytas pūstas neaustinis lakštas | | | | 17,8 | 38,5 |

**3 sluoksnių prototipas su elektriniu sluoksniu**

Tvarių elektrinio verpimo nanopluoštų įtraukimo į aplinkai nekenksmingą ir biologiškai skaidų neaustinį medicininių veido kaukių ar respiratorių filtravimo sluoksnį metodu siekiama padidinti filtravimo efektyvumą derinant kelių sluoksnių pranašumus su pažangiomis nanopluošto savybėmis. Nanopluoštai yra tiesiogiai nusodinami ant neaustinio lakšto naudojant kolektoriaus būgną, užtikrinant stabilią

struktūrą ir sprendžiant problemas, susijusias su atskyrimu ir lūžimu. Ant neaustinio lakšto surinkus elektrinio verpimo pluoštus, yra du galimi šio derinio panaudojimo medicininių veido kaukių gamyboje būdai. Ir jie aptariami toliau:

***Spunbondo-nanopluošto-spunbondo*** **struktūra:** Šis metodas apima trijų sluoksnių medicininių veido kaukių struktūrą. Viršutinis ir apatinis sluoksniai yra pagaminti iš spunbondo lakštų, užtikrinančių mechaninę atramą, o vidurinį sluoksnį sudaro nanopluoštai, užtikrinantys puikų filtravimą, kad būtų galima efektyviai užfiksuoti daleles ir virusus. Ši konfigūracija žinoma kaip spunbondo-nanopluošto-spunbondo mazgas.

**Filjerinės neaustinės medžiagos su nanopluoštu struktūra:** Šioje alternatyvioje konfigūracijoje nanopluoštai, surinkti ant neaustinės medžiagos, sukuria dviejų sluoksnių struktūrą, viršutiniame sluoksnyje yra nanopluoštai, o priešingoje pusėje – filjerinė neaustinė medžiaga. Sulenkus šią konstrukciją, išorinėse pusėse susidaro neaustinės medžiagos sluoksnis, todėl susidaro unikali neaustinės medžiagos-nanopluošto-nanopluošto-neaustinės medžiagos struktūra. Ši konfigūracija padidina dalelių ir virusų filtravimo efektyvumą medicininėse veido kaukėse ir respiratoriuose, nes juose yra du nanopluošto sluoksniai, o išoriniai spunbondo sluoksniai palaiko struktūrinį vientisumą ir užtikrina nanopluošto sluoksnių funkcionalumą.

.

## 5.4. Išvados

1. Optimizavus tirpalo parametrus, elektrinio verpimo būdu buvo sėkmingai suformuoti PVA ir PLA pluoštai. Nustatyta, kad 10 % PVA vandeniniame tirpale pakako elektrinio verpimo būdu suverpti pluoštus, o su 12 % PLA DMF buvo matomas tik elektrinis purškimas, ir pluoštai nesusidarė. Taip buvo todėl, kad PVA turi daug didesnę molekulinę masę nei PLA. 19 % PLA (koncentracija DMF) ir 10 % PVA (koncentracija vandenyje) buvo optimalus sprendimas jų elektriniam verpimui.
   Taip pat buvo nustatyta, kad tirpalo klampa ir laidumas yra svarbūs elektrinio verpimo būdu pagamintų pluoštų morfologijai:
   - PVA pluoštų mažesnis skersmuo buvo gautas esant 0,056 S/m laidumui ir 1490 mPa·s klampai.
   - PLA pluoštų gera morfologija buvo gauta esant 0,129 S/m laidumui ir 358 mPa·s klampai.

2. Atlikus elektrinio verpimo būdu suverptų pluoštų, funkcionalizuotų antibakteriniais preparatais, paviršiaus morfologijos ir jų cheminės sudėties analizę, gautos tokios išvados:
   AV/PVA/ZnO pluoštai:
   - Nustatyta, kad bandiniuose su skirtingomis AV koncentracijomis, esant 4 % AV PVA, gaunamos plonesnės gijos, kurių vidutinis skersmuo yra 130 nm diapazone. Taip pat buvo nustatyta, kad, esant 4 % ZnO, gaunamos plonesnės pluošto gijos, kurių vidutinis skersmuo yra 145 nm.
   - Visų bandinių FTIR analizė parodė, kad elektrinio verpimo būdu pagamintuose pluoštuose papildomų smailių neaptikta, ir tai reiškia, kad gaminant šiuos pluoštus jokios kitos cheminės reakcijos nevyksta.
   - Nustatyta, kad 4% AV PVA ir 4% ZnO PVA yra optimali koncentracija funkcionalizuotiems PVA pluoštams gaminti elektrinio verpimo būdu.

   PLA/CNDs pluoštai:
   - Nustatyta, kad maža (12 %) PLA koncentracija DMF lėmė lašelių, o ne pluošto susidarymą elektrinio verpimo metu. Iš 19 % PLA DMF su 4 % CND suverpti pluoštai, kurių vidutinis skersmuo yra 88 nm.
   - Atlikus FTIR analizę nustatyta kad, palyginti su grynu PLA, papildomų smailių nėra, o tai rodo, kad šiuose pluoštuose DMF likučio nėra. Todėl galima daryti išvadą, kad juos saugu naudoti medicininėse veido kaukėse.

- Taip pat buvo nustatyta, kad iš 19% PLA su 4% CND suverpti mažesnio skersmens pluoštai, ir šis derinys laikomas geriausiu iš visų kitų tirtų.

3. Įrodyta, kad PVA funkcionalizavimas su antibakterinėmis medžiagomis, tokiomis kaip AV ir ZnO NP, ir PLA funkcionalizavimas su fotoaktyviomis CND medžiagomis suteikia antibakterinį poveikį gramteigiamoms ir gramneigiamoms bakterijoms. Įvertinus jų antibakterinį aktyvumą buvo nustatyta, kad:
    - 4 % AV PVA turi didžiausią antibakterinį poveikį (91,2 %) *S. Aureus* ir 86,9 % *E. coli*.
    - 4 % ZnO PVA suteikė puikių antibakterinių savybių sunaikinant 100% *S. Aureus* ir 99,2% s *E. coli bakterijų*.
    - Ištyrus PLA elektrinio verpimo būdu pagamintus pluoštus nustatyta, kad 4 % CND PLA užtikrino didžiausią antibakterinį aktyvumą sunaikinant 77,3% *S. Aureus* ir 62,5% *E. coli* bakterijų.
    - Taip pat buvo nustatyta, kad, esant vienodai masei, bendras CND antibakterinis aktyvumas buvo mažesnis, palyginti su AV ir ZnO, o priežastis gali būti siejama su faktu, kad CND buvo įterpti į hidrofobinų PLA ir ant jo paviršiaus, o AV ir ZnO buvo įterpti į hidrofilinį PVA ir ant jo paviršiaus.
4. Tiriant barjerinį veikimą, kietųjų dalelių filtravimo efektyvumą (PFE) ir diferencinį slėgį, buvo nustatyta, kad su PLA/CND suformuota gijinė struktūra pasižymėjo geresnėmis savybėmis, palyginti su AV/PVA/ZnO gijine struktūra. Nustatyta, kad, PVA/ZnO4 verpiant 90 minučių, PFE buvo 84,3%, o kai PLA/CND buvo verpiamas 90 minučių, jo PFE buvo 96,5%. Ši PLA/CNDs elektrinio verpimo būdu pagaminta gijinė struktūra puikiai tinka naudoti medicininėms veido kaukėms, nes turi minimalų barjerinį kietųjų dalelių filtravimo efektyvumą, t. y. 96,5 %, ir priimtiną slėgio skirtumą, t. y. 39 $Pa/cm^2$ .
5. Palyginti su įprastomis neaustinėmis medžiagomis, elektrinio verpimo būdu pagamintos dangos pasižymi geresnėmis filtravimo savybėmis. PLA gijinė danga, kurios paviršinis tankis 4,47 $g/m^2$, pasižymi didesniu kietųjų dalelių filtravimo ir slėgio skirtumo efektyvumu nei lydymo-pūtimo būdu pagamintos neaustinės medžiagos, kurių paviršinis tankis yra 17,8 $g/m^2$. Vadinasi, PLA gijinių dangų panaudojimas leidžia 75 % sumažinti medžiagų sąnaudas, palyginti su įprastomis lydymo-pūtimo būdu pagamintomis neaustinėmis medžiagomis. Be to, naudojant PLA ir PVA elektrinio verpimo būdu pagamintą pluoštą, galima veiksmingai išspręsti su veido kaukėmis susijusias atliekų problemas, nes ir PLA, ir PVA yra tvarūs ir biologiškai skaidūs polimerai.

## REFERENCES


1. SPITERI, Gianfranco, FIELDING, James and DIERCKE, Michael. First cases of coronavirus disease 2019 (COVID-19) in the WHO European Region, 24 January to 21 February 2020. *Eurosurveillance*. 2020. Vol. 25, no. 9. DOI 10.2807/1560-7917.ES.2020.25.9.2000178.
2. WHO Director-General's opening remarks at the media briefing on COVID-19 - 11 March 2020. Online. [Accessed 2 May 2023]. Available from: https://www.who.int/director-general/speeches/detail/who-director-general-s-opening-remarks-at-the-media-briefing-on-covid-19---11-march-2020
3. SU, Wen-lin, LU, Kuo-cheng, CHAN, Chih-yu and CHAO, You-chen. Since January 2020 Elsevier has created a COVID-19 resource centre with free information in English and Mandarin on the novel coronavirus COVID- 19 . The COVID-19 resource centre is hosted on Elsevier Connect , the company ' s public news and information . . 2020. No. January.
4. Personal Protective Equipment [PPE] Market Size | Trends, 2029. Online. [Accessed 3 May 2023]. Available from: https://www.fortunebusinessinsights.com/personal-protective-equipment-ppe-market-102015
5. Five things you should know about disposable masks and plastic pollution | UN News. Online. [Accessed 3 May 2023]. Available from: https://news.un.org/en/story/2020/07/1069151
6. MORAWSKA, Lidia and MILTON, Donald K. It Is Time to Address Airborne Transmission of Coronavirus Disease 2019 (COVID-19). *Clinical Infectious Diseases*. 2020. Vol. 71, no. 9, p. 2311–2313. DOI 10.1093/cid/ciaa939.
7. LUZIO, Alessandro, CANESI, Eleonora Valeria, BERTARELLI, Chiara and CAIRONI, Mario. Electrospun polymer fibers for electronic applications. *Materials*. 2014. Vol. 7, no. 2, p. 906–947. DOI 10.3390/ma7020906.
8. HAN, Ziyi, WANG, Lina, LIU, Yueyan, CHAN, Tatleung, SHI, Zhandong and YU, Mingzhou. Since January 2020 Elsevier has created a COVID-19 resource centre with free information in English and Mandarin on the novel coronavirus COVID- 19 . The COVID-19 resource centre is hosted on Elsevier Connect , the company ' s public news and information . . 2020. No. January.
9. ULLAH, Sana, ULLAH, Azeem, LEE, Jaeyun, JEONG, Yeonsu, HASHMI, Motahira, ZHU, Chunhong, JOO, Kye Il, CHA, Hyung Joon and KIM, Ick Soo. Reusability Comparison of Melt-Blown vs Nanofiber Face Mask Filters for Use in the Coronavirus Pandemic. *ACS Applied Nano Materials*. 2020. Vol. 3, no. 7, p. 7231–7241. DOI 10.1021/acsanm.0c01562.
10. TUCKER, Nick, STANGER, Jonathan J., STAIGER, Mark P., RAZZAQ, Hussam and HOFMAN, Kathleen. The history of the science and technology of electrospinning from 1600 to 1995. *Journal of Engineered Fibers and Fabrics*. 2012. Vol. 7, no. 3, p. 63–73. DOI 10.1177/155892501200702s10.
11. Face Masks, Barrier Face Coverings, Surgical Masks, and Respirators for COVID-19

| FDA. Online. [Accessed 3 May 2023]. Available from: https://www.fda.gov/medical-devices/coronavirus-covid-19-and-medical-devices/face-masks-barrier-face-coverings-surgical-masks-and-respirators-covid-19

12. Medical devices. Online. [Accessed 3 May 2023]. Available from: https://www.who.int/health-topics/medical-devices#tab=tab_2

13. GU, Hongbo, GUO, Zhanhu, NAIK, Nithesh, SHETTY, Dasharathraj K., HAMEED, B. M.Zeeshan, CHAKRABORTY, Udit Kumar and PAUL. Frontiers of Advanced Sciences and Technologies: Results, Challenges and Perspectives. *Engineered Science*. 2021. Vol. 16, no. December, p. 1–4. DOI 10.30919/es8e557.

14. BABAAHMADI, Vahid, AMID, Hooman, NAEIMIRAD, Mohammadreza and RAMAKRISHNA, Seeram. Since January 2020 Elsevier has created a COVID-19 resource centre with free information in English and Mandarin on the novel coronavirus COVID- 19 . The COVID-19 resource centre is hosted on Elsevier Connect , the company ' s public news and information . . 2020. No. January.

15. DHIVYADHARSHINI, J, SOMASUNDARAM, Jayalakshmi and BRUNDHA, M P. Composition and uses of N95 masks -a review. *European Journal of Molecular and Clinical Medicine*. 2020. Vol. 7, no. 1, p. 1529–1540.

16. TCHARKHTCHI, A., ABBASNEZHAD, N., ZARBINI SEYDANI, M., ZIRAK, N., FARZANEH, S. and SHIRINBAYAN, M. An overview of filtration efficiency through the masks: Mechanisms of the aerosols penetration. *Bioactive Materials*. Online. 2021. Vol. 6, no. 1, p. 106–122. DOI 10.1016/j.bioactmat.2020.08.002.

17. ADANUR, Sabit and JAYSWAL, Ajay. Filtration mechanisms and manufacturing methods of face masks: An overview. *Journal of Industrial Textiles*. 2022. Vol. 51, no. 3, p. 3683S-3717S. DOI 10.1177/1528083720980169.

18. ISO 9092:2011 - Textiles — Nonwovens — Definition. Online. [Accessed 4 May 2023]. Available from: https://www.iso.org/standard/50397.html

19. Home. Online. [Accessed 4 May 2023]. Available from: https://www.edana.org/

20. POURMOHAMMADI, A. Nonwoven materials and joining techniques. *Joining Textiles: Principles and Applications*. 2013. P. 565–581. DOI 10.1533/9780857093967.4.565.

21. Home. Online. [Accessed 4 May 2023]. Available from: https://www.inda.org/

22. KOTHARI, Vijay K., DAS, A. and SINGH, S. Filtration behaviour of woven and nonwoven fabrics. *Indian Journal of Fibre and Textile Research*. 2007. Vol. 32, no. 2, p. 214–220.

23. ZHANG, Xiayun, LI, Ting Ting, PENG, Hao Kai, WANG, Zhike, HUO, Junli, LOU, Ching Wen and LIN, Jia Horng. Synergistic Effects of Needle Punching and Shear-Thickening Fluid on Sandwich-Structured Composites Made of Nonwoven and Woven Fabrics. *Fibers and Polymers*. 2020. Vol. 21, no. 7, p. 1515–1522. DOI 10.1007/s12221-020-9967-8.

24. AJMERI, J.R. and AJMERI, C.J. Nonwoven personal hygiene materials and products. *Applications of Nonwovens in Technical Textiles*. 2010. P. 85–102. DOI 10.1533/9781845699741.2.85.

25. YILMAZ, Korhan Babacan, SABUNCUOGLU, Baris, YILDIRIM, Bora and SILBERSCHMIDT, Vadim V. A brief review on the mechanical behavior of nonwoven fabrics. *Journal of Engineered Fibers and Fabrics*. 2020. Vol. 15. DOI 10.1177/1558925020970197.

26. VARGHESE P. J, George, DAVID, Deepthi Anna, KARUTH, Anas, MANAMKERI JAFFERALI, Jabeen Fatima, SABURA, Sabura Begum, GEORGE, Jinu Jacob, RASULEV, Bakhtiyor and RAGHAVAN, Prasanth. Experimental and Simulation Studies on Nonwoven Polypropylene-Nitrile Rubber Blend: Recycling of Medical Face Masks to an Engineering Product. *ACS Omega*. 2022. Vol. 7, no. 6, p. 4791–4803. DOI 10.1021/acsomega.1c04913.

27. VENKATARAMAN, Dhanya, SHABANI, Elnaz and PARK, Jay H. Advancement of Nonwoven Fabrics in Personal Protective Equipment. *Materials*. 2023. Vol. 16, no. 11. DOI 10.3390/ma16113964.

28. Nonwoven Processes and Applications (MELT BLOWN NON-WOVEN) - Fibre2Fashion. Online. [Accessed 19 May 2023]. Available from: https://www.fibre2fashion.com/industry-article/1280/nonwoven-processes-and-applications

29. SILVA, Edmir. The Melt-Blowing Process. *Lecture Notes TT 505.601*. 2010. P. 1–10.

30. HUTTEN, Irwin M. Processes for Nonwoven Filter Media. *Handbook of Nonwoven Filter Media*. 2007. P. 195–244. DOI 10.1016/b978-185617441-1/50020-2.

31. GEUS, H. G. *Developments in manufacturing techniques for technical nonwovens*. Online. Elsevier Ltd, 2016. ISBN 9780081005842.

32. Nonwoven Fabric Processing|Nonwoven Line-DKM. Online. [Accessed 19 May 2023]. Available from: https://dkm.com/nonwoven/nonwoven-fabric-production-system.html

33. XUE, Jiajia, XIE, Jingwei, LIU, Wenying and XIA, Younan. Electrospun Nanofibers: New Concepts, Materials, and Applications. *Accounts of Chemical Research*. 2017. Vol. 50, no. 8, p. 1976–1987. DOI 10.1021/acs.accounts.7b00218.

34. WILSON, A. The formation of dry, wet, spunlaid and other types of nonwovens. *Applications of Nonwovens in Technical Textiles*. 2010. P. 3–17. DOI 10.1016/B978-1-84569-437-1.50001-X.

35. Size of the Nanoscale | National Nanotechnology Initiative. Online. [Accessed 19 May 2023]. Available from: https://www.nano.gov/nanotech-101/what/nano-size

36. LEENA, M. Maria, YOHA, K. S., MOSES, J. A. and ANANDHARAMAKRISHNAN, C. *Nanofibers in Food Applications*. Online. Elsevier, 2020. ISBN 9780128157824.

37. ZHANG, Wenshuo, HE, Ziying, HAN, Ying, JIANG, Qinyuan, ZHAN, Chenhao, ZHANG, Kaiji, LI, Zekun and ZHANG, Rufan. Structural design and environmental applications of electrospun nanofibers. *Composites Part A: Applied Science and Manufacturing*. Online. 2020. Vol. 137, no. May, p. 106009.

DOI 10.1016/j.compositesa.2020.106009.

38. MA, Jian, ZHANG, Qian, ZHANG, Yin, ZHOU, Lei, YANG, Juekuan and NI, Zhonghua. A rapid and simple method to draw polyethylene nanofibers with enhanced thermal conductivity. *Applied Physics Letters*. 2016. Vol. 109, no. 3. DOI 10.1063/1.4958905.

39. SIMFUKWE, Joseph, MAPASHA, Refilwe Edwin, BRAUN, Artur and DIALE, Mmantsae. Biopatterning of Keratinocytes in Aqueous Two-Phase Systems as a Potential Tool for Skin Tissue Engineering. *MRS Advances*. Online. 2017. Vol. 357, no. May, p. 1–8. DOI 10.1557/adv.201.

40. ZHANG, Xiangwu and LU, Yao. Centrifugal spinning: An alternative approach to fabricate nanofibers at high speed and low cost. *Polymer Reviews*. 2014. Vol. 54, no. 4, p. 677–701. DOI 10.1080/15583724.2014.935858.

41. AGARWAL, Seema, WENDORFF, Joachim H. and GREINER, Andreas. Use of electrospinning technique for biomedical applications. *Polymer*. Online. 2008. Vol. 49, no. 26, p. 5603–5621. DOI 10.1016/j.polymer.2008.09.014.

42. ZHONG, Wen. Nano fi bres for medical textiles. . 2016. DOI 10.1016/B978-1-78242-379-9.00003-7.

43. HOHMAN, Moses M. Electrospinning and Electrically Forced Jets . I . Stability Theory Electrospinning and electrically forced jets . I . Stability theory. . 2015. No. August 2001. DOI 10.1063/1.1383791.

44. LI, By Dan and XIA, Younan. Electrospinning of Nanofibers : Reinventing the Wheel ?**. . 2004. No. 14, p. 1151–1170. DOI 10.1002/adma.200400719.

45. TAYLOR, Geoffrey and A, Proc R Soc Lond. Disintegration of Water Drops in an Electric Field Article cited in : . 1964. P. 383–397. DOI 10.1098/rspa.1964.0151.

46. AL-HAZEEM, Nabeel Zabar Abed and AL-HAZEEM, Nabeel Zabar Abed. Nanofibers and Electrospinning Method. *Novel Nanomaterials - Synthesis and Applications*. Online. 18 April 2018. [Accessed 19 May 2023]. DOI 10.5772/INTECHOPEN.72060.

47. SAHAY, Rahul, THAVASI, Velmurugan and RAMAKRISHNA, Seeram. Design Modifications in Electrospinning Setup for Advanced Applications. . 2011. Vol. 2011. DOI 10.1155/2011/317673.

48. AGRAHARI, Vibhuti, AGRAHARI, Vivek, MENG, Jianing and MITRA, Ashim K. *Electrospun Nano fi bers in Drug Delivery : Fabrication , Advances , and Biomedical Applications*. Online. Elsevier, 2017. ISBN 9780323429788.

49. RAHMATI, M, MILLS, D K, URBANSKA, A M, SAEB, M, VENUGOPAL, J R, RAMAKRISHNA, S and MOZAFARI, M. Electrospinning for Tissue Engineering Applications. *Progress in Materials Science*. Online. 2020. P. 100721. DOI 10.1016/j.pmatsci.2020.100721.

50. HU, Xiuli, LIU, Shi, ZHOU, Guangyuan, HUANG, Yubin, XIE, Zhigang and JING, Xiabin. Electrospinning of polymeric nano fi bers for drug delivery applications. *Journal of Controlled Release*. Online. 2014. Vol. 185, p. 12–21. DOI 10.1016/j.jconrel.2014.04.018.

51. WU, Shaohua, DONG, Ting, LI, Yiran, SUN, Mingchao, QI, Ye, LIU, Jiao, KUSS, Mitchell A, CHEN, Shaojuan and DUAN, Bin. State-of-the-art review of advanced electrospun nanofib er yarn-base d textiles for biomedical applications. . 2022. Vol. 27. DOI 10.1016/j.apmt.2022.101473.

52. LIU, Jiao, ZHAI, Huiyuan, SUN, Yaning, WU, Shaohua and CHEN, Shaojuan. Developing high strength poly ( L-lactic acid ) nanofiber yarns for biomedical textile materials : A comparative study of novel nanofiber yarns and traditional microfiber yarns. *Materials Letters*. Online. 2021. Vol. 300, no. June, p. 130229. DOI 10.1016/j.matlet.2021.130229.

53. LU, Tao, CUI, Jiaxin, QU, Qingli, WANG, Yulin, ZHANG, Jian, XIONG, Ranhua, MA, Wenjing and HUANG, Chaobo. Multistructured Electrospun Nano fi bers for Air Filtration : A Review. . 2021. DOI 10.1021/acsami.1c06520.

54. GUERRERO-P, M Olga. Research Progress on the Applications of Electrospun Nanofibers in Catalysis. . 2022.

55. SUN, Guiru, SUN, Liqun, XIE, Haiming and LIU, Jia. Electrospinning of Nanofibers for Energy Applications. . 2016. DOI 10.3390/nano6070129.

56. XUE, Jiajia, WU, Tong, DAI, Yunqian, XIA, Younan and STATES, United. Electrospinning and Electrospun Nano fi bers : Methods , Materials , and Applications. *Chemical Reviews*. 2018. DOI 10.1021/acs.chemrev.8b00593.

57. HOMAEIGOHAR, Shahin. The Electrospun Ceramic Hollow Nanofibers. . 2017. DOI 10.3390/nano7110383.

58. BUBAKIR, Mahmoud Mohammed, LI, Haoyi and BARHOUM, Ahmed. *Advances in Melt Electrospinning Technique Advances in Melt Electrospinning Technique*. . 2017. ISBN 9783319427898.

59. NAYAK, R, PADHYE, R and ARNOLD, L. *Melt-electrospinning of nanofibers*. Online. Elsevier Ltd., 2017. ISBN 9780081009079.

60. KOENIG, Kylie, BEUKENBERG, Konrad, LANGENSIEPEN, Fabian and SEIDE, Gunnar. A new prototype melt-electrospinning device for the production of biobased thermoplastic sub-microfibers and nanofibers. . 2019. P. 1–12.

61. BACHS-HERRERA, Anna, YOUSEFZADE, Omid and VALLE, Luis J. applied sciences Melt Electrospinning of Polymers : Blends , Nanocomposites , Additives and Applications. . 2021.

62. TOBY, Author, PAUL, D Brown and DIETMAR, D Dalton. Ac ce pt e d cr t. *Progress in Polymer Science*. Online. 2016. DOI 10.1016/j.progpolymsci.2016.01.001.

63. AFGHAH, Ferdows, DIKYOL, Caner, ALTUNBEK, Mine and KOC, Bahattin. Biomimicry in bio-manufacturing: Developments in melt electrospinning writing technology towards hybrid biomanufacturing. *Applied Sciences (Switzerland)*. 2019. Vol. 9, no. 17. DOI 10.3390/app9173540.

64. SURESH, Sinduja and BECKER, Alexander. Impact of Apparatus Orientation and Gravity in Electrospinning — A Review of Empirical Evidence. . 2020. No. Figure 1, p. 1–15.

65. ISAAC, Blesson, TAYLOR, Robert M. and REIFSNIDER, Kenneth. Mechanical and dielectric properties of aligned electrospun fibers. *Fibers*. 2021. Vol. 9, no. 1, p. 1–32. DOI 10.3390/fib9010004.

66. HEKMATI, Amir Houshang, RASHIDI, Abosaeed, GHAZISAEIDI, Reza and DREAN, Jean Yves. Effect of needle length, electrospinning distance, and solution concentration on morphological properties of polyamide-6 electrospun nanowebs. *Textile Research Journal*. 2013. Vol. 83, no. 14, p. 1452–1466. DOI 10.1177/0040517512471746.

67. ODULARU, Ayodele Temidayo. Basic Principles of Electrospinning, Mechanisms, Nanofibre Production, and Anticancer Drug Delivery. *Journal of Chemistry*. 2022. Vol. 2022. DOI 10.1155/2022/9283325.

68. HE, Jianxin and ZHOU, Yuman. *Multineedle electrospinning*. Online. Elsevier Inc., 2018. ISBN 9780323512701.

69. BEAUDOIN, Étienne J., KUBASKI, Maurício M., SAMARA, Mazen, ZEDNIK, Ricardo J. and DEMARQUETTE, Nicole R. Scaled-Up Multi-Needle Electrospinning Process Using Parallel Plate Auxiliary Electrodes. *Nanomaterials*. 2022. Vol. 12, no. 8. DOI 10.3390/nano12081356.

70. WANG, Nü and ZHAO, Yong. *Coaxial electrospinning*. Online. Elsevier Inc., 2018. ISBN 9780323512701.

71. AYTAC, Zeynep and UYAR, Tamer. *Applications of core-shell nanofibers*. Online. Elsevier Ltd, 2018. ISBN 9780081021989.

72. PARTHENIADIS, Ioannis, NIKOLAKAKIS, Ioannis, LAIDMÄE, Ivo and HEINÄMÄKI, Jyrki. A mini-review: Needleless electrospinning of nanofibers for pharmaceutical and biomedical applications. *Processes*. 2020. Vol. 8, no. 6. DOI 10.3390/PR8060673.

73. YAN, Guilong, NIU, Haitao and LIN, Tong. *Needle-less electrospinning*. Online. Elsevier Inc., 2018. ISBN 9780323512701.

74. SASITHORN, Nongnut and MARTINOVÁ, Lenka. Needleless Electrospinning of Silk Fibroin/Gelatin Blend Nanofibres. *Applied Mechanics and Materials*. 2015. Vol. 804, p. 213–216. DOI 10.4028/www.scientific.net/amm.804.213.

75. KIM, Bum Jin, CHEONG, Hogyun, CHOI, Eun Som, YUN, So Hee, CHOI, Bong Hyuk, PARK, Ki Soo, KIM, Ick Soo, PARK, Dae Hwan and CHA, Hyung Joon. Accelerated skin wound healing using electrospun nanofibrous mats blended with mussel adhesive protein and polycaprolactone. *Journal of Biomedical Materials Research - Part A*. 2017. Vol. 105, no. 1, p. 218–225. DOI 10.1002/jbm.a.35903.

76. SHARMA, Deepika and SATAPATHY, Bhabani K. Optimization and physical performance evaluation of electrospun nanofibrous mats of PLA, PCL and their blends. *Journal of Industrial Textiles*. 2022. Vol. 51, no. 4, p. 6640S-6665S. DOI 10.1177/1528083720944502.

77. CHENG, Tong, HUND, Rolf Dieter, AIBIBU, Dilibaier, HORAKOVA, Jana and CHERIF, Chokri. Pure chitosan and chitsoan/chitosan lactate blended nanofibres made by single step electrospinning. *Autex Research Journal*. 2013. Vol. 13, no. 4, p. 128–133. DOI 10.2478/v10304-012-0040-6.

78. STEYAERT, I., VAN DER SCHUEREN, L., RAHIER, H. and DE CLERCK, K. An alternative solvent system for blend electrospinning of polycaprolactone/chitosan nanofibres. *Macromolecular Symposia*. 2012. Vol. 321–322, no. 1, p. 71–75. DOI 10.1002/masy.201251111.

79. PEESAN, Manisara, RUJIRAVANIT, Ratana and SUPAPHOL, Pitt. Journal of Biomaterials Science , Electrospinning of hexanoyl chitosan / polylactide blends. . 2012. No. August, p. 37–41.

80. CHEN, Zonggang, MO, Xiumei and QING, Fengling. Electrospinning of collagen-chitosan complex. *Materials Letters*. 2007. Vol. 61, no. 16, p. 3490–3494. DOI 10.1016/j.matlet.2006.11.104.

81. PAKRAVAN, Mehdi, HEUZEY, Marie Claude and AJJI, Abdellah. A fundamental study of chitosan/PEO electrospinning. *Polymer*. Online. 2011. Vol. 52, no. 21, p. 4813–4824. DOI 10.1016/j.polymer.2011.08.034.

82. XU, Jia, ZHANG, Jinhui, GAO, Weiquan, LIANG, Hongwei, WANG, Hongyan and LI, Junfeng. Preparation of chitosan/PLA blend micro/nanofibers by electrospinning. *Materials Letters*. Online. 2009. Vol. 63, no. 8, p. 658–660. DOI 10.1016/j.matlet.2008.12.014.

83. SORLIER, P., DENUZIÈRE, A., VITON, C. and DOMARD, A. Relation between the degree of acetylation and the electrostatic properties of chitin and chitosan. *Biomacromolecules*. 2001. Vol. 2, no. 3, p. 765–772. DOI 10.1021/bm015531+.

84. CONFEDERAT, Luminita Georgeta, TUCHILUS, Cristina Gabriela, DRAGAN, Maria, SHA'AT, Mousa and DRAGOSTIN, Oana Maria. Preparation and Antimicrobial Activity of Chitosan and Its Derivatives: A Concise Review. *Molecules (Basel, Switzerland)*. 2021. Vol. 26, no. 12. DOI 10.3390/molecules26123694.

85. ARANAZ, Inmaculada, ALCÁNTARA, Andrés R., CIVERA, Maria Concepción, ARIAS, Concepción, ELORZA, Begoña, CABALLERO, Angeles Heras and ACOSTA, Niuris. Chitosan: An overview of its properties and applications. *Polymers*. 2021. Vol. 13, no. 19. DOI 10.3390/polym13193256.

86. MIKUČIONIENĖ, Daiva, MILAŠIUS, Rimvydas, DAUGELAVIČIUS, Rimantas, RAGELIENĖ, Lina, VENSLAUSKAITĖ, Neringa, RAGAIŠIENĖ, Audronė and RUKUIŽIENĖ, Žaneta. Preliminary investigation into the antimicrobial activity of an electrospun polyamide nanofibrous web with micro particles of Baltic amber. *Fibres and Textiles in Eastern Europe*. 2016. Vol. 24, no. 5, p. 34–37. DOI 10.5604/12303666.1215524.

87. FOMBY, Paula, CHERLIN, Andrew J, HADJIZADEH, Afra, DOILLON, Charles J, SUEBLINVONG, Viranuj, WEISS, Daniel J., BATES, Jason H T, GILBERT, Thomas, LILES, W. Conrad, LUTZKO, Carolyn, RAJAGOPAL, Jay, PROCKOP, Darwin J., CHAMBERS, Daniel, GIANGRECO, Adam, KEATING, Armand, KOTTON, Darrell, LELKES, Peter I., WAGNER, Darcy E. and PROCKOP, Darwin J. Stem cells and cell therapies in lung biology and diseases: Conference report. *Annals of the American Thoracic Society*. Online. 2010. Vol. 12, no. 3, p. 181–204. DOI 10.1002/term.

88. BISWAS, Dew, MANDAL, Sujata, CHATTERJEE SAHA, Suchismita, TUDU, Champa Keeya, NANDY, Samapika, BATIHA, Gaber El Saber, SHEKHAWAT, Mahipal S., PANDEY, Devendra Kumar and DEY, Abhijit. Ethnobotany, phytochemistry, pharmacology, and toxicity of Centella asiatica (L.) Urban: A comprehensive review. *Phytotherapy Research*. 2021. Vol. 35, no. 12, p. 6624–6654. DOI 10.1002/ptr.7248.

89. CHAN, Wing P., HUANG, Kuan Chen and BAI, Meng Yi. Silk fibroin protein-based nonwoven mats incorporating baicalein Chinese herbal extract: preparation, characterizations, and in vivo evaluation. *Journal of Biomedical Materials Research - Part B Applied Biomaterials*. 2017. Vol. 105, no. 2, p. 420–430. DOI 10.1002/jbm.b.33560.

90. SADRI, Minoo, ARAB-SORKHI, Saedeh, VATANI, Hossein and BAGHERI-PEBDENI, Azam. New wound dressing polymeric nanofiber containing green tea extract prepared by electrospinning method. *Fibers and Polymers*. 2015. Vol. 16, no. 8, p. 1742–1750. DOI 10.1007/s12221-015-5297-7.

91. SUWANTONG, Orawan, PANKONGADISAK, Porntipa, DEACHATHAI, Suwanna and SUPAPHOL, Pitt. Electrospun poly(l-lactic acid) fiber mats containing crude Garcinia mangostana extracts for use as wound dressings. *Polymer Bulletin*. 2014. Vol. 71, no. 4, p. 925–949. DOI 10.1007/s00289-014-1102-9.

92. MAMAT, S. F., AZIZAN, K. A., BAHARUM, S. N., MOHD NOOR, N. and AIZAT, W. M. The influence of two solvent extraction ratios in GC-MS-based metabolomics of different Garcinia mangostana Linn. fruit tissues. *International Food Research Journal*. 2019. Vol. 26, no. 5, p. 1447–1457.

93. YANG, Zhe, PENG, Hongdan, WANG, Weizhi and LIU, Tianxi. Crystallization behavior of poly(ε-caprolactone)/layered double hydroxide nanocomposites. *Journal of Applied Polymer Science*. 2010. Vol. 116, no. 5, p. 2658–2667. DOI 10.1002/app.

94. VALIZADEH, Moharam, BEIGOMI, Maryam and FAZELI-NASAB, Bahman. Antibacterial and Antibiofilm Effects of Ethanol and Aceton Leaf Extract of Momordica charantia and Tecomella undulata against Acinetobacter baumannii. *International Journal of Advanced Biological and Biomedical Research*. Online. 2020. Vol. 8, no. 4, p. 403–418. DOI 10.33945/SAMI/IJABBR.2020.4.6.

95. RADHA, Maharjan H. and LAXMIPRIYA, Nampoothiri P. Evaluation of biological properties and clinical effectiveness of Aloe vera: A systematic review. *Journal of Traditional and Complementary Medicine*. 2015. Vol. 5, no. 1, p. 21–26. DOI 10.1016/j.jtcme.2014.10.006.

96. BOZZI, A., PERRIN, C., AUSTIN, S. and ARCE VERA, F. Quality and authenticity of commercial aloe vera gel powders. *Food Chemistry*. 2007. Vol. 103, no. 1, p. 22–30. DOI 10.1016/j.foodchem.2006.05.061.

97. GENTILINI, Roberta, BOZZINI, Sabrina, MUNARIN, Fabiola, PETRINI, Paola, VISAI, Livia and TANZI, Maria Cristina. Pectins from Aloe Vera: Extraction and production of gels for regenerative medicine. *Journal of Applied Polymer Science*. 2014. Vol. 131, no. 2, p. 1–9. DOI 10.1002/app.39760.

98. FANI, Mohammadmehdi and KOHANTEB, Jamshid. Inhibitory activity of Aloe vera gel on some clinically isolated cariogenic and periodontopathic bacteria.

*Journal of oral science*. 2012. Vol. 54, no. 1, p. 15–21. DOI 10.2334/josnusd.54.15.

99. SUGANYA, S., VENUGOPAL, J., AGNES MARY, S., RAMAKRISHNA, S., LAKSHMI, B. S. and GIRI DEV, V. R. Aloe vera incorporated biomimetic nanofibrous scaffold: A regenerative approach for skin tissue engineering. *Iranian Polymer Journal (English Edition)*. 2014. Vol. 23, no. 3, p. 237–248. DOI 10.1007/s13726-013-0219-2.

100. ISFAHANI, Fatemeh Rafieian, TAVANAI, Hossein and MORSHED, Mohammad. Release of aloe vera from electrospun aloe vera-PVA nanofibrous pad. *Fibers and Polymers*. 2017. Vol. 18, no. 2, p. 264–271. DOI 10.1007/s12221-017-6954-9.

101. IBRAHIM, Illani, SEKAK, Khairunnadim Ahmad and HASBULLAH, Norazurean. Preparation and characterization of chitosan/Aloe Vera composite nanofibers generated by electrostatic spinning. *AIP Conference Proceedings*. 2015. Vol. 1674, no. December 2022. DOI 10.1063/1.4928842.

102. MARTÍNEZ-BURGOS, Walter Jose, SERRA, Josilene Lima, MARSIGLIAF, Ronald M., MONTOYA, Pedro, SARMIENTO-VÁSQUEZ, Zulma, MARIN, Oranys, GALLEGO-CARTAGENA, Euler and PATERNINA-ARBOLEDA, Carlos D. Aloe vera: From ancient knowledge to the patent and innovation landscape – A review. *South African Journal of Botany*. 2022. Vol. 147, p. 993–1006. DOI 10.1016/j.sajb.2022.02.034.

103. LIN, Neil, VERMA, Daksh, SAINI, Nikhil, ARBI, Ramis, MUNIR, Muhammad, JOVIC, Marko and TURAK, Ayse. Antiviral nanoparticles for sanitizing surfaces: A roadmap to self-sterilizing against COVID-19. *Nano Today*. Online. 2021. Vol. 40, p. 101267. DOI 10.1016/j.nantod.2021.101267.

104. LEKHA, D. Chandra, SHANMUGAM, R., MADHURI, K., DWARAMPUDI, L. Priyanka, BHASKARAN, Mahendran, KONGARA, Deepak, TESFAYE, Jule Leta, NAGAPRASAD, N., BHARGAVI, V. L.Nirmal and KRISHNARAJ, Ramaswamy. Review on Silver Nanoparticle Synthesis Method, Antibacterial Activity, Drug Delivery Vehicles, and Toxicity Pathways: Recent Advances and Future Aspects. *Journal of Nanomaterials*. 2021. Vol. 2021. DOI 10.1155/2021/4401829.

105. PILAQUINGA, Fernanda, MOREY, Jeroni, TORRES, Marbel, SEQQAT, Rachid and PIÑA, María de las Nieves. Silver nanoparticles as a potential treatment against SARS-CoV-2: A review. *Wiley Interdisciplinary Reviews: Nanomedicine and Nanobiotechnology*. 2021. Vol. 13, no. 5, p. 1–19. DOI 10.1002/wnan.1707.

106. ADOMAVIČIUTE, Erika, PUPKEVIČIUTE, Solveiga, JUŠKAITE, Vaida, ŽILIUS, Modestas, STANYS, Sigitas, PAVILONIS, Alvydas and BRIEDIS, Vitalis. Formation and investigation of electrospun PLA materials with propolis extracts and silver nanoparticles for biomedical applications. *Journal of Nanomaterials*. 2017. Vol. 2017. DOI 10.1155/2017/8612819.

107. ROY, Anupam, BULUT, Onur, SOME, Sudip, MANDAL, Amit Kumar and YILMAZ, M. Deniz. Green synthesis of silver nanoparticles: Biomolecule-nanoparticle organizations targeting antimicrobial activity. *RSC Advances*. 2019. Vol. 9, no. 5, p. 2673–2702. DOI 10.1039/c8ra08982e.

108. JEREMIAH, Sundararaj S., MIYAKAWA, Kei, MORITA, Takeshi, YAMAOKA,

Yutaro and RYO, Akihide. Potent antiviral effect of silver nanoparticles on SARS-CoV-2. *Biochemical and Biophysical Research Communications*. Online. 2020. Vol. 533, no. 1, p. 195–200. DOI 10.1016/j.bbrc.2020.09.018.

109. ALMANZA-REYES, Horacio, MORENO, Sandra, PLASCENCIA-LÓPEZ, Ismael, ALVARADO-VERA, Martha, PATRÓN-ROMERO, Leslie, BORREGO, Belén, REYES-ESCAMILLA, Alberto, VALENCIA-MANZO, Daniel, BRUN, Alejandro, PESTRYAKOV, Alexey and BOGDANCHIKOVA, Nina. Evaluation of silver nanoparticles for the prevention of SARS-CoV-2 infection in health workers: In vitro and in vivo. *PLoS ONE*. 2021. Vol. 16, no. 8 August, p. 1–14. DOI 10.1371/journal.pone.0256401.

110. BLOSI, Magda, COSTA, Anna Luisa, ORTELLI, Simona, BELOSI, Franco, RAVEGNANI, Fabrizio, VARESANO, Alessio, TONETTI, Cinzia, ZANONI, Ilaria and VINEIS, Claudia. Polyvinyl alcohol/silver electrospun nanofibers: Biocidal filter media capturing virus-size particles. *Journal of Applied Polymer Science*. 2021. Vol. 138, no. 46, p. 1–10. DOI 10.1002/app.51380.

111. SELVAM, Arun Karthick and NALLATHAMBI, Gobi. Polyacrylonitrile/silver nanoparticle electrospun nanocomposite matrix for bacterial filtration. *Fibers and Polymers*. 2015. Vol. 16, no. 6, p. 1327–1335. DOI 10.1007/s12221-015-1327-8.

112. HeiQ Viroblock | Antiviral and Antibacterial Technology. Online. [Accessed 19 May 2023]. Available from: https://www.heiq.com/products/textile-technologies/heiq-viroblock-antiviral/?utm_campaign=GB_HeiQ_Viroblock&utm_adgroup=HeiQ_Viroblock&utm_source=google_paid&utm_medium=search&utm_content=&utm_position=&gad=1&gclid=CjwKCAjwvJyjBhApEiwAWz2nLXeguk57gbyGiNsNFK8YIu84ktsujiqkS-G44Bp4GCP3w2ODbdjZlxoCTnIQAvD_BwE

113. SALAM, Abdul, HASSAN, Tufail, JABRI, Tooba, RIAZ, Shagufta, KHAN, Amina, IQBAL, Kanwal Muhammad, KHAN, Saif Ullah, WASIM, Muhammad, SHAH, Muhammad Raza, KHAN, Muhammad Qamar and KIM, Ick Soo. Electrospun nanofiber-based viroblock/ZnO/PAN hybrid antiviral nanocomposite for personal protective applications. *Nanomaterials*. 2021. Vol. 11, no. 9. DOI 10.3390/nano11092208.

114. Resusable Face Masks - Viroblock – Medsales. Online. [Accessed 19 May 2023]. Available from: https://www.medsales.com.au/products/viroblock-resusable-face-mask

115. ROMÁN, Luz E., GOMEZ, Enrique D., SOLÍS, José L. and GÓMEZ, Mónica M. Antibacterial Cotton Fabric Functionalized with Copper Oxide Nanoparticles. *Molecules*. 2020. Vol. 25, no. 24, p. 1–21. DOI 10.3390/MOLECULES25245802.

116. FUJIMORI, Yoshie, SATO, Tetsuya, HAYATA, Taishi, NAGAO, Tomokazu, NAKAYAM, Mikio, NAKAYAM, Tsuruo, SUGAMAT, Ryuichi and SUZUKI, Kazuo. Novel antiviral characteristics of nanosized copper(i) iodide particles showing inactivation activity against 2009 pandemic H1N1 influenza virus. *Applied and Environmental Microbiology*. 2012. Vol. 78, no. 4, p. 951–955. DOI 10.1128/AEM.06284-11.

117. ARCHANA, K. M., RAJAGOPAL, Revathy, KRISHNASWAMY, Veena Gayathri

and AISHWARYA, S. Application of green synthesised copper iodide particles on cotton fabric-protective face mask material against COVID-19 pandemic. *Journal of Materials Research and Technology*. Online. 2021. Vol. 15, p. 2102–2116. DOI 10.1016/j.jmrt.2021.09.020.

118. DELUMEAU, Louis Vincent, ASGARIMOGHADDAM, Hatameh, ALKIE, Tamiru, JONES, Alexander James Bryan, LUM, Samantha, MISTRY, Kissan, AUCOIN, Marc G., DEWITTE-ORR, Stephanie and MUSSELMAN, Kevin P. Effectiveness of antiviral metal and metal oxide thin-film coatings against human coronavirus 229E. *APL Materials*. 2021. Vol. 9, no. 11. DOI 10.1063/5.0056138.

119. KUMAR, Sumit, KARMACHARYA, Mamata, JOSHI, Shalik Ram, GULENKO, Oleksandra, PARK, Juhee, KIM, Gun Ho and CHO, Yoon Kyoung. Photoactive Antiviral Face Mask with Self-Sterilization and Reusability. *Nano Letters*. 2021. Vol. 21, no. 1, p. 337–343. DOI 10.1021/acs.nanolett.0c03725.

120. JUNG, Sunghoon, BYEON, Eun Yeon, KIM, Do Geun, LEE, Da Gyum, RYOO, Sungweon, LEE, Sanggu, SHIN, Cheol Woong, JANG, Ho Won, YANG, Jun Yeoung, KIM, Hyo Jung and LEE, Seunghun. Copper-coated polypropylene filter face mask with SARS-COV-2 antiviral ability. *Polymers*. 2021. Vol. 13, no. 9, p. 1–10. DOI 10.3390/polym13091367.

121. KUMAR, Abhishek, SHARMA, Anu, CHEN, Yi, JONES, Megan M., VANYO, Stephen T., LI, Changning, VISSER, Michelle B., MAHAJAN, Supriya D., SHARMA, Rakesh Kumar and SWIHART, Mark T. Copper@ZIF-8 Core-Shell Nanowires for Reusable Antimicrobial Face Masks. *Advanced Functional Materials*. 2021. Vol. 31, no. 10, p. 1–13. DOI 10.1002/adfm.202008054.

122. TURNLUND, Judith R. Human whole-body copper metabolism. *American Journal of Clinical Nutrition*. Online. 1998. Vol. 67, no. 5 SUPPL., p. 960S-964S. DOI 10.1093/ajcn/67.5.960S.

123. HEJAZY, Marzie, KOOHI, Mohammad Kazem, POUR, Adele Bassiri Mohamad and NAJAFI, Davod. Toxicity of manufactured copper nanoparticles - A review. *Nanomedicine Research Journal*. 2018. Vol. 3, no. 1, p. 1–9. DOI 10.22034/NMRJ.2018.01.001.

124. SPORTELLI, Maria Chiara, IZZI, Margherita, LOCONSOLE, Daniela, SALLUSTIO, Anna, PICCA, Rosaria Anna, FELICI, Roberto, CHIRONNA, Maria and CIOFFI, Nicola. On the Efficacy of ZnO Nanostructures against SARS-CoV-2. *International Journal of Molecular Sciences*. 2022. Vol. 23, no. 6, p. 1–12. DOI 10.3390/ijms23063040.

125. BARZINJY, Azeez Abdullah and AZEEZ, Himdad Hamad. Green synthesis and characterization of zinc oxide nanoparticles using Eucalyptus globulus Labill. leaf extract and zinc nitrate hexahydrate salt. *SN Applied Sciences*. Online. 2020. Vol. 2, no. 5. DOI 10.1007/s42452-020-2813-1.

126. KARAGOZ, Sultan, BURAK KIREMITLER, N., SARP, Gokhan, PEKDEMIR, Sami, SALEM, Samaa, GOKSU, Ayse Gencay, SERDAR ONSES, M., SOZDUTMAZ, Ibrahim, SAHMETLIOGLU, Ertugrul, OZKARA, Ergun Samet, CEYLAN, Ahmet and YILMAZ, Erkan. Antibacterial, antiviral, and self-cleaning mats with sensing capabilities based on electrospun nanofibers decorated with ZnO

nanorods and Ag nanoparticles for protective clothing applications. *ACS Applied Materials and Interfaces*. 2021. Vol. 13, no. 4, p. 5678–5690. DOI 10.1021/acsami.0c15606.

127. JIANG, Shengjie, LIN, Kaili and CAI, Ming. ZnO Nanomaterials: Current Advancements in Antibacterial Mechanisms and Applications. *Frontiers in Chemistry*. 2020. Vol. 8, no. July, p. 1–5. DOI 10.3389/fchem.2020.00580.

128. PARDO-FIGUEREZ, Maria, CHIVA-FLOR, Alberto, FIGUEROA-LOPEZ, Kelly, PRIETO, Cristina and LAGARON, Jose M. Antimicrobial nanofiber based filters for high filtration efficiency respirators. *Nanomaterials*. 2021. Vol. 11, no. 4, p. 1–17. DOI 10.3390/nano11040900.

129. SHAKEEL, Muhammad, JABEEN, Farhat, SHABBIR, Samina, ASGHAR, Muhammad Saleem, KHAN, Muhammad Saleem and CHAUDHRY, Abdul Shakoor. Toxicity of Nano-Titanium Dioxide (TiO2-NP) Through Various Routes of Exposure: a Review. *Biological Trace Element Research*. Online. 2016. Vol. 172, no. 1, p. 1–36. DOI 10.1007/s12011-015-0550-x.

130. ATTIA, Gouda H., MOEMEN, Yasmine S., YOUNS, Mahmoud, IBRAHIM, Ammar M., ABDOU, Randa and EL RAEY, Mohamed A. Antiviral zinc oxide nanoparticles mediated by hesperidin and in silico comparison study between antiviral phenolics as anti-SARS-CoV-2. *Colloids and Surfaces B: Biointerfaces*. Online. 2021. Vol. 203, no. January, p. 111724. DOI 10.1016/j.colsurfb.2021.111724.

131. MUTALIK, Chinmaya, WANG, Di-yan, KRISNAWATI, Dyah Ika and JAZIDIE, Achmad. Light-Activated Heterostructured Nanomaterials for Antibacterial Light-Activated Heterostructured Nanomaterials for Antibacterial Applications. . 2020. No. March. DOI 10.3390/nano10040643.

132. HARTATI, Sri, ZULFI, Akmal, MAULIDA, Pramitha Yuniar Diah, YUDHOWIJOYO, Azis, DIOKTYANTO, Mudzakkir, SAPUTRO, Kurniawan Eko, NOVIYANTO, Alfian and ROCHMAN, Nurul Taufiqu. Synthesis of Electrospun PAN/TiO2/Ag Nanofibers Membrane As Potential Air Filtration Media with Photocatalytic Activity. *ACS Omega*. 2022. Vol. 7, no. 12, p. 10516–10525. DOI 10.1021/acsomega.2c00015.

133. BOBO, Daniel, ROBINSON, Kye J., ISLAM, Jiaul, THURECHT, Kristofer J. and CORRIE, Simon R. Nanoparticle-Based Medicines: A Review of FDA-Approved Materials and Clinical Trials to Date. *Pharmaceutical Research*. Online. 2016. Vol. 33, no. 10, p. 2373–2387. DOI 10.1007/s11095-016-1958-5.

134. ABO-ZEID, Yasmin, ISMAIL, Nasser S., MCLEAN, Gary R. and HAMDY, Nadia M. A molecular docking study repurposes FDA approved iron oxide nanoparticles to treat and control COVID-19 infection. *European Journal of Pharmaceutical Sciences*. Online. 2020. Vol. 153, no. July, p. 105465. DOI 10.1016/j.ejps.2020.105465.

135. DE MAIO, Flavio, PALMIERI, Valentina, BABINI, Gabriele, AUGELLO, Alberto, PALUCCI, Ivana, PERINI, Giordano, SALUSTRI, Alessandro, SPILMAN, Patricia, DE SPIRITO, Marco, SANGUINETTI, Maurizio, DELOGU, Giovanni, RIZZI, Laura Giorgia, CESAREO, Giulio, SOON-SHIONG, Patrick, SALI, Michela and

PAPI, Massimiliano. Graphene nanoplatelet and graphene oxide functionalization of face mask materials inhibits infectivity of trapped SARS-CoV-2. *iScience*. Online. 2021. Vol. 24, no. 7, p. 102788. DOI 10.1016/j.isci.2021.102788.

136. DE TOLEDO, Gabriel G., TOLEDO, Victor H., LANFREDI, Alexandre J.C., ESCOTE, Marcia, CHAMPI, Ana, DA SILVA, Maria Cristina C. and NANTES-CARDOSO, Iseli L. Promising nanostructured materials against enveloped virus. *Anais da Academia Brasileira de Ciencias*. 2020. Vol. 92, no. 4, p. 1–22. DOI 10.1590/0001-3765202020200718.

137. DAHANAYAKE, Madushani H., ATHUKORALA, Sandya S. and JAYASUNDERA, A. C.A. Recent breakthroughs in nanostructured antiviral coating and filtration materials: a brief review. *RSC Advances*. 2022. Vol. 12, no. 26, p. 16369–16385. DOI 10.1039/d2ra01567f.

138. DONG, Xiuli, LIANG, Weixiong, MEZIANI, Mohammed J, SUN, Ya-ping and YANG, Liju. Theranostics Carbon Dots as Potent Antimicrobial Agents. . 2020. Vol. 10, no. 2. DOI 10.7150/thno.39863.

139. The environmental toll of disposable masks | MIT News | Massachusetts Institute of Technology. Online. [Accessed 19 May 2023]. Available from: https://news.mit.edu/2021/covid-masks-environment-0720

140. Five things you should know about disposable masks and plastic pollution | UN News. Online. [Accessed 19 May 2023]. Available from: https://news.un.org/en/story/2020/07/1069151

141. SALIU, Francesco, VERONELLI, Maurizio, RAGUSO, Clarissa, BARANA, Davide, GALLI, Paolo and LASAGNI, Marina. The release process of microfibers: from surgical face masks into the marine environment. *Environmental Advances*. Online. 2021. Vol. 4, no. March, p. 100042. DOI 10.1016/j.envadv.2021.100042.

142. DAS, Oisik, NEISIANY, Rasoul Esmaeely, CAPEZZA, Antonio Jose, HEDENQVIST, Mikael S., FÖRSTH, Michael, XU, Qiang, JIANG, Lin, JI, Dongxiao and RAMAKRISHNA, Seeram. The need for fully bio-based facemasks to counter coronavirus outbreaks: A perspective. *Science of the Total Environment*. Online. 2020. Vol. 736, p. 139611. DOI 10.1016/j.scitotenv.2020.139611.

143. TILIKET, G., SAGE, D. Le, MOULES, V., ROSA-CALATRAVA, M., LINA, B., VALLETON, J. M., NGUYEN, Q. T. and LEBRUN, L. A new material for airborne virus filtration. *Chemical Engineering Journal*. 2011. Vol. 173, no. 2, p. 341–351. DOI 10.1016/j.cej.2011.07.059.

144. PATIL, Nikhil Avinash, GORE, Prakash Macchindra, JAYA PRAKASH, Niranjana, GOVINDARAJ, Premika, YADAV, Ramdayal, VERMA, Vivek, SHANMUGARAJAN, Dhivya, PATIL, Shivanand, KORE, Abhay and KANDASUBRAMANIAN, Balasubramanian. Needleless electrospun phytochemicals encapsulated nanofibre based 3-ply biodegradable mask for combating COVID-19 pandemic. *Chemical Engineering Journal*. Online. 2021. Vol. 416, no. December 2020, p. 129152. DOI 10.1016/j.cej.2021.129152.

145. CHOI, Sejin, JEON, Hyeonyeol, JANG, Min, KIM, Hyeri, SHIN, Giyoung, KOO, Jun Mo, LEE, Minkyung, SUNG, Hye Kyeong, EOM, Youngho, YANG, Ho Sung,

JEGAL, Jonggeon, PARK, Jeyoung, OH, Dongyeop X. and HWANG, Sung Yeon. Biodegradable, Efficient, and Breathable Multi-Use Face Mask Filter. *Advanced Science*. 2021. Vol. 8, no. 6, p. 1–8. DOI 10.1002/advs.202003155.

146. WANG, Zhe, PAN, Zhijuan, WANG, Jigen and ZHAO, Ruizhi. A Novel Hierarchical Structured Poly(lactic acid)/Titania Fibrous Membrane with Excellent Antibacterial Activity and Air Filtration Performance. *Journal of Nanomaterials*. 2016. Vol. 2016. DOI 10.1155/2016/6272983.

147. HE, Haijun, GAO, Min, ILLÉS, Balázs and MOLNAR, Kolos. 3D Printed and electrospun, transparent, hierarchical polylactic acid mask nanoporous filter. *International Journal of Bioprinting*. 2020. Vol. 6, no. 4. DOI 10.18063/ijb.v6i4.278.

148. KADAM, Vinod, TRUONG, Yen Bach, SCHUTZ, Jurg, KYRATZIS, Ilias Louis, PADHYE, Rajiv and WANG, Lijing. Gelatin/β–Cyclodextrin Bio–Nanofibers as respiratory filter media for filtration of aerosols and volatile organic compounds at low air resistance. *Journal of Hazardous Materials*. Online. 2021. Vol. 403, no. September 2020, p. 123841. DOI 10.1016/j.jhazmat.2020.123841.

149. AL-HAZEEM, Nabeel. Manufacture of fibroustructure facemask to protect against coronavirus using electrospinning. *Medico Research Chronicles*. 28 April 2021. Vol. 8, no. 2, p. 103–110. DOI 10.26838/medrech.2021.8.2.480.

150. LEZA, Daniela Salado. Development of platinum based nanoparticles to enhance cancer cell killing by gamma rays and carbon Daniela Salado Leza To cite this version : HAL Id : tel-02458848 L ' U NIVERSITE P ARIS -S ACLAY PREPAREE A L ' U NIVERSITE P ARIS S UD Daniela Edith Salad. . 2020.

151. ISO 20645:2004 - Textile fabrics — Determination of antibacterial activity — Agar diffusion plate test. Online. [Accessed 17 November 2023]. Available from: https://www.iso.org/standard/35499.html

152. ISO 20743:2021 - Textiles — Determination of antibacterial activity of textile products. Online. [Accessed 17 November 2023]. Available from: https://www.iso.org/standard/79819.html

153. ASTM. Standard Test Method for Determining the Initial Efficiency of Materials Used in. . 2010. Vol. 03, no. Reapproved, p. 1–8. DOI 10.1520/F2299.

154. ASTM. F2100-19e1 Standard Specification for Performance of Materials Used in Medical Face Masks. *ASTM International*. 2020. Vol. 11, no. 2018, p. 10–13. DOI 10.1520/F2100-20.2.

155. STANDARISATION, Bureau for. Belgian Standard EN 14683 : 2019 + AC : Medical face masks - Requirements and test methods. . 2019.

156. HULLE, Nishant R Swami, PATRUNI, Kiran and RAO, P Srinivasa. RHEOLOGICAL PROPERTIES OF ALOE VERA ( ALOE BARBADENSIS MILLER ) JUICE CONCENTRATES. . 2014. DOI 10.1111/jfpe.12093.

157. MAG, Phcog, KHAN, Abdul Wadood, KOTTA, Sabna, ANSARI, Shahid Hussain, SHARMA, Rakesh Kumar, KUMAR, Amit and ALI, Javed. Formulation development , optimization and evaluation of aloe vera gel for wound healing. . 2013. Vol. 9, no. 36, p. 2–6. DOI 10.4103/0973-1296.117849.

158. ABUTALIB, M M and RAJEH, A. Structural , thermal , optical and conductivity studies of Co / ZnO nanoparticles doped CMC polymer for solid state battery applications. *Polymer Testing*. Online. 2020. Vol. 91, no. June, p. 106803. DOI 10.1016/j.polymertesting.2020.106803.

159. WANG, Hongqiang, LI, Caihong, ZHAO, Haigang, LI, Ru and LIU, Jinrong. Synthesis , characterization , and electrical conductivity of ZnO with different morphologies. . 2013. Vol. 239, no. 3, p. 266–271. DOI 10.1016/j.powtec.2012.12.045.

160. FONG, Hao. Bending Instability of Electrically Charged Liquid Jets of Polymer Solutions in Electrospinning Bending instability of electrically charged liquid jets of polymer solutions in electrospinning. . 2014. No. May. DOI 10.1063/1.373532.

161. SHIRATORI, Seimei. Formation of novel 2D polymer nanowebs via electrospinning Formation of novel 2D polymer nanowebs via electrospinning. . 2014. No. August 2006. DOI 10.1088/0957-4484/17/15/011.

162. Electrospinning Process. . 2004. P. 90–154.

163. CHEMISTRY, Cellulose, JAFARBEGLOU, Maryam and HAGHI, A K. Electrospun biodegdadable and biocompatible natural nanofibers : A detailed review ELECTROSPUN BIODEGDADABLE AND BIOCOMPATIBLE NATURAL NANOFIBERS : A DETAILED REVIEW. . 2008. No. January.

164. LAGE-RIVERA, Silvia, ARES-PERNAS, Ana, CARLOS, Juan, PERMUY, Becerra and GOSSET, Anne. Enhancement of 3D Printability by FDM and Electrical Conductivity of PLA / MWCNT Filaments Using Lignin as Bio-Dispersant. . 2023.

165. PRABHAKAR, Pranav Kumar and DOBLE, Mukesh. Interaction of Cinnamic Acid Derivatives with Commercial Hypoglycemic Drugs on 2-Deoxyglucose Uptake in 3T3-L1 Adipocytes. . 2011. P. 9835–9844.

166. LALLO, Bruna, ABUÇAFY, Marina Paiva, MANAIA, Eloisa Berbel and CHIAVACCI, Leila Aparecida. Relationship Between Structure And Antimicrobial Activity Of Zinc Oxide Nanoparticles : An Overview. . 2019. P. 9395–9410.

167. SALAM, Abdul, KHAN, Muhammad Qamar, HASSAN, Tufail, HASSAN, Nafees, NAZIR, Ahsan, HUSSAIN, Tanveer, AZEEM, Musaddaq and KIM, Ick Soo. In - vitro assessment of appropriate hydrophilic scaffolds by co - electrospinning of poly ( 1 , 4 cyclohexane isosorbide terephthalate )/ polyvinyl alcohol. *Scientific Reports*. Online. 2020. P. 1–10. DOI 10.1038/s41598-020-76471-x.

168. MAI-PROCHNOW, Anne, CLAUSON, Maryse, HONG, Jungmi and MURPHY, Anthony B. Gram positive and Gram negative bacteria differ in their sensitivity to cold plasma. *Scientific Reports*. 2016. Vol. 6, no. November, p. 1–11. DOI 10.1038/srep38610.

## CURRICULUM VITAE

**Muhammad Usman Munir**
Muhammad.munir@ktu.edu

**Education:**
2009 – 2013 Bachelor's in Textile Engineering (Textile Processing), National Textile University, Faisalabad, Pakistan

2014 – 2017 Master's in Advanced Materials Engineering, National Textile University, Faisalabad, Pakistan

2019 – 2023 PhD in Materials Engineering, Kaunas University of Technology, Kaunas, Lithuania

**Professional experience:**
2013 – 2019 Denim Dyeing Head, Crescent Bahuman Limited, Pakistan.
03/2021 – 12/2021 Biomedical Engineer, Consultant, United States Pharmacopeia.

**Areas of research interest:**
Textiles, nanomaterials, nanofibers, electrospinning, dyes and chemicals, sustainable textiles, denim, antimicrobial finishes.

**Scientific papers on the topic of dissertation:**

1. **Munir, Muhammad Usman**; Mikucioniene, Daiva; Khanzada, Haleema; Khan, Muhammad Qamar. Development of eco-friendly nanomembranes of aloe vera/PVA/ZnO for potential applications in medical devices // Polymers. Basel: MDPI. ISSN 2073-4360. 2022, Vol. 14, iss. 5, art. No. 1029, p. 1–14. DOI: 10.3390/polym14051029. [Science Citation Index Expanded (Web of Science); Scopus; MEDLINE] [IF: 4.967; AIF: 5.162; IF/AIF: 0.962; Q1 (2021, InCites JCR SCIE)] [Field: T 008].
2. **Munir, Muhammad Usman**; Mayer-Gall, Thomas; Gutmann, Jochen S; Ali, Wael; Etemad-Parishanzadeh, Omid; Khanzada, Haleema; Mikučionienė, Daiva. Development of carbon-nanodot-loaded PLA nanofibers and study of their barrier performance for medical applications // Nanomaterials. Basel: MDPI. ISSN 2079-4991. 2023, Vol. 13, iss. 7, art. No. 1195, p. 1–13. DOI: 10.3390/nano13071195. [Science Citation Index Expanded (Web of Science); Scopus; MEDLINE] [IF: 5.719; AIF: 7.191; IF/AIF: 0.795; Q1 (2021, InCites JCR SCIE)] [Field: T 008].

3. Ivanoska-Dacikj, Aleksandra; Oguz-Gouillart, Yesim; Hossain, Gaffar; Kaplan, Müslüm; Sivri, Çağlar; Ros-Lis, José Vicente; Mikucioniene, Daiva; **Munir, Muhammad Usman**; Kizildag, Nuray; Unal, Serkan; Safarik, Ivo; Akgül, Esra; Yıldırım, Nida; Bedeloğlu, Ayşe Çelik; Ünsal, Ömer Faruk; Herwig, Gordon; Rossi, René M.; Wick, Peter; Clement, Pietro; Sarac, A. Sezai. Advanced and smart textiles during and after the COVID-19 pandemic: issues, challenges, and innovations // Healthcare. Basel: MDPI. ISSN 2227-9032. 2023, Vol. 11, iss. 8, art. No. 1115, p. 1–27. DOI: 10.3390/healthcare11081115. [Science Citation Index Expanded (Web of Science); Scopus; MEDLINE] [IF: 3.160; AIF: 4.049; IF/AIF: 0.780; Q2 (2021, InCites JCR SCIE)] [Field: T008].

**Scientific conferences:**

1. **Munir, Muhammad Usman**; Mikučionienė, Daiva. Study on barrier performance of medical face masks available to Lithuanian public // Advanced materials and technologies: book of abstracts of 24th international conference-school, 22–26 August 2022, Palanga, Lithuania. Kaunas: Kaunas University of Technology. ISSN 2669-1930. 2022, A-P97, p. 136. [Field: T 008] CNBCNHVDH6HU.
2. **Munir, Muhammad Usman**; Mikučionienė, Daiva. Development of eco-friendly nanomembranes of aloe vera/PVA/ZnO for potential applications in PPEs // Polymers 2022 – New trends in polymer science: health of the planet, health of the people, Turin, Italy, 25–27 May 2022: book of abstracts. Basel: MDPI. 2022, A.6, p. 80. [Field: T 008]
3. Khanzada, Haleema; Salam, Abdul; Qadir, Muhammad Bilal; Phan, Duy-Nam; Hassan, Tufail; **Munir, Muhammad Usman**; Pasha, Khalid; Hassan, Nafees; Khan, Muhammad Qamar; Kim, Ick Soo. Antimicrobial aloe vera/PVA electrospun nanofibers for protective textiles // AUTEX 2021 – Unfolding the future: 20th world textile conference, 5–9 September 2021, Guimarães, Portugal & online: book of abstracts / edited by Sciencentris. Guimarães: Local organizing committee, 2021, ID55. ISBN 9789895480869. p. 78–79. [Field: T008]
4. **Munir, Muhammad Usman**; Mikučionienė, Daiva. Modelling and optimization of Aloe vera/PVA/ZnO nanomembranes and their applications in nonwoven masks // Advanced materials and technologies: book of abstracts of 23rd international conference-school, 23–27 August 2021, Palanga, Lithuania. Kaunas: Kaunas University of Technology. ISSN 2669-1930. 2021, B-P34, p. 64. [Field: T 008]
5. **Munir, Muhammad** Usman; Mikučionienė, Daiva. A study on barrier performance of medical face masks // AUTEX conference proceedings: 21st World textile conference AUTEX 2022: Passion for Innovation: June 7–10, 2022, Łódź, Poland. Łódź: Łódź University of Technology Press, 2022.

ISBN 9788366741751. p. 115–119. DOI: 10.34658/9788366741751.24. [Field: T 008] [Contribution: 0.500].

## ACKNOWLEDGEMENTS

I attribute all my achievements and the ability to overcome challenges during my demanding PhD study to the blessings and strengths bestowed upon me by Allah Almighty.

I dedicate the completion of my PhD to the loving memory of my dear mom, Naseem Akhtar. Although she is no longer with us, her presence continues to inspire and guide me every step of the way. You were my biggest supporter, my rock, and my guiding light throughout this academic journey. Your unwavering belief in my abilities and your constant encouragement gave me the strength to persevere, especially during the challenging moments. Your wisdom, love, and sacrifices have shaped the person I am today, and I am forever grateful.

This achievement is a testament to your enduring influence in my life. I carry your values, resilience, and determination within me as I embark on new adventures and contribute to the world in meaningful ways. I hope that I can make you proud, just as you always made me proud.

While I deeply miss your presence, I find solace in knowing that you are watching over me from above. Your memory will forever be etched in my heart, and I will continue to honour you in all that I do.

Although my name appears alone on the title page of this thesis, I humbly acknowledge that I am not its sole contributor. The successful completion of this doctoral thesis would not have been feasible without the unwavering support and encouragement of numerous individuals who have directly or indirectly played a part. Hence, I express my heartfelt gratitude and extend a sincere ‘thank you’ to all those who have contributed to this accomplishment.

I would like to express my utmost appreciation and profound admiration to my esteemed supervisor, Professor Daiva Mikučionienė, for the unwavering support, exceptional guidance, and profound motivation provided throughout my academic journey. I extend my heartfelt gratitude for accepting me as a doctoral candidate. Throughout the entirety of my doctoral studies, you bestowed upon me relentless trust and considerable autonomy to delve into intriguing research areas. Your systematic encouragement and support during my endeavours left a lasting impression on me. It is an immense privilege to have had the opportunity to be mentored by such an accomplished scholar. Let us never bid farewell, graduation signifies not the termination but rather the commencement of a new chapter in everyone’s life.

I would also like to thank my loving family, my son, my little daughter, and my loving wife. As balancing the demands of pursuing a doctorate while also being a loving wife and mother is no easy task, yet you managed to do it with grace and selflessness. Your sacrifices and understanding during those long nights of studying, countless hours spent researching, and moments of self-doubt have been invaluable to me. Your belief in my abilities and constant motivation kept me going, even when I

felt overwhelmed. To my son and my daughter, although you may not fully comprehend the significance of this accomplishment at your tender age, your smiles, hugs, and laughter were the light that brightened my darkest days. Your innocent joy and unconditional love served as a constant reminder of why I pursued this dream in the first place – to create a better future for our family.

Regards,
Muhammad Usman Munir

UDK 615.46 + 615.479.4 + 677.022.3/.5](043.3)
SL344. 2024-01-30, 16,5 leidyb. apsk. l. Tiražas 14 egz. Užsakymas 12.
Išleido Kauno technologijos universitetas, K. Donelaičio g. 73, 44249 Kaunas
Spausdino leidyklos „Technologija“ spaustuvė, Studentų g. 54, 51424 Kaunas